NANOSCALE STUDIES OF METAL REDUCTION BY MICROBIAL BIOCATALYSTS USING IN VITRO BIOMIMETIC PLATFORMS

By

Bhushan Prabhakar Awate

A DISSERTATION

Submitted to
Michigan State University
in partial fulfillment of the requirements
for the degree of

Chemical Engineering—Doctor of Philosophy

2014

ABSTRACT

NANOSCALE STUDIES OF METAL REDUCTION BY MICROBIAL BIOCATALYSTS USING IN VITRO BIOMIMETIC PLATFORMS

By

Bhushan Prabhakar Awate

Metal-reducing bacteria like *Geobacter sulfurreducens* use cytochrome proteins to reductively precipitate water-soluble uranium salts. However, the mechanism by which the cytochromes achieve multistep electron transfer to extracellular metals is not yet understood. Previous studies of cytochromes' role in electron transfer have involved a genetic approach, in which specific cytochromes are either deleted or overexpressed. However, results of these genetic studies are difficult to interpret, because mutation of one gene can cause multiple phenotypic changes, resulting in complex alterations of the cell's electron-transfer machinery. These limitations can be bypassed using a biomimetic approach, in which *Geobacter* cytochromes are assembled into nanostructured interfaces that mimic the cell envelope and electron-carrier machinery.

In this study, we heterologously expressed some of *Geobacter's* most abundant and conserved cytochromes in *Escherichia coli*. We then used these cytochromes to fabricate nanostructured biomimetic interfaces that mimicked *Geobacter*'s double-membrane cell envelope. A self-assembled monolayer of alkanethiols on a gold electrode mimicked the inner membrane; an aqueous layer containing PpcA (a periplasmic cytochrome) mimicked the periplasmic space; and a synthetic bilayer lipid membrane containing OmcB (an outer membrane cytochrome) mimicked the outer membrane. Cytochrome-mediated electron transfer from the gold electrode to soluble metal salts was characterized using cyclic voltammetry. The PpcA was

found to transfer electrons to U(VI) more rapidly than to other soluble electron acceptors, consistent with the observation that U(VI) is reductively precipitated in *Geobacter's* periplasm. Spectroelectrochemical characterization of PpcA and OmcB demonstrated for the first time electron transfer between these two proteins, suggesting that they may be redox partners in *Geobacter's* electron transport chain.

Fabrication of electrochemically active nanostructured bioelectronic interfaces that mimic *Geobacter's* double-layered cell envelope establishes a new experimental platform with which to characterize *Geobacter's* electron transfer machinery. Addition of more *Geobacter* components will make the interface more realistic and enable hypotheses about electron-transfer mechanisms to be systematically tested. An improved understanding of *Geobacter's* ability to reduce metals may lead to new technologies for *in situ* reductive immobilization of uranium and other toxic metals.

ACKNOWLEDGEMENTS

I would like to thank my advisor Dr. R. Mark Worden for all the help and guidance he provided for this research. And I would also like to thank him for being patient and supportive during the challenging times I faced. I wish to convey thanks to Dr. Gemma Reguera for providing me the opportunity to work with this extremely interesting multidisciplinary project. I wish to thank Dr. Scott Calabrese - Barton for his time and help he provided me as a committee member and also as a graduate coordinator. I would also like to thanks Dr. Ilsoon Lee for his helpful suggestions and for providing expertise in nanotechnology area.

I would also like to give special thanks to Dr. Denise Proshlyakov and his graduate student Chris John for helping and guidance me regarding the spectrophotometric techniques. My work here has been possible because of the help form fellow graduate students and post docs in my and my collaborator's labs. therefore, I would like to thank Lee Alexander, Chloe, Ying, Becky, Mike, Blaire and Dr. Jihwan. I would also like to convey my gratitude to Dr. Alicia Pastor for help regarding TEM, and Dr. Yuri Londer for providing me plasmid for protein expression.

And finally last but not the least, I would like to thank my family for being extremely supportive.

TABLE OF CONTENTS

LIST OF TABLES

LIST OF FIGURES

KEY TO ABBREVIATIONS

Chemicals

ACN	Acetonitrile
Ag/AgCl	Silver/silver chloride
ATP	Adenosine triphosphate
$CaCl_2$	Calcium chloride
DMR	Dissimilatory metal reducing microorganisms
DOPC	1,2-dioleoyl-*sn*-glycero-3-phosphocholine
DTT	Dithiothreitol
EDC	1-ethyl-3-[3-dimethylaminopropyl]carbodiimide
EDTA	Ehtylenediamine tetraacetic acid
HEPES	4-(2-hydroxyethyl)-1-piperazineethanesulfonic acid
IPTG	Isopropyl-β-D-thiogalactopyranoside
KCl	Potassium chloride
LB	Luria Bertani
$MgCl_2$	Magnesium chloride
NaCl	Sodium Chloride
NHS	N-hydroxysuccinimide
NTA	Nitrilotriacetic acid
TFA	Trifluoroacetic acid

UA Uranyl acetate

Symbols

A Electrode area

C_{DL} Double layer capacitance

C_F Faradaic capacitance

C_M Membrane capacitance

CPE Constant phase element

D Diffusion coefficient

F Faradays constant

i_P Peak faradaic current

kDA Kilodalton

Q Charge transferred during oxidation/reduction

R_{CT} Charge transfer resistance

R_M Membrane resistance

R_S Solution resistance

t Time

τ Surface coverage

T Temperature

ν Scan rate

V	Applied potential
Y	Admittance
Z	Impedance
Z_I	Imaginary part of impedance
Z_R	Real part of impedance
θ_M	Phase delay
ω	Frequency

Terminologies

BLM	Bilayer lipid membrane
BRACE	Biomimetic redox active cell envelope
DET	Direct electron transfer
ET	Electron transfer
SAM	Self assembled monolayer
sBLM	Supported BLM
tBLM	Tethered BLM

Instrumentation

CA	Chronoamperometry
CV	Cyclic voltammetry
DLS	Dynamic light scattering
EIS	Electrochemical impedance spectroscopy

MS	Mass spectrometry
QCM	Quartz crystal microbalance
TEM	Transmission electron microscopy
UV-vis	Ultraviolet- visible

1.0 INTRODUCTION

1.1 Motivation

Anthropogenic use of uranium has lead to the contamination of vast areas of subsurface waters and sediments, resulting in an environmental hazard. (1) More than 100 uranium-contaminated sites has been identified by U.S. Department of Energy (DOE) as a target for remediation. (2) *Ex situ* pump and treat decontamination methods involve sorption, volatilization, and biotic or abiotic treatments along with groundwater flushing. Disadvantage of these techniques is that they cannot be applied to the larger area with low localized concentration of contaminants and their high cost. (3) *In situ* bioremediation is proposed to be the most cost effective technique to clean up subsurface and groundwater contamination. (1) Bioelectronic reduction of uranium from soluble U (VI) form to insoluble (IV) form decreases its mobility and can limit the spread of uranium contamination through the groundwater. (4) Lab-scale as well as at pilot-scale field studies found that microbes from the bacterial family *Geobacteraceae* were instrumental in this bioremediation process. (5-10) Stimulating the activity of metal-reducing bacteria such as *Geobacter* spp. *in situ* shows promise for the immobilization of uranium, which is concomitantly reduced to its less soluble form, U(IV). (11) The reduction of U(VI) by *Geobacter* is concomitant to the reduction of Fe(III) oxides, a process that relies on the extracellular transfer of metabolically-generated electrons across electron carriers of the cell envelope. However, *Geobacter's* mechanism of biological metal reduction is still not understood at the molecular level. The objective of our project is to elucidate the electron transfer (ET) mechanism of the *Geobacter* using a nanostructured biomimetic interface.

1.2 Background

Dissimilatory metal reducing microorganisms (DMR) like *Geobacter* obtain energy by oxidizing organic compounds inside the cell and then transferring the electrons to the electron acceptors (mostly metal oxides) located outside the cell. Genome sequence analysis of different *Geobacter* species have identified some of conserved respiratory pathways (Fig. 1.1). (12) Electrons obtained from oxidation of organic carbon are used to reduce electron carriers like NAD^+, which transfer the electrons to the menaquinone pool. Then these electrons travel from the inner membrane of bacteria, across the periplasm with the help of number of periplasmic cytochrome proteins. It was postulated that heme network (cytochrome proteins) exists in this bacterium to either shuttle the electrons to the extracellular electron acceptors or to serve as an electron-storage depot in the absence of them. (13) A periplasmic cytochrome PpcA which is conserved across different families of *Geobacter* is thought to be most important of them. (14, 15) The electrons are passed by the periplasmic cytochromes to the outer membrane cytochromes, and finally to the electron acceptors outside the cell. Although the overall framework of energy metabolism inside the cell remains same in most of the DMRs, ET to extracellular electron acceptors can occur through a variety of mechanisms, including (1) indirect ET by solubilization of iron with organic chelators, (2) indirect transfer using electron shuttles (3) direct ET from the outer membrane *c*-cytochromes, and (4) direct ET with microbial protein nanowires - pili. The first mechanism has been claimed to be the mode of ET in *Shewanella putrefaciens* (16, 17), still this mechanism is yet to be accepted without reservations as a mode of ET in different *Shewanella* species. In *Shewanella*, the second mechanism is thought to be more predominant as *Shewanella* secrete soluble electron shuttles like riboflavin and flavin mononucleotides. (18, 19) However *Geobacter* species do not produce small shuttling

molecules, and electron shuttle with cytochrome secretion may not be metabolically economical for the bacteria. A lot of emphasis has been given to the third model due to the large number of *c*- cytochromes present in the *Geobacter* and *Shewanella* species, which are capable of reducing iron *in vitro*. (20-23) *G. sulfurreducens* has been shown to transfer electrons to an electrode via its outermost membrane cytochromes. (24) Various studies have well documented the important roles of different outer membrane cytochromes like OmcZ (25, 26), OmcB (27), OmcS, and OmcT (28) in *Geobacter* ET. However, very little homology exists among different species of *Geobacter* and related *Pelobacter* species regarding the content of cytochrome related genome, yet they all are capable of growing with Fe (III) oxide, and are present in uranium contaminated environments. (29)

While these variances create uncertainties about the exact role of outer membrane cytochromes, a highly conserved pili protein emerge as a likely candidate for final electron transfer in these organisms. Pili are the hair like appendages present on the surface of many bacteria, and are involved in DNA transfer, motility and surface attachment. *G.* sulfurreducens specifically produces pili during the growth on insoluble metal salts. (30) When pilA gene was deleted, *G. sulfurreducens* could not produce pili and failed to reduce insoluble electron acceptors such Fe(III) oxides. However these mutants could still use soluble electron acceptors like Fe(III) citrate and fumarate. These results point out that the pili might have a more direct role in electron transfer to Fe(III) oxides. (30) *Geobacter* pili were analyzed with a conductive probe atomic force microscope (AFM) and found to be conductive. This suggests a crucial role of pili in *Geobacter* for Fe(III) oxide reduction, as pili can serve as a nanowires to conduct electron transfer between the cell surface of the Fe(III) oxides. The exact nature of conduction of electrons along the length of pili is still under investigation. It was hypothesized that OmcS is

localized along the length of pili and the OmcS is responsible for the ET from pili to Fe(III) oxide. (31) However this interpretation is questionable, because a recent publication has shown that pili are primarily responsible for the extracellular reduction and localization of the uranium. (32) The *Geobacter* strains with mutation designed to produce higher amount of pili, reduced more uranium than native wild type pili, but OmcS content of both the strains were same, suggesting the pili mediated ET is not directly dependent on OmcS expression. (32) Studies carried out to measure the conductivity of these microbial nanowires has verified the conductive nature of pili. (33) A recent study showed that *Geobacter* strain with deletion of multiple outer membrane cytochrome decrease the rate of extracellular U reduction. (34) It is possible that one of the deleted cytochrome may be electron donor to pili. Still the mechanism by which pili receive the electrons remains unidentified, and is under investigation. Figure 1.2 represents a schematic description of our understanding of the *Geobacter* ET process based on current literature review. (22, 35, 36)

1.3 Problem description

The theoretical energy gained (ΔG) for bacteria is directly related to the potential difference between electron donor and acceptor:

$$\Delta G = -n F E_{emf}$$

where n is the number of electron exchanged, F is Faraday's constant and E_{emf} is the potential difference. Bacteria will try to maximize the energy gain by selecting the electron acceptor with higher potential and electron donor with lower potential. Therefore it is crucial to gain knowledge about thermodynamic properties of this electron transport carrier proteins to understand their significance in bacterial ET. A putative picture of energy coupling with ET

process is shown in Figure 1.3. Biological approaches to identify these electron carriers are limited by pleiotropic effects resulting from alterations in the native uranium reductase machinery. For example, deletion of OmcF gene also led to reduced expression of OmcB protein, and resultant cells showed impaired growth on Fe (III) citrate (37) Absence of OmcG and OmcH, did not affect the transcript levels of OmcB; however, expression of OmcB was affected negatively in those strains. (38) Deletion of OmcB led to reduced growth of the cells, but cells eventually recovered with increased expression of other outer membrane cytochromes like OmcS and OmcT. (39) These pleiotropic constraints can be bypassed through the use of *in vitro* platform that mimic the *Geobacter* cell membrane electron carrier machinery.

The objective of this research was to construct biomimetic redox active cell envelope (BRACE) containing *Geobacter*'s most abundant and conserved electron carriers to mimic *Geobacter* cell membrane electron carrier machinery. We identified periplasmic cytochrome protein PpcA and an outer membrane cytochrome OmcB as an integral components of designed biomimetic interface. These proteins were expressed heterologously in *E. coli* host in order to achieve high yields of proteins necessary for the study, and to isolate the target cytochromes from bacteria without any interference from other redox proteins. The BRACE interfaces were assembled on a gold or carbon electrode (cathode) that act as a source of electrons. An example BRACE interface consist of (1) a self-assembled monolayer of lipids that simulate the inner membrane of *Geobacter*; (2) a layer containing periplasmic cytochrome PpcA, which act as an intermediate electron carrier to either outer membrane cytochrome and/or pili; (3) a lipid layer, which act as an outer membrane and will insulate the PpcA layer from the solution, thus creating an artificial periplasmic space; (4) an outer membrane cytochrome OmcB embedded in the lipid

layer; (5) a self assembled monolayer of lipids, with immobilized PpcA deposited on optically transparent electrode.

Till date a very few studies are available about the kinetics of the reduction reaction of metal species and DRMs, (40-42) and even fewer studies are available about the kinetics of specific cytochromes from *Shewanella* and metals, (40, 43, 44) but none of the specific cytochromes from *Geobacter* has been analyzed for their kinetics of metal reduction. Our present research aims to bridge the knowledge gap about the putative role of these individual cytochrome in *Geobacter* ET. Furthermore our aim has been to provide a versatile biomimetic interface in the form of BRACE, which can be used to study different proteins, and which can be adapted to diverse application such as biosensor development.

These novel biomimetic interfaces will provide the platform necessary to investigate the flow of electrons from *Geobacter* membrane to the electrons acceptors. Information gained from these studies will enhance understanding of *Geobacter* ET and may guide efforts to engineer uranium bioremediation strategies.

1.3.1 Heterologous expression of cytochrome in *E. coli*

Heterologous expression of cytochrome in *E. coli* is highly desirable for the possibility of mass production and purification; but it can be very challenging because of the posttranslational modification required for the activity of these proteins. Therefore till date very few recombinant cytochromes have been expressed in *E. coli*. To best of our knowledge *Shewanella* cytochromes: MtrA (45), CymA (46), and OmcA (47) and *Geobacter* cytochrome PpcA (48) are the only cytochrome that has been successfully expressed in *E. coli*. Careful understanding of the cytochrome *c* biogenesis is required to design its heterologous expression strategy.

Cytochrome *c* proteins are hemoproteins in which iron-protoporphyrin IX (heme b) groups are covalently bound to the polypeptide chain. Cytochrome *c* proteins have at least one heme binding motif (C_1XXC_2H), where the cysteines forms two thioether bonds with vinyls at position 2 and 4 of the tetrapyrrole rings of heme b. (49) The histidine residue serves as one of the axial ligand to the heme-iron. Methionine or another histidine residue located farther away in amino acid sequence forms the other ligand. The stereo-selectivity of heme attachment to the cytochrome *c* polypeptide chain is same in all known examples of cytochrome *c*.(50) Heterologous expression of cytochrome *c* is challenging because none of the cytochrome *c* are cytoplasmic proteins. They are either expressed in the intermediates space of mitochondria or in the periplasmic space or are membrane associated via transmembrane helix or a lipid anchor. (51) For biogenesis of a functional cytochrome *c*, both apoprotein and heme moieties must transloacte through inner membrane. Then the apoprotein and heme must be brought together by series of enzymes and chaperon proteins to form a thioether bond. Cytochrome *c* biogenesis processes are still being discovered, but based on current knowledge about the proteins involved in the apocytochrome assembly and chaperoning, heme handling and thioether bond formation, they are divided into three classes: system I, II and III. (52)

Many gram negative bacteria including *E. coli* use system I (also called the Ccm system) for cytochrome *c* assembly. The Ccm system employs up to ten different membrane bound components (CcmABCDEFGHI and DsbD/CcdA) whose operation can be divided into three different modules. (53) Module 1 consists of Ccm proteins A to E and are involved in the translocation and relaying of heme b. The exact mechanism of the heme translocation across the membrane is still unclear and not entirely dependent on presence of Ccm proteins (54) but Ccm proteins are essential for assembly of *c*-type cytochromes where heme is covalently bound.

Module 2 is involved in apocytochrome *c* thioreduction (to make it ligand competent) and chaperoning process. It is important that after translocation across the membrane the cysteine moiety of apocytochrome *c* destined to bind heme must be in reduced state in the oxidative environment of periplasmic space. This is proposed to be achieved by first oxidizing the cysteines with DsbA-DsbB pathway to form disulfide bond making it less susceptible to degradation. Then the cysteine is reduced by CcmG/CcmA pathway. Cysteines of CcmH are also involved although not directly in the reduction of cysteine of apocytochrome *c*. Module 3 consisting of CcmH, CcmF and CcmI is involved in stereoselctive ligation of apocytochrome *c* to heme b resulting in holocytochrome *c*. In *E. coli* the Ccm protein are located in the inner membrane and on the periplasmic side of inner membrane and are active only in anaerobic conditions. (36) Cloning of the gene cluster ccmABCDEFGH into pACYC184 plasmid enables its constitutive co expression under aerobic conditions. (55) In this study, pEC 86, a derivative of the pACYC184 plasmid was co expressed with cytochrome *c* plasmid in *E. coli* to achieve mature cytochrome *c* expression.

1.3.2 Electrochemical measurements

Electrochemical techniques offer a powerful and convenient way of analyzing the redox proteins of interest in controlled environment. Some of the cytochromes are capable of direct electron transfer (DET) from the electrode without any additional redox mediators. We have taken advantage of this capability to study the kinetic and thermodynamic properties of these cytochrome on biomimetic interface using a variety of techniques like cyclic voltammetry, chronoamperometry, square wave voltammetry, and electrochemical impedance analysis.

1.3.3 Spectro-electrochemical measurements

Spectroelectrochemical techniques combines electrochemistry and spectroscopic measurements, and offers advantage offering capability to assess changes in specific molecules in the system as a function of electric potential. We built working electrode form a transparent slide coated with gold (~100 A^{o} thickness) and covered with self assembled monolayer (SAM) of thiolipids. Formation of SAM on the gold electrodes shielded the protein solution from degradation at the electrode surface, and furthermore provided us with the capability of controlling the access of species in solution towards working electrode. Redox activity of *Geobacter* cytochromes was measured electrochemically by technique like cyclic voltammetry and chronoamperometry, and multipotential analysis where changes in current at the working electrode are monitored as a function of applied potential. High transparency of the working electrode allowed us to measure reduction of cytochromes spectrophotometrically by presence of three characteristic absorption bands.

Despite its enormous importance in bioremediation as well as its potential application in MFCs, the ET mechanisms in DRMs has not been established yet. We have identified the unmet need about the tools required to study the *Geobacter* ET *in vitro*. The research presented in this dissertation focuses on building biomimetic systems that will help bridge the knowledge gap in this field. We have recognized the challenges associated establishing the theory about the ET mechanism, and have made a conscious effort to build a novel BRACE system that will facilitate the understanding about these complex processes in a more controlled environment.

1.4 Dissertation Outline

Chapter 2 of this dissertation describes a method to heterologously express and purify periplasmic cytochrome form *Geobacter*: PpcA in *E. coli*. Initial electrochemical characterization of the protein and method to immobilize it on electrode are presented. Kinetic of electron transfer reaction between protein and electrode are calculated. Chapter 3 describes the calculation of electron transfer kinetics between immobilized protein and soluble metal electron acceptors determined by cyclic voltammetry and rotating disk electrode technique. Chapter 4 describes our efforts to express *Geobacter* outer membrane protein OmcB in *E. coli*, confirmation of its identity and its localization to outer membrane of the *E. coli*. Chapter 5 describes development of spectroelectrochemical interface to study the redox active proteins on a thin layer electrode. Chapter 6 describes the formation of a BRACE interface with both PpcA and OmcB and its electrochemical characterization. Chapter 7 summarizes conclusions of this studies.

2.0 EXPRESSION, PURIFICATION, IMMOBILIZATION AND ELECTROCHEMISTRY OF RECOMBINANT PPCA

2.1 Introduction

One hallmark feature of *Geobacter* species as revealed by examination of genome sequence of *Geobacter sulfurreducens* is the presence of more than 70 *c*-type cytochromes. (57) It has been hypothesized that *c*-cytochromes acts as intermediate electron carriers from cytoplasm to outer membrane and then pili proteins complete the circuitry between cells and electron acceptors. A family of periplasmic triheme cytochromes was identified, (58) which was thought to be responsible for the periplasmic reduction of iron (59) and possibly as an intermediate in the transfer of electrons to the electron acceptor outside the cells. (60) PpcA is one of the most abundant of these periplasmic cytochromes and gene knockdown studies have shown its importance in Fe (III) and U (VI) reduction. (15) We have chosen PpcA as a protein of interest in our studies because it is one of the most conserved periplasmic cytochromes across different *Geobacter* species. (14) PpcA is a small protein of molecular size about 9.6 kDa, made up of 71 amino acids, and a very high proportion of lysine residues. (58) This protein has been studied by X-ray diffraction, (58) and nuclear magnetic resonance (NMR) to elucidate its structure and redox thermodynamics in great detail. (61-63) (64) The study of ^{15}N labeled PpcA with NMR spectroscopy was used to elucidate the structure of the protein, its backbone dynamics and the conformational changes based on the pH of the solution. (65) However, identity of the redox partner of PpcA in *Geobacter* ET is unknown.

2.1.1. Immobilization of PpcA on biomimetic interface

The studies mentioned in the previous section were done with the protein in solution. However, the biological compartments are much more viscous than the buffer solutions in which

these studies were done. For example, PpcA is located in the periplasm of bacteria, which environment resembles more like a thick gel (66), and the width of this space is about 10-25 nm. (66, 67) The diffusion processes inside the cell are slower for the biomolecules and even much slower for the proteins. (68, 69) Therefore, to better mimic the biological conditions inside the cells, we developed a protein immobilization strategy. The literature reviews showed large number of strategies available to immobilize cytochrome *c* on electrode; for example with N-acetyl cysteine, (70) cysteamine-modified gold with EDC coupling, (71) polypyrrole matrix, (72) functionalized vertically aligned carbon nanofiber scaffold, (73) beta-cyclodextrin-modified gold nanoparticles, (74) and even bare gold (75) to name just a few. We chose a self assembled monolayer (SAM) of alkanethiols on gold electrode as our substrate for immobilization. Gold oxides are formed on the surface of the electrode by the method employed to clean the surface (such as oxygen plasma cleaning), which are reduced by thiol terminated alkanes which self assemble on the gold electrode. (76, 77) Immobilization of cytochrome on this SAM is preferable because based on the functional group (e.g. carboxyl, hydroxy), and the chain length of carbon the chemistry of SAM can be fine-tuned to obtain optimum immobilization. (78-83)

2.1.2 Electrochemical characterization

Electrochemical characterization of interface was done by technique called cyclic voltammetry (CV). In CV technique, the voltage is swept between two potential values at a fixed scan rate. (84) In the forward scan, potential is swept from voltage V1 to voltage V2. Once the voltage reaches V2 the scan is reversed and the voltage is swept back to V1. The current is plotted as a function of applied voltage in a cyclic voltammogram. The shape of the voltammogram depends on the quality of electrode surface and the mass transfer effects. The redox couple present at the electrode surface get reduced or oxidized at the standard redox

potential value for the corresponding redox reaction. CV measurements can be used to determine the surface coverage of the immobilized redox species, diffusion coefficient of the redox species in the solution, and to gain insights into the mechanism of the reaction (such as multistep reactions).

2.2 Materials and methods

2.2.1 Production of PpcA

PpcA was heterologously expressed in *Escherichia coli* strain BL21 (DE3), as previously reported. (48) *E. coli* cells were co-transformed with plasmids pEC 86 and pCK 32. Plasmid pEC 86 contains the *ccm* genes that enable heme incorporation and maturation of PpcA in *E. coli.* (85) Plasmid pCK 32 plasmid is a derivative of plasmid pkIVlen004 with the *ppcA* fused to the signal peptide of the *E. coli* OmpA leader sequence for periplasmic expression of PpcA. Cells were grown in 2X YT liquid or solidified media containing 100 μg/ml ampicillin and 34 μg/ml chloramphenicol. The cultures used for purification of PpcA were initiated by growing a single colony of freshly co-transformed *E. coli* cells in 50 ml of 2x YT liquid medium supplemented with antibiotics. After overnight incubation at 30^{o} C with 250 rpm gyratory agitation, 10 ml of the culture were transferred into a 1 L of fresh medium and incubated under the same conditions to an optical density at 600 nm of approximately 1. PpcA expression was then induced with 100 μM of isopropyl β-D-1-thiogalactopyranoside (IPTG) during overnight incubation. Expression of PpcA was monitored by taking a sample of the inoculated fermentation media during the growth centrifugation at 5000X G to get a cell pellet. The pellet was digested by O.D. normalized value of Laemmle buffer with SDS, and running a SDS PAGE. Cells were harvested by centrifugation (4000 g, 4^{o} C, 15 min).

2.2.2. Purification of PpcA

Periplasmic protein fractions were separated by osmotic shock using lysis buffer containing 100 mM Tris-HCl, pH 8, 0.5 mM EDTA, 20% sucrose and 0.5 mg/ml lysozyme. Cells were ground gently using a rubber scraper and incubated at room temperature for 15 min. After addition of ice-cold water, the cells were incubated on ice for 15 min with gentle agitation. The periplasmic fraction was recovered in supernatant fluid after centrifugation (12000 g, 4^{o} C, 20 min) and filter-sterilized through 0.2 μm syringe filters. PpcA was separated from other periplasmic proteins in the supernatant fluid by cation exchange chromatography using a SP Sepharose® fast flow column (GE health care) equilibrated with 20 mM Tris-HCl pH 8.5 and eluted with a step salt gradient with 20 mM Tris-HCl, pH 8.5, 1 M NaCl at flow rate of 2 ml/min. Excess salt was removed from the sample using gel filtration column. Final purification was done using the same cation exchange column but eluting the protein with a 0-300 mM NaCl salt gradient in 10 mM Tris HCl, pH 8.5. Five ml fractions eluted from the column were collected, and their protein and heme content was monitored spectrophotometrically as UV absorbance at 210 nm (peptide bonds) and 408nm (heme). Those fractions having ratio of A_{408}/A_{210} close to 1 were pooled together, and their protein composition was analyzed by sodium dodecyl sulfate polyacrylamide gel electrophoresis (SDS-PAGE) using 4-15 % Biorad Tris Glycine precast gel and Coomassie blue staining. The redox activity of the purified PpcA protein was confirmed by dithionite-reduced minus air-oxidized difference spectra (420-700 nm), with the peak at 530 nm corresponding to the oxidized heme and peak maxima at 522 and 552 nm corresponding to the reduced hemes. (86)

2.2.3 Immobilization of PpcA on biomimetic interfaces

Recombinant PpcA was immobilized onto a SAM of mixed alkanethiols on a gold electrode as described below. Commercial gold substrates (LG thin films, Santa Clara, CA) were cleaned by dipping in Piranha solution (7 parts sulfuric acid and 3 parts 30% hydrogen peroxide solution) for 30 s and then rinsing with distilled water. For SAM formation, the cleaned substrates were dipped in 5 mM ethanolic solution of 11-mercaptoundecanoic acid and 11-mercapto 1 undecanol in a 1:3 ratio for 24 h, and then rinsed with ethanol and distilled water. PpcA was bound to the SAM via an amide linkage using 50 mM 1-ethyl-3-[3-dimethylaminopropyl]carbodiimide hydrochloride (EDC) and 5 mM *N*-hydroxysuccinimide (NHS) solutions. The electrodes were then washed in 20 mM phosphate buffer to remove unbound protein.

2.2.4 Electrochemical measurements

CV experiments were performed using a three cell electrode setup that included the gold substrate described above as the working electrode, a Ag/AgCl reference electrode and a platinum wire counter electrode. Gold electrodes for rotating disk experiments were purchased from Pine Research Instrumentation Inc., Raleigh, NC. All other electrodes were purchased from Bioanalytical Systems Inc, West Lafayette, IN. Electrochemical measurements were conducted using a CHI660B and CHI660D electrochemical potentiostats (CH instruments Inc, Austin TX). Before CV experiments, all solutions were purged with argon gas for a minimum of 30 min to remove oxygen, and the experiments were performed in an argon atmosphere at 25^{o} C. During the CV experiments, the voltage was alternately swept between 0.2 and -0.8 V (versus Ag/AgCl) at scan rates (scan rates ranging from 20-700 mV/s). The midpoint redox potential of the immobilized PpcA was calculated by averaging the anodic and cathodic peak potentials of CV

scan at low scan rate (10mV/s). The midpoint redox potential of PpcA in solution was measured similarly using 1 mg/ml solution of protein in an argon atmosphere. Unless specified otherwise, all experiments were done in presence of 100 mM NaCl as a supporting electrolyte.

2.2.5 Ellipsometric measurements

Ellipsometric measurements were carried out using M-44 rotating analyzer ellipsometer (J.A. Woollan Co. Inc., Lincoln, NE) running WVASE32 software. The refractive index and the extinction coefficient values were assumed to be 1.5 and 0 for all measurements. For immobilized cytochrome c measurements, the film was modeled as a transparent "Cauchy" layer with *refractive* index of 1.5. A minimum of three measurement were taken for each sample.

2.3 Results and discussion

2.3.1 Production and purification of PpcA

SDS PAGE results of the samples taken during fermentation indicated the cytochrome *c* expression in *E. coli*. The first step of purification with SP sepharose® column captured the cationic charged proteins from the periplasmic fraction (Fig. 2.1A). The protein eluted with a step gradient had very high concentration of salt, which may interfere with binding of protein on ion exchange resin. Buffer exchange of the protein samples using gel filtration column reduced the conductivity below 4 ms/cm (Fig. 2.1B). These pooled protein fractions were further purified by second step of cation exchange chromatography with NaCl gradient. The Purified recombinant PpcA obtained by cation exchange chromatography (Fig. 2.2) had a ratio of A_{210}/A_{408} (peptide bond/heme absorption) near 1, consistent with the incorporation of the protein's three hemes. (85) The protein samples displayed a single protein band in an SDS-PAGE gel that exhibited a relative mass of approximately 9.6 kDa (Fig. 2.2, inset), as reported

for the native PpcA protein. (87) The redox difference spectra of dithionite-reduced versus oxidized recombinant PpcA (Fig. 2.3) showed the three absorption bands at wavelengths of 420, 522, and 552 nm, characteristic of *c*-type cytochromes.

2.3.2 Electrochemistry of PpcA in solution

The electrochemical behavior of PpcA was first investigated with protein in solution. The bare gold working electrode contributed to protein degradation during CV runs. Therefore all the electrochemical characterization were done on SAM modified gold electrode. Also presence of oxygen interfered with PpcA electro analysis. Therefore all the measurements were done under the constant stream of argon with buffers purged by nitrogen or argon. The CV curves for recombinant PpcA in solution at 10 mV/s (Fig. 2.4) displayed defined oxidation and reduction peaks that gave a mid-point potential of -375 mV vs. a Ag/AgCl electrode. This value matches closely the midpoint potential of -374.5 mV versus Ag/AgCl (-169.5 mV versus a standard hydrogen electrode) estimated for the native PpcA by cyclic voltammetry at the same scan rate. (88) The peak separation was about 130 mV at scan rate of 100 mV/s and increased with increasing scan rates consistent with quasireversible redox species. The relationship between peak currents and scan rate is give by Randles-Sevcik equation. (84)

$$i_p = 2.69 * 10^5 * n^{3/2} * A * D^{1/2} * C * v^{1/2} \quad \text{.....Eq.(2.1)}$$

where, i_p is the peak current, n is the number of electrons transferred, A is the area of the electrode, D is the diffusion coefficient, C is the bulk concentration of the analyte and ν is the scan rate. The relationship between i_p and square root of ν was linear for alkane terminated

SAM indicating diffusion controlled reaction. This relationship was linear for SAM coated gold electrode, indicating diffusion limited current of PpcA at electrode (Fig. 2.5).

2.3.3 Immobilization of PpcA and its electrochemistry

Ellipsometric measurements revealed the monolayers have thickness of 15 A^{o}, which is consistent the literature reported height for a 11 carbon chain link with a slight tilt. (89) Thickness of the SAM after cytochrome *c* deposition was about 30 A^{o}, indicating cytochrome *c* adsorption in a monolayer.

The midpoint potential obtained from CV of immobilized PpcA at a scan rate of 10 mV/s (data not shown) was -372 mV against Ag/AgCl, which is virtually identical to that obtained for PpcA in solution and the native PpcA. (88) Hence, the biomimetic interface with immobilized PpcA is well suited to investigate the electrochemical activity of PpcA under biologically relevant conditions. The CV curves for PpcA immobilized on SAM-functionalized gold collected at increasing scan rates from 25 to 700 mV/s (Fig. 2.6) displayed distinct cathodic and anodic peaks, indicating that the protein was being reversibly oxidized and reduced, respectively. Plotting cathodic peak height for the SAM-immobilized PpcA vs. scan rate (Fig. 2.6, inset) gave a linear correlation (R^2 =0.997), consistent with a surface-controlled electrochemical reaction. (90)

The Laviron equation expresses the relationship between peak current I_p, scan rate ν and surface coverage τ:

$$I_p = \frac{n^2F^2A\tau\nu}{4RT} \quad \text{.....Eq.(2.2)}$$

where A is area of electrode, n is number of electrons transported, F is Faraday's constant, R is the universal gas constant and T is absolute temperature.

Also,

$$I_p = \frac{nFQv}{4RT} \quad \text{.....Eq.(2.3)}$$

From the area under the peak for a voltammogram, we calculated the charge Q. And from this relationship, we calculated value of n to be 1. From the area under the CV cathodic peak, we calculated PpcA surface coverage values (τ) of 20 to 50 pmol/cm^2, which are 2-5 times greater than the values reported for other immobilized *c*-cytochromes, such as horse heart *c*-cytochrome and cytochrome *c* 552. (81, 91, 92) This large difference in τ (20 to 50 vs. ~10 pmol/cm^2) is surprising given the similar size of the cytochromes (e.g., 9.6 kDa for PpcA vs 12 kDa for horse heart cytochrome) and the same alkane thiols (MUA and MU) being used to make the SAM for both PpcA and horse heart cytochrome *c*. (27) The difference is likely due to variations of the immobilization methods, suggesting that the immobilization strategy may need to be optimized for each cytochrome to be tested under biologically relevant conditions.

Laviron analysis was used to determine the apparent electron transfer rate constant k_s for PpcA immobilized on a gold electrode. Laviron's calculations for the variation of parameter m^{-1} (m = (RT/F)*(k/nν)) with peak potential separation (ΔE_p) were fitted to a third order polynomial, which was then used to determine the values of m^{-1} at different sweep rates from the experimental ΔE_p results.

$$\Delta E_{p,a} = \frac{RT}{(1-\alpha)nF} ln\left[\frac{(1-\alpha)}{m}\right] \quad \text{.....Eq. (2.4)}$$

$$\therefore \Delta E_{p,a} = \frac{RT}{(1-\alpha)nF} ln(1-\alpha) + \frac{RT}{(1-\alpha)nF} ln(m^{-1}) \text{.....Eq. (2.5)}$$

Where, α is a transfer coefficient. Plot of experimental Δ E_{pa} vs ln(m^{-1}) and Δ E_{pc} vs. ln (m^{-1}) can be used to calculate the k_s values (Fig. 2.7).

$$\Delta E_{p,a} = \frac{RT}{(1-\alpha)nF} ln\left[\frac{(1-\alpha)nF}{RT} \frac{\vartheta}{k^o}\right] \quad \text{.....Eq. (2.6)}$$

where, $m = \frac{RTk^o}{nF\vartheta}$ .....Eq. (2.7)

Similarly,

$$\Delta E_{p,c} = -\frac{RT}{\alpha nF} ln\left[\frac{\alpha nF}{RT} \frac{\vartheta}{k^o}\right] \text{.....Eq. (2.8)}$$

Fitting the equations 2.6 and 2.8, the k_s for reaction was found to be 0.05 s^{-1}. These results indicate relatively rapid ET between immobilized PpcA and the electrode.

In summary, we have successfully expressed and purified *Geobacter* periplasmic cytochrome *c* PpcA in *E. coli*. The heterologously expressed PpcA is electroactive and have redox properties similar to the native *Geobacter* cytochrome. The PpcA protein is capable of direct electron transfer with electrode. Furthermore, we have successfully immobilized the PpcA protein on SAM covered gold electrode and studied the redox properties of the immobilized protein. This work is an important step in developing biomimetic redox active cell envelope or

BRACE interface on the electrode, where we need the protein to be able to interact with the electrode in a controlled fashion.

3.0 ELECTROCHEMICAL CHARACTERIZATION OF *GEOBACTER SULFURREDUCENS* PPCA *C*-CYTOCHROME USING BIOMIMETIC INTERFACES REVEALS GREATER REDUCTION RATES OF URANIUM THAN IRON

3.1 Abstract

The reductive precipitation of uranium by *Geobacter* bacteria shows promise for the *in situ* bioremediation of contaminated sites. However, genetic approaches to identify the redox components involved in the reaction are often limited by compensatory effects of the mutations, which often lead to adapted phenotypes. To bypass this limitation we developed nanostructured biomimetic interfaces that mimic the cell envelope of *Geobacter* cells and permit the interrogation of specific redox components. We used this approach to investigate the electrochemical role of the most abundant periplasmic *Geobacter c*-cytochrome, PpcA, in uranium reduction. The studies revealed a much greater rate constant of PpcA for the reduction of uranium than for iron electron acceptors, providing a plausible explanation for the rapid reduction and precipitation of uranium, and loss of cell viability, observed when the radionuclide permeates into the periplasm. As a result, *Geobacter* cells have evolved mechanisms for the extracellular reduction of uranium to prevent it from traversing the outer membrane. The studies highlight the value of biomimetic interfaces to interrogate individual redox components of the *Geobacter* cell envelope and gain novel insights into their biological role, and also show promise for the development of sensors and deployable devices for uranium bioremediation.

3.2 Introduction

Uranium (U) is naturally present at low levels in many terrestrial environments and can reach higher concentrations in seawater and U-rich ores. (93) Its anthropogenic use in nuclear research, fuel production, coal combustion, phosphate fertilizers, and weapons manufacturing has also

resulted in the accumulation of toxic levels of the radionuclide in many soils and groundwater. (94) In these environments, U is easily oxidized into the water-soluble and highly mobile uranyl cation (UO_2^{+2}), which facilitates its dispersal. This results in vast volumes of groundwater contaminated with U in complex mixtures with other radionuclides and toxic metals, making environmental remediation via standard excavation-and-removal or pump-and-treat approaches impractical. (95)

Despite its toxicity even at trace concentrations, (96) some microorganisms inhabit environments with naturally high U content and contribute to its cycling. (97) Among these microorganisms are dissimilatory metal reducing bacteria in the family *Geobacteraceae*, which can gain energy for growth by transferring respiratory electrons to the uranyl cation. (98, 99) The biological reduction of the hexavalent U (U[VI]) in the uranyl cation by these organisms generates sparingly soluble phases of tetravalent U (U[IV]), (99-101) thereby reducing the mobility and bioavailability of the contaminant. Furthermore, the reductive precipitation of U by these microorganisms can also be stimulated *in situ* with field-scale additions of selected electron donors such as acetate, (102, 103) thus slowing the migration of the contaminant and mitigating health risks associated with U exposure. Studies with the model representative *Geobacter sulfurreducens* show that the reduction of U by these organisms is extracellular and dependent on the expression of conductive protein filaments or pili and outer membrane *c*-cytochromes. (100) The contribution of outer membrane *c*-cytochromes is likely small, because protease treatment to remove proteins exposed on the outer membrane does not affect U reduction. (60) Furthermore, the extent of U reduction correlates linearly with the piliation levels (100) but not with the outer membrane *c*-cytochrome content. (104)

Some U can also traverse the outer membrane of *Geobacter* cells, especially if non-piliated. (100, 104) Once inside the periplasmic space, U is rapidly reduced to a mononuclear U(IV) phase bound to carbon ligands consistent with the involvement of periplasmic proteins. (100) As the degree of periplasmic precipitation increases, the cellular respiratory activities decline rapidly and the cell's viability is severely compromised. (100) The periplasm of *Geobacter* cells contains abundant small *c*-cytochromes, which could catalyze this reduction and influence the cells' ability to remain viable during exposure to U. One such periplasmic protein is PpcA, (88) a triheme *c*-cytochrome that is conserved in all the sequenced *Geobacteraceae* genomes. (56, 105) PpcA has been proposed to function as a periplasmic electron carrier during acetate oxidation (88) and to contribute to the H^+ electrochemical potential gradient through a coupled e^-/H^+ transfer mechanism. (106) However, the role of PpcA in U reduction remains controversial. Resting cell suspensions of a PpcA-deficient mutant were originally reported to be impaired in the acetate-dependent reduction of U(VI) but were not affected when hydrogen served as the electron donor. (88) However, later studies failed to replicate the acetate-dependent mutant phenotype. (107) Such contrasting results could have been the result of compensatory effects of the mutation, as reported for other *c*-cytochromes in *Geobacter*. (108, 109)

To bypass these limitations, we studied the catalytic activities of PpcA in a controlled *in vitro* environment using electrochemical interfaces structured to mimic the native cell envelope. Cyclic voltammetry was used to investigate the electron transfer (ET) kinetics of PpcA to Fe(III) and U(VI), provided as soluble complexes with various ligands. The studies revealed much higher rate constants for U(VI) than for Fe(III) independently of the ligand, consistent with a much higher affinity for U than for the natural electron acceptor Fe. The results provide novel insights into the role of PpcA in U reduction that are relevant for the *in situ* U bioremediation.

3.3 Materials and Methods

3.3.1 Recombinant PpcA expression and purification.

PpcA was heterologously expressed in *Escherichia coli* strain BL21 DE3, as reported in chapter 2.

3.3.2 Biomimetic interfaces with PpcA.

The conceptual design for the biomimetic interfaces constructed and interrogated in this work includes a gold electrode, a self-assembled monolayer of alkanethiols (SAM), a PpcA monolayer, and, when indicated, an external synthetic lipid bilayer. The conceptual design is shown in the Figure 3.1, where the SAM and PpcA layers serve as mimics of the inner membrane (IM) and periplasm space (PS), respectively, and the external, synthetic lipid bilayer, as the outer membrane (OM) analogue. PpcA was immobilized onto SAM coated gold electrode as described in chapter 2. When indicated, a synthetic lipid bilayer was deposited by incubating the PpcA-containing SAM interface with a 0.25 mM solution of 1,2-dioleoyl-s*n*-glycero-3-phosphocholine (DOPC) liposomes in 50 mM HEPES buffer. The resulting interface, designated DOPC interface, mimicked the cell envelope of *G. sulfurreducens*, with its PpcA-containing periplasmic space sealed by an outer membrane.

3.3.3 Electrochemical measurements.

Cyclic voltammetry (CV) experiments were performed using a three-electrode setup consisting of the PpcA-functionalized gold substrate described above as the working electrode, a Ag/AgCl reference electrode, and a platinum wire counter electrode. All the electrodes were purchased from Bioanalytical Systems Inc (West Lafayette, IN), except for rotating disk electrodes (RDE), which were purchased from Pine Research Instrumentation Inc. (Raleigh,

NC). Prior to SAM deposition, the RDE were polished with alumina slurries (1, 0.3, and 0.05 micron grade) on polishing pads. Electrochemical measurements were conducted using a CHI660B electrochemical potentiostat (CH instruments Inc, Austin TX) and, for RDE experiments, a modulated speed disk electrode rotator (Pine Research Instrumentation Inc., Raleigh, NC). Prior to CV, all solutions were purged with argon gas for a minimum of 30 min to remove oxygen, and the experiments were performed in an argon atmosphere at 25^{o}C. During the CV experiments, the voltage was alternately swept between 0.2 and -0.8 V (versus Ag/AgCl) at scan rates (ν) ranging from 25-700 mV/s. Unless specified otherwise, the supporting electrolyte in all the experiments was 100 mM NaCl. When indicated, CV of the PpcA or DOPC interfaces was performed in the presence of various concentrations of the following soluble, chelated forms of iron (Fe) and uranium (U): ferric nitrilotriacetate (Fe-NTA), ferric citrate (Fe-citrate), ferric nitrate (Fe-nitrate), uranyl acetate (U-acetate), and uranyl nitrate (U-nitrate).

Rotating Disc Electrode Voltammetry (RDE):

The second order rate constant k_o' values were also validated using the RDE technique, which allows the interface mass transfer limitations to be controlled. The PpcA interface was constructed in the same way as described for the static cyclic voltammetry studies but using a circular (5-mm diameter) gold electrode (Pine Research Instruments) and attached to the rotating shaft of the RDE apparatus. The stability of the PpcA interface was first investigated using variable speeds to determine the maximum rotation speed (2500 rpm) it withstood. Then, Fe species were added at various concentrations to collect the voltammograms. Fig. 3.5 shows a representative rotating disc voltammogram for Fe-NTA. For all the RDE experiments, the potential of the working electrode was maintained at -500 mV against Ag/AgCl. The steady state

current (i_{ss}) was measured for a range of rotation speeds (ω) and the inverse of the steady state current values ($1/i_{ss}$) were plotted against $\omega^{-1/2}$. Fig. 3.6A shows the Fe-NTA plot, as an example. The limiting current i_{lim} was inferred from the Y axis intercept value of the regression line for each electron acceptor concentration. This value was plotted against the electron acceptor concentration to generate a regression line whose slope corresponds to the second order rate constant k_o'. The i_{lim} values follow a linear correlation with the concentration of the electron acceptors. Fig. 3.6B shows the linear plot for Fe NTA, as an example. The linearity of the correlation can be used to calculate the k_o'values as previously described (110) using the equation:

$$i_{lim} = nFAC\tau k_o' \quad \text{.....(Eq. 3.1)}$$

where *n* is the number of electrons transferred, *F* is Faraday's constant, *A* is the area of electrode, *C* is the concentrations of the electron acceptor, and τ is the PpcA surface coverage.

Calculation of rate constants:

The reduction of a soluble electron acceptor by PpcA immobilized on the SAM-functionalized gold electrode is a two-step reaction that first involves reduction of PpcA by the electrode and then the reduction of the electron acceptor by PpcA, as exemplified in the following reactions:

$$PpcA_O + e^- \leftrightarrows PpcA_R \qquad \text{(PpcA reduction by gold electrode)}$$

$$PpcA_R + M_O \xrightarrow{k_o'} PpcA_O + M_R \qquad \text{(PpcA oxidation by electron acceptor)}$$

where $PpcA_O$ and $PpcA_R$ are the oxidized and reduced forms of PpcA, respectively, and M_O and M_R are the oxidized and reduced forms of the soluble electron acceptor, respectively. The second order rate constant for reduction of M_O by $PpcA_R$ is k_o'.

To calculate k_o', we performed CV on PpcA immobilized on SAM-functionalized gold electrodes at scan rates of 25-750 mV/s in the presence or absence of the soluble electron acceptors, provided at various concentrations, as indicated for each experiment. The CV curves were normalized by subtraction of the background current recorded with phosphate buffer on SAM coated electrode in potential sweep voltammetry. (111) The peak current values (i_p) were measured for the PpcA interface in the absence of electron acceptors and peak potential values (E_p) were noted. The catalytic current values (i_k) were measured at the E_p in the presence of the soluble electron acceptors. From the ratio of i_p to i_k, we determined the kinetic parameter φ using the working relationship given by Nicholson and Shain for catalytic reactions. (90) The φ values obtained for each of the catalytic reactions involving a particular electron acceptor were plotted versus the reverse of the scan rate (1/υ). The slope of the linear regression line, designated K^o, was used to calculate the K_f^o constant using Eq. 1:

$$K_f^o = K^o \, {nF}/{RT} \quad \text{.....(Eq. 3.2)}$$

where n is the number of electrons transferred, F is Faraday's constant, R is the universal gas constant, and T is the absolute temperature. The K_f^o value obtained from Eq. 1 was plotted

against the electron acceptor concentration and the slope of the regression line corresponded to k_o'. We measured the second order rate constant in triplicate independent experiments for each electron acceptor. In addition, second order rate constants for Fe species were also measured by rotating disc voltammetry. Pairwise comparisons between the electron acceptor rate constants were statistically analyzed using the *t*-test function of the Microsoft® Excel® software. Statistically significant data sets ($p < 0.05$ or < 0.005) were indicated with one or two star symbols, respectively.

3.4 Results and Discussion

3.4.1 Catalytic activity of PpcA with iron and uranium salts.

The reduction of soluble Fe and U species by PpcA was investigated in the PpcA biomimetic interfaces (Fig. 3.2). Control experiments performed with the PpcA interface in the absence of soluble metal species resulted in Nernstian CV curves with well-defined, reversible peaks, indicating that PpcA was engaging in one-step redox reactions with the gold electrode. Addition of Fe-NTA (Fig. 3.2A) or U-acetate (Fig. 3.2B) to the PpcA interface increased the cathodic current, but no anodic peaks were detected, as expected of an irreversible reductive reaction. The addition of the soluble electron acceptors also resulted in sigmoidal CV curves typical of two-step electron transfer reactions, (90) which in this case involved the electron transfer from the electrode to PpcA and then from PpcA to the electron acceptor. Furthermore, the cathodic current of the PpcA interface increased with increasing electron acceptor concentration. By contrast, control interfaces of SAM-functionalized gold electrodes without PpcA lacked faradic current even when in the presence Fe-NTA or U-acetate (Fig. 3.2A and 3.2 B, respectively). Hence, the SAM layer effectively blocked access of the soluble electron

acceptors to the underlying gold electrode, and any cathodic current detected by CV was due to electron transfer via PpcA.

In the native environment, PpcA is trapped in the periplasmic space between the inner and outer lipid membranes. We mimicked this architecture by depositing 1,2-dioleoyl-*sn*-glycero-3-phosphocholine (DOPC) liposomes on the PpcA biomimetic interface and form a lipid bilayer (112, 113) that completely covered the interface. The addition of the DOPC lipid bilayer prevented the increases in the PpcA catalytic current observed in the presence of Fe-NTA or U-acetate, and the CV curves only exhibited the peaks corresponding to the transfer of electrons between the gold electrode and the PpcA (Fig. 3.2, insets). Hence, the synthetic lipid bilayer prevented the permeation of the soluble metal species inside the periplasmic mimic and thereby blocked their access to PpcA. These results are particularly significant to understand how metals transverse the outer membrane and are reduced in the periplasm of *Geobacter* cells. Our results suggest, for example, that the outer membrane functions as a mechanical barrier for metal ions, effectively preventing them from reaching the periplasmic space. However, in the biological setting, the outer membrane contains porins and transporters, which facilitate the diffusion and/or transport of soluble species and allow metals and metal chelators into the periplasm. One of the most abundant proteins in the *G. sulfurreducens* outer membrane is, for example, a putative porin that is required for the reduction of soluble, chelated forms of Fe^{3+}. (114) This porin may allow soluble metal species to enter the periplasm, where they can be reduced by periplasmic *c*-cytochromes such as PpcA.

3.4.2 PpcA exhibits high second order rate constants (k_o') for the reduction of U.

The electrochemical studies of PpcA reduction in the biomimetic interfaces allowed us to calculate the second order rate constant (k_o') for the reduction of various Fe and U electron acceptors. The calculations used the Nicholson and Shain model, (90) which is based on the following assumptions (115, 116) : (i) the reaction of PpcA with the electrode is a fast, reversible, one-electron transfer reaction (as we validated experimentally); (ii) the reaction between PpcA and the soluble electron acceptor follows pseudo first order kinetics and is irreversible (which we showed under the experimental conditions, Fig. 3. 2); (iii) no adsorption of products or reactants occurs; and (iv) the diffusion coefficients of all species are the same. From the CV curves recorded at various scan rates for the PpcA interface alone or in the presence of different electron acceptor concentrations (Fe-NTA, Fe-citrate, Fe-nitrate, U-acetate, and U-nitrate), we calculated the ratio of i_k to i_p, and then the kinetic parameter φ. (90) This kinetic parameter relates the ratio of i_k to i_p with the reaction rates as described in the case of catalytic reaction with reversible charge transfer. (90)

Provided all the assumptions of the Nicholson and Shain model are approximately met, the φ versus 1/ υ (reverse of scan rate) plot is expected to yield a straight line. We did obtain linear correlations for all the electron acceptors but only at scan rates of 300 mV/s or higher. For example, the correlation between φ and 1/ υ was linear for Fe-NTA concentrations above 800 μM (Fig. 3.3A). This suggests that some of the model's assumptions are not met at the lowest scan rates. The Nicholson and Shain model was developed for soluble species under the assumption that all reactants and products had the same diffusion coefficient. (90) In our system, where PpcA is immobilized on the SAM-functionalized electrode, this assumption is only valid

at higher scan rates, at which the reactant concentration profiles at the surface is only partially developed, and the observed rate depends solely on the reaction kinetics. However, at lower scan rates, the electrochemical measurements are influenced by not only reaction kinetics but also by the diffusion of the reactant to the surface.

From the slope of the regression line within the linear region of the φ versus 1/ υ, we calculated the K^o parameter and used Eq. 3.2, described in the Materials and Methods section, to calculate the K_f^o constant. From the linearity of the plot of K_f^o versus the concentration of the electron acceptor, we calculated the second order rate constant k_o' for the reduction of various Fe and U chemical species by PpcA (Table 3.1). Fig. 3.3 B shows, as an example, the plot used to estimate the second order rate constant k_o' for Fe-NTA. Pairwise comparisons between Fe-NTA and the other Fe species (Fe-citrate and Fe-nitrate) revealed significant variations in the rates of reduction (Fe-nitrate > Fe-NTA > Fe-citrate) (Fig. 3.4). Similar results were obtained by rotating disc electrode voltammetry (Table 3.1), suggesting that the differences in the rates of reduction were not an artifact of the electrochemical measurements. Rather, the chemical ligand of Fe influenced the rates of reduction. This result is in agreement with kinetic studies of *c*-cytochromes from the metal-reducing bacterium *Shewanella oneidensis*, which also reduce Fe(III) species at rates that are influenced by the type of ligand complexed to the metal. (117) The charge and molecular size of the ligand affects the kinetics of binding to the cytochrome and also the position and distance between metal electron acceptor and the heme Fe of the protein. This, in turn, influences the rates of electron transfer.

Interestingly, the k_o' values for the reduction of the U species (U-acetate and U-nitrate) were significantly higher than for the Fe species (Fig. 3.4). On average, the rates of reduction of Fe species were 0.06 (± 0.04), whereas those for U species were more than 10 times greater (0.79 ± 0.01). Such differences cannot be attributed to the type of ligand because the reduction rates of U-nitrate were, for example, 8-fold greater than for Fe-nitrate (p = 0.003), although the two electron acceptors have the same ligand. Hence, the faster kinetics of the reduction of U electron acceptors by PpcA is likely the consequence of increased thermodynamic driving force for U reduction over Fe and/or differences in protein-metal interactions.

3.4.3 Specific interactions between U and PpcA promote reduction rates.

The parameters that influence the rate constant (k_{et}) for electron transfer between donor and acceptor can be interpreted using semiclassical theory, (118-120) as shown in Eq. 3.3:

$$k_{et} = \sqrt{\frac{4\pi^3}{h^2 \lambda k_B T}}\, H_{AB}^2\, exp\left\{-\frac{(\Delta G^0 + \lambda)^2}{4\lambda k_B T}\right\} \quad \text{(Eq. 3.3)}$$

where k_B is Boltzmann's constant, h is Plank's constant, ΔG^0 is the free energy of the reaction, H_{AB} is the electronic coupling matrix element, and λ is the nuclear reorganization energy.

The rates of redox reactions involving metals are often proportional to the thermodynamic driving force, ΔG^0, (121) which is dependent on the reduction potentials of the oxidized/reduced metal pair and, to a lesser extent, on the type ligand complexation through the reaction's electrochemical potential difference (ΔE^o). (117) To investigate a similar influence in

the PpcA-mediated reactions we used Eq. 3.4 to calculate ΔG^0 for the various U and Fe electron acceptors tested.

$$\Delta G^o = -nF(\Delta E^o) \quad \text{.....(Eq. 3.4)}$$

To minimize the ligand's contribution, we focused on the reduction of the U-nitrate and Fe-nitrate, which share the same ligand (nitrate). The standard redox potential (E°) of the half reaction of UO_2^{2+}, as shown below, results in a free energy value of -87 kJ/mol.

$$UO_2^{2+} + 2e^- + 4H^+ \rightarrow U^{4+} + 2H_2O, \qquad E^0 = 280\, mV\ vs.SHE$$

For the half reaction of Fe^{3+}, shown below, we calculated a free energy of -91 kJ/mol.

$$Fe^{3+} + e^- \rightarrow Fe^{2+}, \qquad E^0 = 771\, mV\ vs.SHE$$

The free energy of the two reactions is remarkably similar, failing to explain the greater rates of U-nitrate reduction by PpcA compared to Fe nitrate determined experimentally (Fig. 3.4).

With similar ΔG^0 values for Fe and U acceptors, only larger donor-acceptor electronic couplings, $H_{AB,}$ and/or lower reorganization energies, λ, can explain the greater reaction rates of the PpcA-U pair compared to PpcA-Fe. Both of these variables are intimately connected with the type of coordination between PpcA and the metal acceptor. Prior to electron transfer, the metal forms a precursor complex, which positions the metal in a fashion that influences the rates of electron transfer. The H_{AB} variable indicates the probability of electron transfer in this metal-protein precursor complex upon thermal activation. (122) Cytochromes can have many sites for

binding the metal electron acceptor, thus forming several precursor complexes in which the donor-acceptor distance and bridge varies. (123) The electronic coupling matrix element and the rates of electron transfer decrease, for example, exponentially with donor-acceptor distance. Hence, greater rates of U reduction could result from PpcA coordinations that reduce the distance between the U acceptor and the electron-donating heme group in the cytochrome. The type of PpcA coordination around the metal acceptor can also have substantial effects on λ, which is the energy required to distort the nuclear configuration of the reactants into the equilibrium configuration of the products prior to electron transfer. The stoichiometry, size, charge, and structural properties of the reacting protein donor and metal acceptor have a profound effect on both the external (outer sphere, λ_o) and internal (inner sphere, λ_i) reorganization energy required to reach the equilibrium configuration of the products. (124) The outer sphere relates to the surrounding medium and refers to changes in the protein matrix and the energy required to rearrange the solvent environment. On the other hand, the inner sphere is influenced by the solvent sheath and the type of ligands involved in creating a geometrically favorable arrangement between the metal and the electron-donating heme group in PpcA prior to electron transfer; hence, it is influenced by redox-dependent nuclear perturbations of redox centers, such as changes in bond angles and lengths.

Extended X-ray Absorption Fine Structure (EXAFS) analyses of the uranyl coordination in wild-type cells of *G. sulfurreducens* with a predominantly periplasmic precipitation (e.g., those not expressing conductive pili) shows U coordinated with carbon-containing ligands. (100) The EXAFS model is consistent with a U atomic environment involving bidentate and monodentate carbon-containing ligands. Bidentate carbon ligands have been reported for other iron-binding proteins such as apotransferrin, which uses the carboxyl coordinations of acidic

amino acids as metal ligands. (125) The uranyl cation also binds to apotransferrin at its iron-binding sites, using some of the amino acids of the Fe coordination sphere as well as specific amino acid ligands. (126) Interestingly, the binding of the uranyl cation to apotransferrin induces conformational changes such that the period of conformation stabilization is reduced compared to Fe. (126) Similar effects could allow PpcA to position the uranyl cation more rapidly than iron in an optimal configuration for electron transfer, thereby increasing the rates of electron transfer to U acceptors over Fe.

3.5 Implications

The rates of electron transfer between cytochromes and metal acceptors reflect the contribution of three rate constants, each corresponding to reactions occurring before, during, and after the transfer of electrons from the protein to the metal, as follows:

$$\mathrm{Cyt} + \mathrm{M} \overset{k1}{\Leftrightarrow} [\mathrm{Cyt\ M}]$$

$$[\mathrm{Cyt\ M}] \overset{ket}{\Leftrightarrow} [\mathrm{Cyt^{+} + M^{-}}]$$

$$[\mathrm{Cyt^{+} + M^{-}}] \overset{kd}{\Leftrightarrow} \mathrm{Cyt^{+} + M^{-}}$$

The first step involves the diffusion of the metal species (M) to the cytochrome (Cyt) and their association to form a precursor complex [CytM] (rate constant k_1). The second step is the transfer of electrons from the Cyt to the M and formation of the reactant complex [$Cyt^+ + M^-$] (rate constant k_{et}). The final step is the dissociation of the [$Cyt^+ + M^-$] complex to generate the products Cyt^+ and M^-, which diffuse apart in the solution (rate constant k_d). Calculation the

overall reaction rate constant, k_{obs}, experimentally and/or by deconvolution of k_{et} from other rate constants is challenging. (86) However, the biomimetic interfaces used in this study provide a well-characterized and reproducible experimental tool to study redox catalyses involving cytochromes despite the inherent complexity of the stepwise reaction. A major advantage of biomimetic interfaces over the natural, biological system is that the former allows virtually all variables (cytochrome content, lipid content, etc.) to be precisely known and controlled to test hypotheses about how each variable influences k_{obs}. The electron transfer rates measured for PpcA under identical conditions but using different metal species revealed, for example, a higher rate constant for U(VI) reduction than for Fe(III) reduction by PpcA. This finding helps explain why U is rapidly reduced in the periplasm of *G. sulfurreducens* once it transverses the outer membrane. (2, 41, 127) The reduction of U(VI) to U(IV) precipitates the radionuclide as a mineral in the periplasmic space, compromising the structural integrity and essential functions of the cell envelope and eventually killing the bacteria. (100) Not surprisingly, *Geobacter* cells have evolved mechanisms to reduce the uranium extracellularly and, in doing so, preserving the cell envelope's essential functions.

Another advantage of biomimetic interfaces is that additional redox components of the *Geobacter* respiratory machinery could be added to extend the kinetic and thermodynamic studies and provide additional insights into bacterial mechanisms for U reduction. This approach could lead to new or improved schemes for the *in situ* remediation of U and other metal contaminants. The higher reaction rate constant for PpcA-mediated reduction of U than of Fe, independently of its complexation with ligands, also shows promise for the developing PpcA-based electrochemical devices for the specific detection of U, providing a valuable tool for the *in*

situ monitoring of U levels in sites undergoing environmental restoration or for long-term stewardship of contaminated sites.

4.0 HETEROLOGOUS EXPRESSION OF OMCB IN *E. COLI* AND ITS LOCALIZATION TO BACTERIAL MEMBRANE

4.1 Abstract

Outer membrane cytochromes play a key role in metal-respiring bacteria like *Geobacter* and *Shewanella* spp. The outer membrane cytochrome OmcB of *Geobacter sulfurreducens* is potentially important protein in *Geobacter*, although it's primary function in electron transport chain remains ambiguous. Very little information is available about the structure and activity of this protein, in part due to difficulty in isolating active OmcB from *Geobacter* membranes and the lack of heterologous expression systems for OmcB. In this paper, we report heterologous expression of OmcB in *E. coli*. Subcellular fractionation localized the protein in *E. coli* outer membrane, and whole cell spectroscopy confirms redox activity of the heterologously expressed OmcB.

4.2 Introduction

Dissimilatory metal reducing microorganisms generating energy in form of ATP through a respiratory process that transfers electrons obtained from intracellular electron donors (commonly organic acids, such as acetate) to extracellular electron acceptors (commonly metal oxides, such as Fe_2O_3). The electrons are shuttled through an electron-transport chain that includes both soluble and membrane-bound cytochromes. (6, 128, 129) Metal-reducing microorganisms have utility in bioremediation (2, 130) and microbial fuel cells. (131-133) Members of the genus *Geobacter* have been extensively studied because of their exceptional electrogenic capacity. Proteins involved in *Geobacter's* electron transport chain are being isolated and characterized to elucidate the metal-reduction mechanisms. The *Geobacter* cells contain multiple outer-membrane *c* type cytochromes that are believed to participate in

extracellular electron transfer (ET), either directly or indirectly. (34) Although a large number of these cytochromes have been identified and implicated in their role in extracellular ET, very few of them been studied in detail. To date, OmcZ (134) and OmcS (20) are the only *Geobacter* outer membrane cytochromes that have been purified and studied in isolation. The lack of high yield system for expressing these proteins is one of the underlying factors. OmcB is a multiheme (12 heme-binding domains) protein partially embedded in *Geobacter* outer membranes. (27) Unlike other *c*-type cytochromes that are loosely bound to the outer membrane, OmcB is very tightly associated with the outer membrane and is only partially exposed. (135) *Geobacter* cells with OmcB deleted were unable to reduce soluble as well as insoluble Fe(III) (27), which may indicate OmcB's importance in iron reduction. However, *Geobacter* cells with OmcB deletion mutation, adapted to grow over time (39), suggesting a compensatory mechanism, in which *Geobacter* upregulates production of other membrane *c* type cytochromes like OmcS and OmcT. (39, 136) Such pleiotropic compensation may explain the ability of *Geobacter* with OmcB deletion to reduce uranium (15) as well as to produce electricity (137) Pleiotropic effects also complicate genetic approaches to identify key electron carriers in *Geobacter's* native uranium reductase machinery. For example, deletion of OmcF gene also led to reduced expression of OmcB protein, and resultant cells showed impaired growth on Fe (III) citrate. (37) Absence of OmcG and OmcH, did not affect the transcript levels of OmcB; however, expression of OmcB was affected negatively in those strains. (38) Deletion of OmcB led to reduced growth of the cells, but cells eventually recovered with increased expression of other outer membrane cytochromes like OmcS and OmcT. (39) These pleiotropic effects can be bypassed through the study of isolated protein(s) of interest using a biomimetic approach, in which only the protein(s) of interest are assembled into an *in vitro* interface designed to mimic portions of the *Geobacter*

electron transport chain. Toward that end, heterologous expression of OmcB in *E. coli* could enable large amounts of the protein to be produced for study. Moreover, because *E. coli* does not produce any outer membrane cytochromes, heterologous expression of an outer membrane cytochrome would enable the protein's activity to characterized while the protein was embedded in the outer membrane without interference by other cytochromes. This capability is particularly valuable for outer membrane cytochromes like OmcB that are difficult to isolate and purify in an active state. Here we report for the first time recombinant expression of OmcB cytochrome in *E. coli*, confirmation of its identity and evidence of its localization to outer membrane of bacteria.

4.3 Methods

4.3.1 Sequence data

To express C-terminal His_6-tagged OmcB in *E. coli*, the signal peptide of *G. sulfurreducens* OmcB was replaced with that of *E. coli* OmpA. The primers OmpA-OmcB 5' *Nde*I (5'-ACCATATGAAAAAGACAGCTATCGCGATTGCAGTGGCACTGGCTGGTTTCGCTACCGTAGCGCAGGCCTGCGGCTCCGAAAACAAGGA-3', coding sequences of *E. coli* OmpA signal peptide are underlined), and OmcB *Xho*I 3' His fusion (5'-GTAAGTCTCGAGCGGACGGGTCGTGCCGAGGTA-3') were used for PCR to amplify the *omcB* gene. The PCR product was digested with *Nde*I and *Xho*I and cloned into the *Nde*I- *Xho*I site of pET21c vector (Novagen), yielding pET21cOmpAOmcB. Plasmid pET21cOmpAOmcB was used as template to substitute the cysteine residue right after signal peptide to alanine by mutagenesis PCR using two primers OmcB Cys mut 5' (5'-GTAGCGCAGGCCGCCGGCTCCGAAAAC-3', mutated sequences are underlined.) and OmcB Cys mut 3' (5'-GTTTTCGGAGCCGGCGGCCTGCGCTAC-3', mutated sequences are

underlined.), yielding pET21cOmpAOmcB24. The primers OmcB 5' *Nco*I (5'-AATACCATGGGCTCCGAAAACAAGGAGGGGAC-3') and OmcB 3' *Xho*I (5'-ATATCTCGAGCGGACGGGTCGTGCCGAGGTAG-3') were used to clone pET22bOmcB that expresses mature OmcB fused to *E. coli* PelB leader sequence and His_6-tag at the N- and C-terminal, respectively. The integrity of each plasmid was confirmed by sequencing analysis. Primers used for cloning of OmcB are listed in Table 1.

4.3.2 Bacterial strains and plasmids

E. coli strain DH5α (Invitrogen) was used for subcloning and strain BL21 (DE3) (Novagen) was used for heterologous expression of protein with and without His tag. *E. coli* cells (BL 21 DE3) were freshly co-transformed with plasmid PEC 86 containing ccm gene which is responsible for the heme maturation of cytochrome *c* as well as OmcB plasmids. The cells were selected, grown, and maintained into 2X YT media (16 g/L Bacto Tryptone, 10 g/L Yeast extract, 5 g/L NaCl) containing selective antibiotics: chloramphenicol (34 μg/ml) and ampicillin (100 μg/ml). For protein expression a single colony was picked from plate and grown into 50 ml 2X YT media at 30^{o} C overnight. 10 ml of this culture was used to inoculate 1L M9 minimal media supplemented with casamino acids (10 ml of 10% solution), vitamin B1 (100 μL of 0.5%), magnesium sulfate (1 ml of 1 M stock solution), glucose (10 ml of 20% solution) and antibiotics chloramphenicol (34 μg/ml) and ampicillin (100 μg/ml). The culture was incubated at 30^{O} C while shaking at 225 rpm until the optical density (O.D.) reached around 0.8, and the cells were induced with isopropyl-1-thio-b-D-galactopyranoside (0.1 mM), and were supplemented with heme (10 μM final from filter sterilized stock of 5 mM) and δ-aminolevulinic acid (0.3 mM). After induction the shaking was reduced to 190 rpm, and cells were grown for additional 15-18

hr before harvesting. In some experiments the induction step was omitted. The 2X YT and LB media were also used at different temperatures and shaking conditions to optimize growth parameters. Samples from the fermentation media were taken periodically, and, after reading optical density at 600 nm, the samples were centrifuged, and digested by boiling with Laemmli buffer containing 2.1 % SDS (100 μl of buffer per 0.1 O.D. reading).

The hexahistidine (His) affinity tag was added to the c-terminus of protein to aid affinity purification of the protein. The *Nco*I-*Xho*I restriction fragment of OmcB was cloned into vector pET-22b(+), which contains pelB leader sequence to facilitate the transport of OmcB polypeptide into the periplasmic space where further posttranslational processing takes place. (49, 53) The OmpA tag of the pET21cOmpAOmcB also targets proteins to the periplasm. Both of the plasmids are under the control of T7*lac* promoter. The plasmid pEC86 allowed constitutive expression of ccm genes (genes required for cytochrome *c* maturation) under the aerobic conditions.(55)

Expression of OmcB was optimized by adjusting variables including temperature, shaking speed and induction time and concentration of the inducer IPTG. Color of the cell pellet (pink for the cells producing mature cytochrome *c*) and spectroscopic analysis of cells reduction by sodium dithionite served as a preliminary indication of mature cytochrome *c* production. SDS PAGE analysis of the whole cells digested by heating with SDS buffer revealed a band of OmcB at ~80 kD which was absent in the control cells without the OmcB plasmids. From the ratio of the cytochrome *c* peak at 552 nm to the intensity of the band at ~80 KD in SDS PAGE, the optimal fermentation conditions for OmcB expression were evaluated.

4.3.3 Subcellular fractionation

Subcellular fractions were prepared using a procedure modified from the previously described methods. (11, 138-140) Briefly, the protein expression cultures were harvested by centrifugation at 6000 X g at 4^{o} C for 20 min. The harvested cells were washed with 40 ml cell resuspension buffer (50 mM Tris HCl pH 8, 100 mM NaCl, 10 mM $MgCl_2$ and 10 μg/ml DNase). The clarified cell expression media at the end fermentation as well as cell resuspension buffer after cell wash were concentrated using an ultrafilter with molecular weight cutoff of 10 kD, and samples were stored for further analysis. The washed cells were pelleted by centrifugation for 10 min at 6000 X g at 4^{o} C and suspended in 100 mM Tris HCl pH 8 followed by addition of sucrose (75 mM), EDTA (50 mM) and lysozyme (0.1 mg/ml) which leads to spheroplast formation. The spheroplasts were separated by centrifugation at 20000 X g at 4^{o} C for 20 min. The supernatant was stored as a periplasmic fraction. The spheroplasts were suspended in resuspension buffer and lysed by Avestin Emulsiflex C3 high pressure homogenizer by 3 passes at 12000 psi. The unbroken cells were separated by centrifugation at 4000 X g at 4^{o} C for 20 min, and the supernatant was ultracentrifuged at 100000 X g at 4^{o} C for 90 min in a Beckman Ti 45 rotor. The supernatant was stored as a cytoplasmic fraction, and the pellet was stored as a membrane pellet. The membrane pellet was resuspended in cytoplasmic membrane solubilization buffer containing 50 mM Tris HCl, pH 8, 100 mM NaCl and 1 % sarkosyl for 30 min. The membrane suspension was ultracentrifuged at 100000 X g at 4^{o} C for 60 min in Beckman Ti 45 rotor. The supernatant was stored as inner membrane fraction (IM), and the pellet was stored as outer membrane fraction (OM). The OMs were resuspended in a series of detergents in 50 mM Tris HCl, pH 8, 150 mM NaCl, 50 mM EDTA and 0.1 mg/ml

lysozyme. The OMs were suspended in different detergents: 2 % *n*-octylpolyoxyethylene (C8POE), 2% *n*-octyl-β-D-glucoside (OG) or 1% *n*-dodecyl-β-D-maltoside (DDM) and homogenized with a Dounce homogenizer and kept stirring overnight at 4^{o} C. The detergent solubilized OMs were separated by ultracentrifugation at 100000 X g at 4^{o}C for 60 min. Alternatively the cells were lysed by pressure homogenizer without spheroplast preparation. Unbroken cells were removed by centrifugation, and the supernatant was ultracentrifuged for 100000 X g for 4^{o} C for 60 min to separate the whole cell envelope. The whole cell envelope was suspended in cell resuspension buffer with DNase, and the suspension was carefully layered over discontinuous gradient made of 75%, 70%, 60%, 50% and 37% sucrose solution in HEPES buffer (pH 7.4). The step gradients were centrifuged in Beckman SW 32 rotor (80000 X g for 4 hr). The material that deposited at the 37% sucrose solution and above was collected, diluted with buffer 20 times and layered on 35% sucrose pad. The material was ultracentrifuged at 120000 X g for 3 hr. The supernatant was diluted 5 times with buffer and was pelleted by ultracentrifugation at 120000 X g for 2 hr. The pellet was stored as IM-enriched fractions. The material at the interface between 60 and 70% sucrose gradient was collected and stored as OM enriched fractions.

For SDS PAGE, the protein samples were resuspended in 2X sample buffer (120 mM Tris HCl, pH 6.8, 4% sodium dodecyl sulfate, 0.2% bromophenol blue, 20% glycerol and 50 mg dithiothreitol). The samples were boiled for 5 min at 100^{o} C, and the proteins were separated by 4-15% SDS-PAGE gel. Proteins were stained with Coomassie brilliant blue dye, and molecular weights were compared using a prestained protein marker ladder.

4.3.4 Mass spectroscopy

The gel bands from SDS PAGE gels were cut and in-gel tryptic digestion was performed from the method modified form the published protocol. (141) Briefly, gel bands were dehydrated using 100% acetonitrile (ACN) and incubated with 10 mM dithiothreitol (DTT) and 50 mM iodoacetamide in 100 mM ammonium bicarbonate for 20 min each. Gel bands were then washed with ammonium bicarbonate and dehydrated again. Sequencing grade modified typsin was diluted to 0.01 μg/μL in 50 mM ammonium bicarbonate and ~50 μL of this solution was added to each gel band in order to completely submerge the gels. Bands were then incubated at 37^{o} C overnight. Peptides were extracted from the gel by water bath sonication in a solution of 60% ACN/1% trichloroacetic acid (TCA) and vacuum dried to ~2μL. Peptides were then re-suspended in 2% ACN/0.1% trifluoroacetic acid (TFA) to 20μL, and 10μL samples were injected by a Waters nanoAcquity Sample Manager^{TM} and loaded for 5 min onto a Waters Symmetry C18 peptide trap and eluted to a Waters BEH C18 nanoAcquity column with a gradient of water and ACN. Eluted peptides were then sprayed into a ThermoFisher LTQ Linear Ion trap mass spectrometer equipped with a Michrom Bioresources Advance nano-spray source. Data-dependent zoom scans was performed onto the top five ions of each survey, followed by low energy collision induced dissociation, and the resulting MS/MS spectra were converted to peak lists using BioWorks Browser v 3.3.1 (ThermoFisher) with the default LTQ instrument parameters. All MS samples were analyzed using Mascot (Matrix Science, London, UK; version 2.4.0). Scaffold (version Scaffold 3.6.0, Proteome Software Inc., Portland, OR) was used to validate MS based protein and peptide identifications.

4.3.5 Biochemical characterization with UV visible spectroscopy

Orientation of heterologously expressed OmcB to outer membrane was assayed by monitoring change in absorption spectra of oxidized versus reduced cytochromes by a UV-visible spectrophotometer. The reduction of low spin cytochrome was observed spectrophotometrically by presence of three characteristic absorption bands, called Soret or gamma peak which shift from ~408 in oxidized form to ~420 in reduced form, alpha (α) peak at ~ 552 nm and beta (β) at ~ 521 nm. Briefly 100 μL of cells at O.D. 2 were washed added to 900 μl of degassed resuspension buffer in a 1 cm path length quartz cuvette. The absorption spectrum of the cytochrome was measured by continuous scan from 380-600 nm. The cell suspensions were then reduced by addition of 5 μL of 0.5 % (w/v) freshly prepared sodium dithionite solution, and reduced spectrum was measured. The ability of cells to oxidize back by transferring electrons to an electron acceptor was tested by adding a soluble electron acceptor like Fe(III)-nitrilotriacetic acid (FeNTA), ferric citrate, uranyl acetate (UA) riboflavin and or an insoluble electron acceptor like ferric oxide particles. Redox activity of membrane fractions was determined similarly using IM and OM preparations at 1-2 mg/ml concentration instead of cell suspensions, and reoxidation was achieved using FeNTA, ferric citrate, ferric oxide, or UA.

4.5 Results and discussion

Fermentation conditions that gave maximum production of apoprotein were not suitable to get maximum expression of mature protein. Cells grown at 30^{o} C at 220 rpm without IPTG addition gave maximum yield of mature protein. Induction was not required due to 'leaky' expression of the plasmid. Addition of δ-aminolevulinic acid and hemin were essential for mature OmcB expression when grown with minimal media. The 2X YT medium without any

additional supplements was sufficient to express OmcB, but the amount of mature OmcB produced with 2 X YT media was lower compared to overall OmcB protein expression. Lowering the temperature to 18^{o} C after initial growth at 30^{o} C slowed the OmcB production rates, but did not increase the ratio of mature protein expression.

The MS analysis revealed the identified peptide cover 51% of the protein sequence (Fig. 4.1). As shown in Figure 4.1, 23 unique peptides were found, resulting 100% protein identification probability. The amino acid sequence was subjected to a BLAST search, which identified protein as cytochrome *c* protein from *Geobacter sulfurreducens* with 12 putative heme-binding sites.

Subcellular fractionation of *E. coli* cells was used to localize heterologously expressed OmcB. The clarified cell expression media at the end fermentation, cell resuspension buffer after cell wash, and cytoplasmic fractions contained no measurable OmcB. An OmcB band was visible mostly in the membrane preparations and to a lesser extent in the periplasmic fraction. EDTA and lysozyme treatment breaks down bacterial outer membrane forming spheroplasts with intact inner membrane. (142) However, complete removal of OM from spheroplasts is challenging. (143) The sucrose density gradient method was used to separate to IM and OM fractions based on different buoyant densities of two membranes. However, cell lysis by pressure homogenization or ultrasonication may lead to formation of mixed membrane fractions. Hypertonic sucrose solution was used in the lysis buffer to minimize formation of mixed membrane pellets. (11) The gradient centrifugation method was optimized using various sucrose concentrations ranging from 20-70%. as well as different concentrations of divalent cations like $MgCl_2$. As shown in Figure 4.3, the IM fractions were localized on the top of 37% the sucrose

gradient, while the OM fractions with higher densities were localized between 60 and 70% sucrose gradient. Both IM and OM fractions showed reddish coloration, but SDS PAGE revealed a very faint band at~ 80 kD for IM fractions, while the OM fractions showed a much darker OmcB band. Although sucrose density gradient was useful in separating *E. coli* membrane fractions based on density gradient, the IM and OM in *E. coli* are fused at several places (144), making the complete separation of the membranes difficult. *N*-lauroylsarcosine or sarkosyl detergent is commonly used to purify outer membrane proteins in *E. coli* and other bacteria (145-147) because it efficiently dissolves cytoplasmic membranes while leaving outer membrane intact. Ultracentrifugation of membrane preparations after sarkosyl detergent treatment yielded dark reddish brown colored pellet of OM fractions. OmcB was a major protein present as a major band in OM preparations. The control OM preparations without OmcB plasmids were white in color and did not show any band in the 75-85 kD range. Yield of OM obtained using sarkosyl treatment was ~ 45 % of total membrane fraction. Compared to OM fractions, the supernatant of the ultracentrifugation step (referred as IM fraction) contain a very small amount of OmcB (Fig. 4.2). Similar results were obtained using 1 % Triton X-100 for differential detergent solubilization.

Evidence of OmcB redox activity was obtained by monitoring UV visible spectra of *E. coli* cell suspension. The cell suspension buffer was purged with argon for 30 min, and the cuvettes used were flushed with nitrogen for 5 min. UV visible spectra of air oxidized cells showed a peak at ~ 410 nm, which shifted to 420 nm after reduction of cells with sodium dithionite. A small peak around 552 nm also became visible in the reduced cells. The reduced cytochrome was then oxidized with Fe NTA or ferric citrate, as evidenced by a Soret peak shift back to 410 nm and disappearance of the 552 peak (Fig. 4.3 A and B). A 520 nm peak often

associated with cytochrome *c* reduction (β peak), and a 530 nm peak with cytochrome *c* oxidation were not very apparent in these spectra, possibly due to higher scattering noise of the cell suspension. Similar reoxidation results were obtained when riboflavin and ferric oxide particles were used as oxidants (Fig.4.3 C and D). The reduction of ferric oxide, an insoluble electron acceptor that is unlikely to traverse through *E. coli's* cell envelope, provides strong evidence that the expression host was able to package heme into the recombinant OmcB and target it to the outer membrane. A similar assay procedure was reported to analyze the orientation of outer membrane cytochromes in *Shewanella oneidensis* and heterologously produced OmcA in *E. coli* by reoxidation of reduced cells with soluble but cell membrane impermeable riboflavin. (148) Additionally substrate accessibility experiments with ferric NTA and insoluble iron oxide mediated reoxidation of sodium dithionite reduced cells concluded that type II secretion system was involved in the transport of heme domain to the outer surface of *E. coli* BL 21 strain. (47) Additionally those studies showed that heterologously expressed OmcA protein was released in the wash solution of the intact cells. In our experiments with OmcB expression we did not observe any release of OmcB in wash solution, which is consistent with the studies showing OmcB expressed in *Geobacter sulfurreducens* cells is only partially accessible to the outer membrane. (135)

SDS PAGE analysis of subcellular fractions of the *E. coli* cells expressing OmcB showed the majority of OmcB to be membrane associated (Fig.4.2, and other data not shown). Inner and outer membrane fractionation by ultracentrifugation with sucrose density gradient and differential detergent extraction revealed majority of the heterologously expressed OmcB is associated with an outer membrane. UV visible analysis of outer membrane fragments showed that the recombinant OmcB was redox active toward a variety of substrates (Figure 4.5). Soluble

electron acceptors like FeNTA, ferric citrate, and UA reoxidize sodium dithionite reduced OmcB OM fractions. Insoluble electron acceptors like iron oxide particles were also able to interact with OmcB OM fractions to reoxidize it back. Interestingly another outer membrane cytochrome of *Geobacter*, OmcZ, was not redox active towards insoluble electron acceptors like iron oxide. (138) This finding is consistent with the observation that OmcZ is released into extracellular matrix while OmcB remains associated with the outer membrane of *Geobacter* and may be important for localized reduction of metals at the bacterial surface. Artifacts generated during membrane protein isolation protocols can lead to formation of mixed membrane fragments (IM and OM); also presence of insoluble periplasmic aggregates can be associated with OM during cell fractionation, leading to false conclusion about the localization of overexpressed protein in *E. coli*. (149) Fractionation with two independent techniques (sucrose density gradient separation and differential detergent extraction), along with whole cell spectroscopy to believe that heterologously expressed OmcB is indeed oriented in the outer membrane of *E. coli*.

The membrane association of OmcB was found to be very strong and resistant to a variety of detergent treatments. A cysteine mutation with alanine in the OmcB leader sequence yielded detergent extractable protein (OmcBc1a). However, UV-visible spectroscopy suggested that the redox activity of this mutant protein did not match the expected cytochrome *c* profile. The Soret peak of the cysteine mutant shifted to 428 nm, with additional peaks at 506, 540 and 560 nm (Fig. 4.6). Therefore it may be possible that the cysteine residue in the protein sequence is important for the redox activity of the protein.

The genome of *Geobacter* predicts around 100 membrane associated cytochrome. (57) The high number of cytochromes involved in the electron transport in this bacteria, makes the study of individual cytochromes extremely challenging. Because of high number of cytochrome

present in these bacteria, there seem to be a functional redundancy. Even though the knock out models can be used to study contribution of specific cytochromes, the bacteria tend to adapt over the time by expressing other cytochromes. One strategy is to use heterologous expression of these *Geobacter* proteins in other hosts like *E. coli*. The heterologous expression can be either used to build a synthetic chain of redox active proteins in bacteria (150) or to purify the protein and study its biochemical properties in detail. (151) However the heterologous expression of these *Geobacter* outer membrane protein in other hosts in challenging, because:

1. The protein needs to be transported across the inner membrane of the bacteria by a pathway like Sec pathway. (152)

2. The apoprotein need to be matured in the periplasmic space with the help of heme maturation machinery in the bacteria, which involves several different proteins such as cytochrome *c* maturation proteins a, b, c, d, e, f, g , h, and I. (53)

3. The protein then need to be transported to the outer membrane, which also requires specific mechanism like Type II secretion system. (44)

Due to these challenges, very few multiheme cytochromes from *Geobacter* have been expressed in *E. coli*.(85, 153) A high-throughput scheme has been proposed to express the multiheme cytochromes in *E. coli* with novel expression vectors. (154) But this scheme utilizes only soluble part of the protein to facilitate the purification. The proteins expressed with such system may not aid in the cellular localization and functional characterization of these proteins.

To the best of our knowledge, we are the first group to express multiheme, outer membrane cytochrome from *Geobacter* in *E. coli*. The advantages of using the whole sequence of the OmcB protein as opposed to only soluble part for the heterologous expression include that

the expressed protein is more likely to be in similar in characteristics to the native OmcB. Another advantage of using *E. coli* host is that under aerobic conditions *E. coli* does not produce cytochromes maturation proteins. The OM fractions separated from control cells of *E. coli* transformed with only pEC86 plasmid, did not show any UV-visible signature peaks for cytochrome *c*. Lack of native cytochromes in *E. coli* is of advantage to us because it means that any cytochrome signal obtained from *E. coli* membrane must be from the heterologously expressed cytochrome. This results enables us to use the membrane vesicles of *E. coli* for further studies of redox activity of OmcB. This saves the efforts of purifying the protein to isolation before studying its redox properties, but more importantly we can study the protein in the environment which is more likely to preserve its activity. Since OmcB sequence indicates putative membrane spanning domains (155) and other studies indicate that OmcB may be embedded in the outer membrane with only partially exposed to the solution side (156), keeping the protein associated with the membrane is more likely to preserve its function. We aim to study this protein further using a biomimetic interface, where the membrane vesicles form *E. coli* containing OmcB will be incorporated to study its electrochemical and spectro-electrochemical properties.

In summary, we demonstrated that heterologously expressed OmcB in *E. coli* cells is membrane associated with majority of protein present in the outer membrane. The OmcB is accessible to and active with a variety of redox partners. These results are a key step towards further analysis of this important redox protein in understanding the redox chemistry of *Geobacter in vitro*.

5.0 SPECTROELECTROCHEMICAL STUDIES OF *GEOBACTER* REDOX PROTEINS EXPRESSED IN *E. COLI*

5.1 Introduction

Spectroelectrochemical technique is a powerful analytical tool offering advantage of both electrochemistry and spectroscopy, allowing quantitative and qualitative characterization of an analyte as a function of changes in electrode potential. A variety of spectroscopic techniques can be coupled with electrochemical analysis which can follow changes in structure of analyte with its redox activity. Examples of the spectroscopic techniques that can be combined with electrochemistry include but are not limited to are electron paramagnetic resonance (EPR) or electron spin resonance which can be useful to study paramagnetic systems such as transition metals and radicals (163-165), vibrational spectroscopies such as Fourier transform infrared spectroscopy (FTIR) and Raman spectroscopy (166-170), and UV- visible spectroscopy. (171-174) UV-visible analysis coupled with electrochemistry has been used to study the redox reactions of biomolecules. (175-177)

Information about the redox thermodynamics of the proteins (178) and kinetics of their reduction reactions with substrates (179) can be obtained by spectroelectrochemical studies. Developments in the optically transparent electrode materials have made it possible to study a variety of biological samples directly on solid substrate. Protein samples can be analyzed by adding them to the protein/lipid films (180, 181), supported lipid bilayers (182), by depositing partially dehydrated protein films on the surface (183) or by immobilizing on an optically transparent electrode. (184, 185) UV-visible spectra of cytochromes can be easily distinguished because of the heme groups associated with the protein. By monitoring changes in the UV-absorption of heme groups because of $\Pi - \Pi^*$ transition (167), the information about the type

of heme, its oxidation state and spin state of iron in the porphyrin ring can be obtained. (167) Further information about the resolution of individual hemes in multiheme cytochrome (186) and conformational changes in individual hemes in different redox states (186) can be obtained by these techniques.

Design of optically transparent cell geometry and selection of electrode material are crucial to build an optimal spectroelectrochemical system. The ideal electrode material should have minimum ohmic resistance, maximum surface area to volume ratio, and wide spectral and potential window. (187) Deposition of optically transparent thin conductive films made of metals (188), metal oxides (189), and carbon material (190, 191) on the substrate offers a variety of spectral regions to be studied. Optically transparent thin cell electrode (OTTLE) system offers several advantages which include (187, 192)

1. Complete and rapid electrolysis of the redox sample.

2. Possibility of using a variety of electrode material like boron doped diamond or SAM coated gold electrode.

3. Requires a small amount of samples, which can be very useful when working with recombinant proteins.

4. Possibility of taking measurements in anaerobic conditions, which can be helpful when working with oxygen sensitive proteins or substrates.

5. Quantitative relationship between experimental and theoretical spectroelectrochemical parameters.

In this study, we have made efforts to develop a substrate on the transparent gold electrodes which will protect the protein in solution from degradation at the electrode while allowing rapid electron transfer. The substrate developed also offers a possibility of

immobilizing the protein on the electrode in an electroactive configuration. We have also explored the possibility of using OTTLE for spectroelectrochemical studies of *Geobacter* multiheme cytochromes heterologously expressed in *E. coli*. We have demonstrated that PpcA is capable of direct electron transfer to metal ions when immobilized on a SAM coated gold electrode. Furthermore we have also studied the electrochemistry of outer membrane protein OmcB embedded in membrane vesicles with different redox mediators. Moreover, we have demonstrated that periplasmic protein PpcA is capable of electron transfer to OmcB. To the best of our knowledge, we are the first group to show evidence of protein-protein electron transfer in OTTLE.

5.2 Materials and methods

5.2.1 Thin-layer spectroelectrochemical system

Schematics of the OTTLE cell are shown in Figure 5.1. (187) The OTTLE cell consists of a holder for the working electrode, which can be 2cm X 2cm with 0.78 cm^2 working area. The working electrode (WE) is pressed against the sample holder with a transparent window made of calcium fluoride (CaF_2) and is the WE separated from the window by a thin spacer. The thickness of spacer can be varied from 25 μM to 125 μM, and thus the volume of the OTTLE cell can be controlled. The diameter of the spacer is slightly larger (1 cm) than the diameter of the transparent window (0.9 cm). An O-ring seals the volume of the spacer. A small fine Pt wire connected to the holder serves as a counter electrode. A small amount of electrolyte such as KCl is added to the counter electrode capillary compartment to complete the circuit. A miniature Ag/AgCl reference electrode is also connected to the counter and working electrode through a fritted glass.

5.2.2 PpcA and OmcB cytochrome *c*

The protein samples of PpcA and OmcB were prepared using the methods described in chapter 2 and chapter 4 respectively. PpcA samples were dissolved in degassed phosphate buffer (50 mM, 150 mM NaCl, pH 7.2), and the concentration was adjusted from 700 μM to 10 μM. OmcB membrane vesicles were stabilized by detergent (0.5% n-dodecyl, b-D-maltoside (DDM)) and sucrose (100-500 mM). OmcB content of the total protein in membrane vesicles determined by densitometry of SDS PAGE gels was from 40-70%.

5.2.3 Electrochemical and Spectroscopic measurements

UV-vis measurements were made by placing the spectroelectrochemical cell in the path length of a Hewlett Packard diode array spectrophotometer (model 8453 Agilent Technologies, Santa Clara, CA). At the beginning of each experiment the optical and electrochemical measurements were synchronized. The electrochemical experiments were performed using CH instrument potentiostat (model 660 b, 760 b, and model 830 c; CH instruments Inc, Austin TX). The potential values reported here are against Ag/AgCl reference electrode. The cathodic current values reported here are positive, and anodic current are reported negative. The data files were saved in ASC II format and were imported into MS excel format™ or plotted by Igor Pro™ software. Baseline noise reduction is achieved by subtracting the average of spectra before the oxidation / reduction step from the following spectra.

Electrochemical techniques used included cyclic voltammetry (CV), chronoamperometry (CA) and multipotential step voltammetry. A more detail explanation of these techniques is give in previous chapters. For multipotential step voltammetry, the potential of the working electrode is changed in small increments and kept constant at each potential for specified time. The change

in current is noted as a function of change in potential. Addition of all the samples to OTTLE were done inside a glove box in nitrogen environment. All the samples and buffers were thoroughly degassed using argon.

Spectroelectrochemical reduction of OmcB membrane vesicles with a mixture of mediators was characterized. The mediator stock solution contained 1 mM of each of the following freshly made mediators: gallocyanine, phenazine methosulfate, 2-hydroxy1-4 naphthoquinone, anthraquinone 2 sulfonic acid, benzyl viologen, and methyl viologen. The mediators were chosen to cover the potential range of interest (+21 mV to -430 mV against SHE). The concentration of mediators used was around 50 μM. The spectra of mediators were recorded using multipotential step voltammetry. Then the spectrum of OmcB was recorded, with and without the mediator mixture.

5.2.4 Preparation of working electrode

The working electrode was a gold coated glass cover slide with 100 A^{o} thickness of gold coating (Sigma-Aldrich) or the custom made electrode with gold grid printed on quartz. The working electrodes were cleaned by Piranha solution or oxygen plasma cleaner. The cleaned electrodes were immediately contacted with ethanolic solution of alkanethiols (~ 5 mM concentration). The chain length of alkanethiols were varied from 6-16 C, and the ratio of carboxy terminal to hydroxy terminal group was adjusted. Protein solutions were contacted either directly with working electrode (for PpcA) or with the help of redox mediators (for OmcB). PpcA was then immobilized on the SAM covered gold working electrode by the procedure described in chapter 2.

5.3 Results and Discussion

5.3.1 Immobilization of PpcA on optically transparent gold electrodes.

The negatively charged SAM deposited on gold surface electrostatically attracts the positively charged PpcA protein at neutral pH. No current was obtained when PpcA protein was initially immobilized using C-16 SAM containing 16-mercaptohexadecanoic acid. However, the number of carbons in the lipid and the ratio of hydroxyl to carboxyl terminated groups in the SAMs were adjusted to optimize the faradic current. We chose mixture of 12-mercaptododecanoic acid with 11-mercapto1-undecanol or 6-mercaptohexanol in 1:3 molar ratio for immobilizing the cytochrome on the electrode. The immobilized PpcA displayed distinct redox peaks for oxidized and reduced forms. The ratio of peak current to the scan rate was linear, consistent with the electrochemistry of the adsorbed protein. The coverage of active adsorbed protein, obtained from integrating the area under CV peak is calculated to be 18 pmol/cm^2. The peak half width (the difference in potential at half the maximum current value) was ~ 140 mV, much higher than the expected value for the reversible species (84), but the redox peaks were stable during multiple runs (data not shown). This finding leads us to believe that the protein was getting completely oxidized and reduced at the electrode reversibly, but maybe due to a large number of lysine residues available. The positively charged lysine residues are attracted towards negatively charged SAM, but because there are multiple residues, the adsorbed protein might be in a range of orientations. Stability of the adsorbed protein was monitored by square wave voltammetry by following decay in the signal. The square wave voltammograms were recorded with amplitude of 50 mV, frequency of 25 Hz, and potential step of 2 mV. The adsorbed cytochrome *c* was very stable for at least 6 hr and the peak current reduced to ~80% of its value after 24 hr (Fig. 5.2). Furthermore CV were recorded at the fast scan rates, and the data obtained

were fitted to the Laviron equation (please refer to chapter 2 for more details) to find the heterogeneous electron transfer rate constant between PpcA and electrode. (data of this section is not shown) Interestingly, we did not observe any peaks associated with cytochrome c during the UV-vis spectroscopic analysis of the optically transparent gold substrates with immobilized PpcA. This observation is not surprising, because of the small size of the protein (~ 2 nm) at the monolayer coverage will not have enough protein at immobilized surface to give UV-vis spectra. Another group working with immobilized cytochrome on a similar SAM reported UV spectra for the protein adsorbed at the monolayer, with the possible explanation that surface plasmons associated with the gold electrode enhance the signal of protein. (184) However, we did not notice such signal augmentation in our studies. Nonetheless, the protein immobilized at the monolayer at the optically transparent electrode provides a possibility of monitoring a redox reaction of proteins with substrates, where the changes in UV-vis spectra of the substrate can be monitored as a function of redox reaction mediated by an immobilized cytochrome.

5.3.2 Spectroelectrochemical characterization of PpcA in solution

Electrode fouling due to adsorption of the inactivated protein (193) or denaturation of proteins (194) during electrochemical measurements at the bare gold substrate can pose experimental problems. Therefore the PpcA was characterized spectroelectrochemicaly with the C-6 SAM coated gold. Distinct oxidation and reduction peaks were observed with 10 μM solution of PpcA on SAM coated gold electrode. The peak potential separation increased with increased scan rates (Fig. 5.3), and the peak current value increased linearly with square root of scan rate as expected for the reaction controlled by the diffusion of the species (Fig. 5.3 inset). Spectroscopic changes associated with the reduction of PpcA at SAM coated electrodes are shown in Figure 5.4A. PpcA cytochrome is capable of direct electron transfer with the electrode

without any redox mediators. Therefore the spectroscopic signal of PpcA in solution is dominated mostly by changes associated with the redox center of the protein of interest and not of any mediators. Figure 5.4 B shows changes in absorption spectra of PpcA at the OTTLE for various electrode potential values. The wavelength values characteristic of the cytochrome *c* protein (315 nm, 408 nm, 420 nm, 520 nm, 530 nm and 552 nm) display the most noticeable changes in absorbance. Moreover the differential spectra also show changes at 280 nm and 430 nm range, which may be associated with the changes in the peptide arrangement of the protein in different redox states. Redox performance of the PpcA solution was monitored by CA measurements, where the potential of the electrode was changed to a large overpotential value (in this case reduction potential of -600 mV vs. Ag/AgCl) and the resulting change in the current was measured. The Cottrell equation (84) describes the relationship between current value (i) at the planar electrode with diffusion coefficient and time as follows:

$$i = \frac{n\,F\,C_o D_o^{1/2}}{\Pi^{1/2} t^{1/2}} \quad \text{.....(Eq. 5.1)}$$

where, n is the number of electrons transferred in the reaction, F is the Faraday's constant, A is the area of the electrode, and C_o and D_o are the concentration and diffusion coefficient, respectively, of the electroactive species. Chronoamperometry experiments were repeated at the multiple potential steps, and the change in current were monitored. The change in current following a potential step for PpcA (Fig 5.5 A) shows a behavior typical of the diffusion species. Interestingly, the change in the absorbance at 552 nm also shows similar behavior, though at apparently slower rate, possibly because the CA measurements follow the change in current mostly at the electrode surface, while the spectroscopy data follow the change in the whole volume of the cell. A common trend is that both signals reach a plateau at around 300 sec,

indicating almost complete reduction of PpcA in solution at that time point. Figure 5.5 B shows the reversibility of the PpcA absorbance signal during multiple CA run, indicating that the SAM of alkanethiols protects the cytochrome from degrading and the electrode from fouling.

5.3.3 Spectroelectrochemical characterization of OmcB in OTTLE

OmcB membrane vesicles were not found to react with the electrode directly, as evidenced by no change in current with a change in applied potential during CA and CV measurements. However, with the addition of mediators, Soret peak absorbance values at 420 and 552 nm peaks were observed that suggested OmcB redox activity (Fig. 5.6).

The changes in absorption spectra with changes in electrode potential were analyzed by the modified Nernst equation (195) :

$$E = E^{o\prime} + \frac{RT}{nF} ln \frac{A - A_r}{A_0 - A} \text{.....(Eq. 5.2)}$$

where, E is the potential of the electrode, $E^{o'}$ is the formal potential of the redox couple, A is the absorbance, A_r and A_o are the absorbance of the fully reduced and fully oxidized species. R, T, n and F are ideal gas constant, absolute temperature, number of electrons transferred, and Faraday's constant respectively. For the electrochemical reaction of proteins in presence of mediators, the Nernst equation can be rearranged in the following form (195, 196) :

$$E = E_M^{o\prime} + \frac{RT}{nF} ln \frac{[O_M]}{[R_M]} = E_P^{o\prime} + \frac{RT}{nF} ln \frac{[O_P]}{[R_p]} \text{.....(Eq. 5.3)}$$

Where, $E^{o'}_{M}$ and $E^{o'}_{P}$ are the formal potential of the mediator and protein respectively and O_M, R_M, O_P and R_P are the concentration of oxidized mediator, reduced mediator, oxidized protein and reduced protein respectively.

From plotting the data of percentage of OmcB reduced (from the change in 410 nm peak) vs the potential of the electrode, and fitting the curve to Nernst equation, a tentative midpoint potential value for OmcB was obtained. Fig 5.7. Furthermore, by carefully changing the electrode parameters it may be possible to further resolve the individual hemes or at least groups of hemes using this technique. (197) Fig 5.7 shows possible resolution of individual heme groups as a the potential was varied. Moreover we found a tentative range for the redox potential of OmcB from these experiments (~ -400 mV vs. Ag/AgCl). In another set of experiments, the mediators were replaced with 50 μM solution of anthraquinone 2,6-disulphonate (AQDS) which serves as a humic acid analogue. (198) OmcB was reduced and oxidized reversibly figure 5.8), indicating that AQDS serves as a redox mediator for OmcB. Quinone moieties are reported to facilitate the extracellular electron transport in *Geobacter* and enhance the rates of bioremediation processes. (199) Considering the outer membrane localization of OmcB, it may be possible that OmcB is one of the *c* cytochrome involved in electron transfer to humic acid moieties found in soil and sediments.

5.3.4 Spectroelectrochemical characterization of PpcA -OmcB interactions

Based on the hypothesis that PpcA may be transfer electrons produced in respiration to OmcB as part of *Geobacter's* electron transport chain, we attempted to demonstrate electron transfer from PpcA to OmcB in OTTLE cell. The CV of PpcA at the scan rate of 50 mV per s shows a distinct redox peak. Addition of OmcB-containing membrane vesicles to the PpcA,

yielded a small increase in the CV peak (Fig.5.9). Since OmcB membrane vesicles, are not capable of direct electron transfer to and from the electrode, the increase in the current can be attributed to the catalytic reduction of OmcB by reduced PpcA. Redox spectra of the cytochromes monitored in the multipotential step experiments showed additional evidence of reduction of OmcB from PpcA (Fig. 5.10 A). Change were observed in the Soret Peak at 410 and 420 nm, and 552 peaks as a function of electrode potential. In the case where only PpcA is getting oxidized and reduced at the electrode, the 410 peak associated with oxidized OmcB will not change. Thus at the reducing potential of PpcA a mixture of peaks in the Soret regions would be observed. The complete disappearance of the 410 peak at reducing potential and complete removal of 420 peak at the oxidizing potential provides the evidence that both cytochromes are getting oxidized and reduced. Spectra of OmcB in multipotential voltammetry can be obtained by subtracting the spectra of PpcA from the spectra of both the cytochromes together (Fig. 5.10 B). Since OmcB was not observed to interact with the electrode, PpcA is apparently acting as a redox mediator between electrode and OmcB.

The biomimetic system assembled here was intended to simulate electron transfer within *Geobacter's* cell envelope, in which electrons produced in respiration are transferred from the inner membrane (mimicked by the SAM coated gold electrode) through the periplasm (mimicked by the PpcA layer bound to the SAM) to outer membrane cytochromes (mimicked by the OmcB-containing microsomes. This study's establishment of a biomimetic redox-active cell envelope (BRACE) provides a new research platform with which to study *Geobacter* electron transport to extracellular electron acceptors.

The use of PpcA and OmcB heterogeneously expressed in *E. coli* helps eliminate the possibility that other *Geobacter* cytochromes that might be difficult to separate from the PpcA

and/or OmcB are participating in the electron transfer. Assuming the redox properties of the heterogeneously expressed OmcB are similar to those of the native OmcB, these experiments support the hypothesis that periplasmic cytochrome PpcA is able to transfer electrons to the outer membrane cytochrome OmcB.

Thus OTTLE system provides two independent measures of redox activity (optical and electrochemical) that provide more insight into the cytochrome electron transfer than either method alone. The ability to simultaneously interrogate a BRACE both optically and electrochemically offers the potential to significantly accelerate progress in elucidating mechanisms of *Geobacter* electron transfer and testing hypotheses about system behavior. For example, another soluble cytochrome could be substituted for PpcA, and the resulting changes in spectroelectrochemical characteristics could be observed. Similarly, vesicles containing different outer membrane cytochromes could be used, and the relative efficiency of inter-cytochrome electron exchange between PpcA and the various outer membrane cytochromes could be explored. This approach could provide insight into the principal redox pathways *Geobacter* uses to transport electron transport to metals.

6.0 ENGINEERING A BIOMIMETIC REDOX ACTIVE CELL ENVELOPE WITH HETEROLOGOUSLY EXPRESSED *GEOBACTER* CYTOCHROMES

6.1 Introduction

Biological systems are often complex in nature, with heterogeneous biomolecules arranged in a specific spatial hierarchy. (200) Such spatial arrangement plays a crucial role in controlling protein-protein interaction, for example close proximity of the proteins reduces the time required for diffusing protein to find the target protein. (201) Metabolic processes take place where multiple species are working in tandem, localized in specific cell compartments. Synthetic biologists and metabolic engineers have been working to understand the multidimensional aspect of these biological processes, yet characterizing these pathways remains challenging. (202) There is an ever increasing demand about understanding these biological routes, in order to optimize the commercially and environmentally important bioprocesses. Dissimilatory metal reduction mediated by anaerobic bacteria *Geobacter* is an example of such important process because of its application in uranium bioremediation and microbial fuel cell technological applications. (203, 204) *Geobacter* display a large number of electron carriers which are located in different cell compartments (57) for e.g.: inner membrane (e.g. cytochrome *bc* complex), periplasmic space (e.g. PpcA cytochrome), outer membrane (e.g. OmcB), and the pili protein protruding out of the membrane. In this work we try to address some key issues about the *Geobacter* electron transfer (ET) process: 1) Is there a possible interaction between the two of the most well conserved *Geobacter* cytochromes (56) (PpcA and OmcB), and 2) Are there any tools available to study these complex and compartmentalized processes in a more controlled manner. Our strategy is to build a nanoscale biomimetic system where these proteins can be

studied in a close proximity yet separated by different compartments similar to the cell envelope of the native bacterium.

Artificial lipid bilayers have emerged as a very useful tool to mimic structure of biological cell membranes. (205, 206) Use of biomimetic membranes allows to study characteristics of biological moieties in an environment which gives more control over experimental parameters without sacrificing functional properties of biomolecules. (207-209) Traditional methods like “patch clamp” to study biological membrane have long given a way to more sophisticated techniques like planar bilipid membrane, in which lipid bilayer is painted over small aperture separating two electrolyte chambers. (210-212) Although this is very sensitive method, the bilayer formed by this method is very fragile. (212) More robust artificial bilayer can be formed by supported bilayer lipid membranes (sBLMs). (213, 214) sBLMs can be deposited on a variety of substrates including surface like gold, (215, 216) glass, (217) silica, (218) and mica. (219) Deposition of lipids by vesicle fusion around the protein immobilized on a glass surface showed that the lipid still maintained its fluidity. (220) Incorporation of membrane proteins into sBLMs using proteoliposomes facilitates study of their structural and functional properties. (221) (222) We have adopted similar methodology to built our proposed biomimetic interface. In this study we have deposited proteoliposomes on a self assembled monolayer (SAM) containing immobilized protein. Rupture of proteoliposomes vesicles on the SAM produces highly insulating film on surface. Because of this blocking layer, any electron transport (ET) must takes place via membrane proteins immobilized in the upper lipid layer of the interface. In this chapter we have demonstrated that the biomimetic redox active cell envelope (BRACE) allows us to study ET in a biomimetic system containing multiple cytochromes. Although more work about BRACE protocol optimization and studies to establish its architecture

needs to be done, we have demonstrated with the use of BRACE that ET is feasible between periplasmic cytochrome PpcA and outer membrane cytochrome OmcB, making them possible redox partners. We are the first group to report use of BRACE to study ET between different *Geobacter* cytochromes and these results suggest that BRACE interface can be used to study the ET between different redox proteins in a more controlled environment.

6.2 Materials and methods

6.2.1 Preparation of protein samples

Please refer to chapter 2 for a detail description about heterologous expression and purification of *Geobacter* periplasmic cytochrome *c* protein: PpcA. Similar method of expression was used to produce PpcA^{-heme} except in this case the *E. coli* cells were transformed with only PpcA plasmid. Omission of pEC86 plasmid necessary for the heme incorporation resulted in expression of apocytochrome without heme. PpcA^{-heme} was purified from periplasmic fraction using cation exchange chromatography and the samples were collected following UV signal. The samples were analyzed by SDS PAGE to verify the presence of the protein. Unlike PpcA, the PpcA^{-heme} is a colorless protein and does not show any UV peaks associated with cytochrome *c* (at 410, 420, and 552 nm on reduction). The PpcA protein samples were stored in phosphate buffer pH 7.2, 100 mM NaCl. Before immobilization experiments, the protein samples were either buffer exchanged or diluted to salt concentration of around 10 mM.

Please refer to chapter 4 for description about isolation of outer membrane vesicles from *E. coli*, expressing *Geobacter* outer membrane cytochrome OmcB. Outer membrane fractions form OmcB with cysteine mutation (OmcBc1) were also isolated with the similar procedure.

The outer membrane vesicles were suspended in 10 mM HEPES buffer containing 150 mM NaCl and sonicated with 20 s pulse and cooling for 40 s between each pulse until the suspension become clear (~10 min). The suspension was then filtered through 450 nm filter.

6.2.2 Preparation of DOPC liposomes

The phospholipid 1,2-dioleoyl-*sn*-glycero-3-phosphocholine (DOPC) was purchased from Avanti Polar Lipids Inc., Alabaster, AL. A chloroform solution of DOPC required to make 1 mM lipid was dried under the stream of nitrogen until it forms a thin white lipid cake. Then the lipids were freeze dried for at least 4 hr. The dried lipids were rehydrated with HEPES buffer (10 mM HEPES, 150 mM NaCl, 2 mM $CaCl_2$, pH 7.4) to form multilamellar vesicles, which were ultrasonicated in bath sonicator for 30 min to obtain small unilamellar vesicles. For formation of proteoliposomes, OmcB outer membrane vesicles were added before or after the sonication of DOPC lipids. In an alternate protocol, the DOPC liposomes were contacted with 0.5 % n-dodecyl-β-D-maltoside (DDM) detergent stabilized OmcB vesicles and dialyzed overnight with HEPES buffer using a 30 kD molecular weight cutoff membrane.

6.2.3 Fabrication of compartmentalized bilipid membrane on gold electrode

Commercial gold substrates (LG thin films, Santa Clara, CA) were cleaned by dipping in Piranha solution (7 parts sulfuric acid and 3 parts 30% hydrogen peroxide solution) for 30 s and then rinsing with distilled water. For SAM formation, the cleaned substrates were dipped in 5 mM ethanolic solution of 12-mercaptododecanoic acid and 11-mercapto 1 undecanol in a 1:3 ratio for 24 h, and then rinsed with ethanol and distilled water. PpcA was bound to the SAM via an amide linkage using 50 mM 1-ethyl-3-[3-dimethylaminopropyl]carbodiimide hydrochloride (EDC) and 5 mM *N*-hydroxysuccinimide (NHS) solutions. The electrodes were then washed in 20 mM phosphate buffer to remove unbound protein. DOPC liposomes or the proteoliposomes

were added to the immobilized PpcA substrate to the final concentration of 500 μM of lipids. The substrates were kept overnight to form the bilayer on the surface, after which the solution was replaced with phosphate buffer, pH 7.2, 100 mM NaCl. Gramicidin activity was tested by adding 1 μM of protein from ethanolic stock solution.

6.2.4 Analytical techniques

The mean diameter and particle size distributions of DOPC liposomes or proteoliposomes were determined by dynamic light scattering (DLS) using a 90 plus nanoparticle size analyzer (Brookhaven Instruments Inc, NY). Liposome solutions were diluted to an appropriate dilution with buffer and measurement were obtained at 90^{o}. Twenty size determination runs were performed for each sample.

A 15 μL aliquots of samples were deposited on a Formvar grid and stained with 2% uranyl acetate. Transmission electron microscopy (TEM) Images were acquired using JEOL 100CX transmission electron microscope (JEOL USA Inc., NJ).

Microgravimetric analysis was done using a quartz crystal microbalance (QCM) (Research Quartz Crystal Microbalance, Maxtek Inc., Santa Fe Springs, CA) controlled by Maxtek RQCM Data Log software. The piezoelectric quartz crystals with 5 MHz oscillating frequency, was held between two gold electrodes. The QCM electrodes were first cleaned by rinsing with ethanol and drying under the stream of nitrogen. Then the crystals were cleaned using an oxygen plasma cleaner. The cleaned crystals were immediately contacted with ethanolic solution of 5 mM mercaptolipids to form SAM. After SAM formation, the crystal were also used to immobilize PpcA. The crystals ready to analyze were mounted on a crystal holder and changes in frequency changes were monitored after addition of DOPC liposomes.

Ellipsometric measurements were carried out using M-44 rotating analyzer ellipsometer (J.A. Woollan Co. Inc., Lincoln, NE) operated by WVASE32 software. The refractive index and the extinction coefficient values were assumed to be 1.5 and 0 for all measurements. The bilayers were removed from the solution just before the measurements. For DOPC bilayers measurements, the film was modeled as a transparent "Cauchy" layer with *refractive index of* 1.5.

Electrochemical analysis was performed using CHI 660 B and CHI 660 D potentiostat (CH Instruments Inc, Austin, TX). Electrochemical techniques used were cyclic voltammetry (CV) and electrochemical impedance spectroscopy (EIS). For more details about the principles of CV, please refer to earlier chapter. EIS is a nondestructive electrochemical technique, which measures the impedance (the net resistance to current flow offered by the interface) at an applied potential. EIS studies were carried out at a bias DC potential (often a open circuit potential) using small sinusoidal potential within a frequency range of 0.01 to 10,000 Hz. The impedance data for the interface was fitted to a Randles equivalent circuit model which include electrical elements such as capacitors and resistors. (84) The impedance (Z) of the system is represented by:

$$Z(\omega) = \frac{1}{Y(\omega)} = \frac{V}{I}\big(\cos(\theta) - i\ sin(\theta)\big) = Z_r + i\ Z_i \quad \text{.....(Eq. 6.1)}$$

where, Y is the admittance, V is the voltage, I is the current, θ is the phase delay, and ω is the radial frequency. Z_r and Z_i are the real and imaginary parts of an impedance. The impedance data is plotted as real vs. imaginary part of the impedance (Nyquist plot); or as the plot of absolute value of impedance vs. frequency function (Bode plot). Addition of films on the surface

of electrode increases the charge transfer resistance (R_m) of the electrode. With addition of each successive layer, the R_m value increases, which help monitoring the interface formation. The impedance data was analyzed using Z -view software (Scribber Associates, NC).

6.3 Results and discussion

6.3.1 Characterization of DOPC liposomes and microsomes

The TEM data show the formation of DOPC liposomes with particle size of about 100 nm in diameter (Fig 6.1 A). The DLS analysis confirmed the size with mean diameter of DOPC liposomes of 110 ± 4 nm. The proteoliposomes measured by DLS had mean particle size of 170 ± 8 nm. The proteoliposomes showed a tendency to aggregate within hours of formation, therefore only freshly formed proteoliposomes were used to form BRACE.

6.3.2 Characterization of BRACE using QCM

QCM is a routinely used technique to monitor deposition at the solution surface interface. (223, 224) Fusion of DOPC liposomes and its kinetics of its rupture on SAM coated gold electrode to form a bilayer was monitored by QCM . In this method we measured changes in oscillating frequency (Δf) of the crystal due to adsorption of the liposomes. The correlation between Δf and mass of the adsorbed species is give by Sauerbrey equation (225, 226) :

$$\Delta f = \frac{-2\Delta m f^2}{A\sqrt{(\mu \varrho_q)}} = -C_f \, \Delta m \quad \text{.....Eq. 6.2}$$

Where, Δm is the change in the mass, f is the intrinsic frequency of the crystal, μ is the shear modulus, A is the electrode area, and ϱ_q is the density of the quartz.

Figure 6.1 B show plot of Δf over the time after addition of liposomes to the SAM coated gold electrode. The curve display a rapid decrease in frequency followed by a slow increase to a steady-state value of lower frequency. This behavior is characteristic of two phase liposome interaction on the surface. (227) In initial phase, the rapid decrease is due to the adsorption of intact liposomes on the surface of the crystals, resulting in decrease in oscillating frequency. In second phase, the liposomes rupture on the surface to form a bilayer. The resultant release of entrapped water in the liposomes reduces the mass of adsorbed species, resulting in slight increase in the frequency. This trend is consistent with the hypothesis, that liposomes rupture on the SAM surface to form a bilayer, though we cannot completely rule of attachment of some non ruptured liposomes on the surface. Ellipsometric characterization of formed after DOPC addition revealed the deposition of film ~75 A^{o} in thickness, which may also indicate formation of lipid bilayer on the surface.

6.3.3 Electrochemical characterization of BRACE

A representative EIS data of BRACE formed with OmcB proteoliposomes is shown in Figure 6.2A. Formation of BRACE was analyzed by fitting the EIS data to the Randle's modified equivalent circuit model as shown in Figure 6.2B. In this model, the double layer capacitance was replaced with constant phase element to accommodate the hydrophilic and heterogeneous lower portion of BRACE. (228, 229) Z value software was used to calculate the membrane resistance (R_m) values of 1.2 $M\Omega cm^2$ and 1.38 $M\Omega cm^2$ for liposomes and proteoliposomes. The capacitance values were 0.51 $\mu F/cm^2$ and 0.59 $\mu F/cm^2$ for BRACE formed with liposomes and proteoliposomes. In both cases the data represents formation of a highly insulating lipid layer. The membrane resistance increased steadily till 6 hrs and reached a steady state. Therefore

the membranes prepared in all the subsequent studies were kept overnight for formation of stable and insulating BRACE.

Periplasmic cytochrome PpcA, immobilized on a SAM display a redox peak in CV measurements. Addition of ferric nitrilotriacetate (FeNTA) solution to the interface results in increase in the catalytic current of the protein (data not shown). Addition of DOPC bilayer to form a BRACE, does not block the redox interaction of PpcA with the underlying gold electrode. However, addition of Fe NTA solution to the BRACE made with DOPC liposomes does not result in increase of the catalytic current (Fig. 6.3A). This is consistent with the formation of the highly insulating lipid bilayer blocking the access of electron acceptors in solution forming separate compartments on the electrode. Formation of BRACE with proteoliposomes containing OmcB protein did not result in observable change in CV signal of PpcA. This may be due to lower amount of membrane protein OmcB getting immobilized in the vicinity of PpcA. This is consistent with observation that immobilized PpcA do not show observable increase in the catalytic current with soluble electron acceptor like Fe NTA until a threshold level is reached (~200 μM). The concentration of OmcB incorporated in proteoliposomes is much smaller (~ 10 μM). However, the BRACE formed with OmcB proteoliposomes displayed noticeable increase in the catalytic current with Fe NTA in a dose dependent manner (Fig. 6.3B). The membrane resistance values calculated by EIS for the BRACE formed with OmcB were still within the range of highly insulating bilayer (~1 $M\Omega cm^2$). Therefore it is unlikely that Fe NTA would have leaked through the bilayer of BRACE to reach PpcA. The more likely explanation is that Fe NTA is getting reduced by the OmcB protein immobilized in BRACE and exposed to the solution side of BRACE. Our hypothesis is that during the cathodic wave of CV, electrons travel from the gold electrode, to PpcA and from PpcA to OmcB and from OmcB to ferric NTA.

In order to investigate our hypothesis further, we immobilized PpcA^{-heme} protein on SAM using EDC and NHS coupling agent. The BRACE formed with these interfaces did not display any redox peaks associated with the PpcA protein (Fig. 6.4A). Also BRACE formed with OmcB and PpcA^{-heme} did not display any catalytic activity of OmcB with Fe NTA. Thus, the presence of immobilized and active PpcA is crucial to form a electron transport chain in BRACE.

In order to investigate importance of OmcB in BRACE, we replaced OmcB proteoliposomes with OmcBc1 proteoliposomes. The BRACEs formed with PpcA and OmcBc1 proteoliposomes did not display the catalytic current increase with soluble electron acceptor Fe NTA (Fig. 6.4B). This is consistent with the observation that cysteine 1 mutation in OmcB sequence causes it to become redox inactive (please refer to chapter 4). And the redox inactive OmcB protein is incapable of transferring electrons from PpcA to the Fe NTA located on the solution side of the BRACE. Thus in order to transfer electrons form a electron transfer chain in BRACE, both PpcA and OmcB need to be present in the active form.

The feasibility of BRACE to characterize ion channel activity was evaluated using gramicidin. Gramicidin is a pore forming antibiotic utilized to test the ion channel formation activity in bilayer lipid membranes. (230, 231) Gramicidin exists in a dimeric form with monomers in upper and lower leaflet, and once aligned, these monomers assemble to form a ion selective channel across the membrane. (232) Addition of gramicidin to the BRACE lead to channel formation in the lipid bilayer resulting a drop in the membrane resistance from 1.2 to 0.32 $M\Omega cm^2$ (Fig.6.5). Addition of Fe NTA solution to this BRACE did not increase the

catalytic current of PpcA entrapped below the bilayer (data not shown). This observation is consistent with the ion selective nature of the gramicidin channels.

6.4 Implications and future work

The biological cell envelopes have a very complex architecture in terms of chemical nature of the components involved as well as its multilayered structural arrangements. (233, 234) Several different types of lipids, carbohydrates and transmembrane proteins make them very complex and dynamic in nature. Therefore it is extremely challenging to characterize the mechanism of the metabolic processes taking place through them. Membrane proteins associated with the biological membranes play a crucial role in these metabolic processes. (235, 236) Membrane proteins constitute over one third of all proteins encoded by the bacteria, (237) yet very little information is available about the role of individual proteins. Because of the difficulties associated with the study of membrane proteins in the living organisms, it is preferable to study the proteins using *in vitro* platforms. Formation of engineered lipid bilayer membranes facilitates the study of these membrane proteins in a more controlled environment. (238) Hybrid bilayer membrane (HBM) is one of such strategies used to study the membrane proteins on the electrode. (239) In HBM, first a SAM is formed on a gold surface and upper leaflet of the lipid bilayer is added by using liposomes. Such HBM structure has been used to study electron transfer process using redox active small biomolecules ubiquinone and NADH. (240) Other approaches to study electron transfer properties of the membrane proteins are its directional immobilization of proteins on the SAM coated electrode (241) or tethering the protein to electrode keeping it in the lipid environment. (242) All of these well designed strategies often focus on studying only one set of specific proteins or biomolecules. With the design of BRACE, we have gone one step forward, where mimic of cell envelope makes study of ET reaction

occurring through different cell envelope compartments possible. In the inner membrane of biological cell envelope, the ET takes place only through some specific redox moieties. Formation of SAM on the gold electrode blocks the access of electrode to some species in solution, forming a mimic of inner membrane. Immobilization of PpcA on SAM, allows direct electron transfer between protein and electrode, and it thus forms a mimic of periplasmic space. Addition of DOPC liposomes leads to formation of bilayer, and forming an insulating layer between immobilized protein and electron acceptors in solution. The DOPC bilayer thus forms a mimic of outer membrane of the bacterial cell envelope. Addition of OmcB through proteoliposomes, adds the dimensionality of outer membrane cytochromes. The cytochrome protein is capable of embedding in the lipid bilayer. (243) It is possible that immobilized protein PpcA has similar interaction with the deposited liposomes, which might bring the OmcB in the proteoliposomes closer to PpcA in a manner to make ET possible. Because of the low concentration of OmcB in the proteoliposomes, we do not observe a change in CV of immobilized PpcA, but addition of soluble electron acceptor may augment the signal of OmcB. Similar increase of signal was reported for the cytochrome *c* oxidase immobilized on the electrode, where no redox current of cytochrome *c* oxidase was observed, but addition of its redox partner cytochrome *c* in solution led to increase in observable catalytic current. (244) Moreover, with the use of inactivated mutant of OmcB (OmcBc1), we have shown that the increase in the catalytic current is dependent on the activity of OmcB. Furthermore, replacement of PpcA with inactive polypeptide of PpcA also led to diminishing of ET, underlining importance of both the redox proteins in ET through BRACE. Formation of ion channels with gramicidin provides an interesting opportunity to add, small porins to the BRACE to mimic the cell envelope even closely.

Thus we have engineered an electron transport chain on artificially constructed mimic of cell envelope using BRACE. A schematic picture of the BRACE comparing it with the components of *Geobacter* cell envelope is drawn in Figure 6.6. Further structural characterization studies will help in optimization of BRACE formation. Also, more studies about optimization of proteoliposomes addition to maximize the loading of OmcB or outer membrane protein to BRACE will increase its sensitivity.

The BRACE is a generic system that can be used with different membrane cytochromes, or even porins to test hypotheses about electrochemical membrane phenomena in gram negative microbes. The bottoms up approach used in the development of BRACE interface allows us to understand the ET at individual steps and build a more complex interface in sequential manner. Understanding dissimilatory metal reduction is a challenging task. The redox state of metallic electron acceptors depends on many factors including pH, presence of complexing agents, and the reduction potential values. The reduction potential values of U(IV)/U(VI) pair varies from -0.042 to 0.086 V (vs SHE) depending on the presence of Ca^{2+} and CO_3^{2-}. (245) Similarly in the absence of precipitation, the midpoint potential values of Fe^{2+}/Fe^{3+} pair is about 0.77 V (vs. SHE); however at pH values > 3, the iron starts precipitating out of the solution and the redox potential values of Fe^{2+}/Fe^{3+} pairs under the environmental condition changes. Table 6.1 summarizes the redox potential values at pH 7 of species relevant to dissimilatory metal reduction in *Geobacter*. ΔG calculations are assumed on standard condition at pH 7, and for iron minerals, the Fe^{2+} concentration is assumed to be 100 μM. (35) Calculations of the bioenergetics based on the redox potential values can help understand the ET mechanism in DRMs, while the BRACE approach can help test the feasibility of the ET between various redox carriers.

Successful fabrication of the functional, nanostructured biomimetic interfaces described above will enable hypotheses about electron transfer mechanisms in *Geobacter* to be tested, to achieve an improved fundamental understanding of *Geobacter* ET process. The interfaces could also potentially lead to better bioremediation strategies for heavy-metal contamination in the environment.

7.0 CONCLUSIONS

The work presented in this dissertation mainly focused on developing a tool to measure the *Geobacter* ET mechanism in a more controlled, in-vitro environment. We utilized a bottom up approach to develop a nanoscale biomimetic interface necessary for such study using a self assembled monolayer of the lipids on electrodes, immobilized periplasmic protein PpcA, a lipid bilayer mimicking the outer membrane of the bacteria and an outer membrane protein OmcB.

The first objective of this work was to establish feasibility of direct electron transfer (DET) between immobilized periplasmic cytochrome PpcA and the electrode. The *Geobacter* periplasmic cytochrome PpcA was expressed *in E. coli* to facilitate its large scale production necessary for the study. The heterologously expressed PpcA was isolated to obtain the pure protein. The purified protein was capable of DET with the electrode. The ratio of carboxyl to hydroxyl terminated lipids in the SAM used to immobilize the PpcA was found to be crucial for the activity of protein.

In the second part of the study, we analyzed the catalytic activity of the immobilized PpcA using CV. The immobilized protein PpcA facilitated the electron transfer between the electrode and soluble electron acceptor species like iron and uranium salts/chelates. We fitted a literature-validated model to the CV data, and found that the reduction rates by PpcA are higher for uranium salts than iron salts. This observation may help explain why uranium gets rapidly precipitated in periplasmic space of *Geobacter*, where this PpcA cytochrome is present in abundance. We also found that the rotating disk voltammetry technique where the effect of mass transfer limitations is minimized enabling us to extract kinetic data can be used to calculate the ET rate constants between PpcA and soluble metal acceptors.

The third part of the study focused on heterologously expressing the *Geobacter* outer membrane cytochrome of OmcB in *E. coli*. We utilized a variety of molecular biology techniques, with the help of our collaborators, to transform *E. coli* cells with the plasmid carrying OmcB gene from *Geobacter*. Heterologous expression of outer membrane cytochromes in *E. coli* is challenging, because the cytochromes require extensive posttranslational modifications, including heme packaging. Moreover, the protein needs to be transported to the outer membrane and inserted in an active confirmation. We have been successful in expressing this multiheme cytochrome in *E. coli*, and based on the localization experiments such as differential detergent extraction and/or cell fractionation followed by ultracentrifugation, the cytochrome was found to be associated with the outer membrane of *E. coli*. To our knowledge, we are the only group to be successful in heterologous expression an outer membrane cytochrome from *Geobacter* in *E. coli*.

The fourth part of this project focused on using spectro-electrochemical techniques in a optically transparent thin layer electrode (OTTLE) system to analyze electrochemical interactions between the PpcA and OmcB cytochromes. The results revealed that PpcA gave stable and reproducible DET in OTTLE and displayed an easily distinguishable UV spectroscopic signature. No evidence of DET by OmcB was observed in OTTLE. However, the addition of redox mediator (e.g., the humic acid analogue AQDS) allowed spectro-electrochemical characterization of OmcB in OTTLE. Experiments conducted with both PpcA and OmcB co-immobilized in the biomimetic interface showed that PpcA can act as a redox mediator for OmcB and is capable of reducing and oxidizing OmcB. This observation is significant because it supports the hypothesis that PpcA and OmcB are redox partners. A putative mechanism involving these proteins is that PpcA transmits electrons generated in respiration to OmcB, which then transmits the electrons to extracellular electron acceptors or

conductive pili. To our knowledge, this study provides the first evidence of direct electron transfer between these two cytochromes. Also, to the best of our knowledge, we are the first group to study protein-protein electron transfer in OTTLE.

The final objective of this study was to develop a novel biomimetic redox active cell envelope (BRACE) to mimic *Geobacter's* ET pathway with a minimum number of components. The BRACE consisted of an electrode to mimic the intracellular source of electrons, a SAM on the electrode to mimic the inner membrane, a layer of periplasmic cytochrome PpcA to mimic the periplasmic space, a bilayer lipid membrane to mimic the outer membrane and the outer membrane cytochrome OmcB added to the bilayer using proteoliposomes to represent outer membrane cytochromes. The BRACE thus formed was capable of transferring electrons from the electrode through the immobilized PpcA and then through the outer membrane cytochrome OmcB to the electron acceptors in solution. Fabrication of these nanoscale biomimetic interfaces has shown to have a great potential for study of electron transfer between redox proteins *in vitro*. Further characterization of these BRACE platforms can make them suitable for even diverse usage and as an important analytical tool. And the knowledge obtained from these systems can be helpful in devising better bioremediation technologies or designing a better microbial fuel system.

APPENDICES

APPENDIX A

OMCB EXPRESSION AND PURIFICATION

A.1 Detergent solubilization of membrane proteins

Membrane proteins like OmcB are difficult to study because they are generally insoluble in aqueous solution. Because of their high hydrophobicity they are difficult to work with. Moreover, membrane proteins are naturally embedded in or are strongly associated with a lipid bilayer, which is a complex and dynamic environment. Therefore, the biophysical studies of the protein such as circular dichroism, NMR, X-ray crystallography and ligand binding studies are difficult to perform.(157) Detergents are an important tool for studying the membrane proteins. Detergents are amphipathic in nature with a lipid tail group and a polar head group. Above a threshold concentration of detergents, called critical micelle concentration (CMC), the detergent self associate and form micelles. Above the CMS, the detergents are capable of solubilizing lipids and membrane proteins. (158) The head group of protein can impart cationic, anionic or zwitterionic properties to the detergent, and in general has stronger influence about its interaction with protein. While the tail group of detergent determine CMC. (159) We attempted solubilization of heterologously expressed OmcB with a variety of detergents at different concentration. The list of name of the detergents and concentrations is give in table A.1. Unfortunately, none of the conditions tried could result in the stable solution of the protein.

Change of the host cell was tried as a mechanism to get better solubility of expressed protein. Instead of BL21 (DE3) *E. coli* cells, Origami2^{TM} and Origami B^{TM} cells were used. Origami strains carry mutation in thioredoxin reductase and glutathione reductase gene, which result in better disulfide bond formation in cytoplasm resulting in higher active protein.(160) Origami B cells are derivative of Bl21 cells. The origami cells were transformed with pEC86 plasmid, and were selected on chloramphenicol plates. The selected cells were grown and made electrocompetent using previously published protocols.(161) The competent cells were

electroporated with OmcB plasmids, to transform the DNA in Origami cell lines. The transformed cells were selected on media containing amp and cmp. The colonies were picked and used for production of OmcB. However the OmcB expressed in these host cell line didn't have better solubility profile.

A.2 Transmission electron microscopy (TEM) of *E. coli* cells

Possibility of inclusion body formation due to overexpressed recombinant protein was tested by TEM. 1 mg/ml suspension of *E. coli* was fixed with gluteraldehyde in 50 mM phosphate buffer and post fixed wit Osmium tetroxide. The post fixed samples were dehydrated with a series of alcohol solutions, infiltrated and embedded with Araldite resin. Sections were taken with glass knife and ultrathin sections were taken with microtome. The ultrathin sections were mounted on the grid and images were taken using a transmission electron microscope (TEM, JEOL 100CX, Peabody, MA) operated at 50 K, 67 k, 100 K, and 200 K accelerating voltage. The *E. coli* cells expressing OmcB did not show any deposits in the periplasmic space ruling out formation of inclusion body type complexes (Fig. A.1).

A.3 Addition of maltose binding protein affinity tag

Maltose-binding protein (MBP) is one of the most popular fusion protein tag added to protein to aid in the affinity purification of protein with gentle elution conditions.(162) Another advantage associated with MBP fusion protein is that it aids in increasing solubility of the overexpressed protein. pMAL^{TM} protein fusion and purification system uses the pMAL vectors designed to insert the target gene results in an MBP fusion protein. pMAL p5G vector was chosen because of its ability to deliver the fusion into the periplasmic space. pMAL p5G vector and OmcB genes were cut with NdeI and EcoRI restriction enzyme and the cut vector and insert

were ligated together. The ligation product was transformed with DH5 α cells and purified plasmid was used to co transform BL 21 cells. The SDS PAGE of the cells showed a band at expected molecular weight of 125 kD (~ 84 kD for OmcB+ 42 kD for MBP) in induced cells. The cells were harvested and the membranes were separated by the method described previously. The fusion protein was found to be membrane associated (Fig A.2). However the fusion protein was still very resistant to solubilization by detergent treatment.

A.4 Gel filtration column chromatography under denaturing conditions

Chaotropic salts like urea were utilized to solubilize OmcB under denaturing condition. The OmcB protein was purified by gel filtration column chromatography using a superdex 200^{TM} column. The flow rate was 1 ml/min. The elution was monitored by UV and the fractions were collected and subjected to SDS PAGE. The fractions with OmcB mol size were pooled together and renaturation was attempted by lowering the concentration of urea. (Fig.A.3) However the yield of this method was unsatisfactory and the renaturation of the protein was not easy to verify without the knowledge of structural characteristic information (like circular dichroism spectra) available.

APPENDIX B

FIGURES AND TABLES

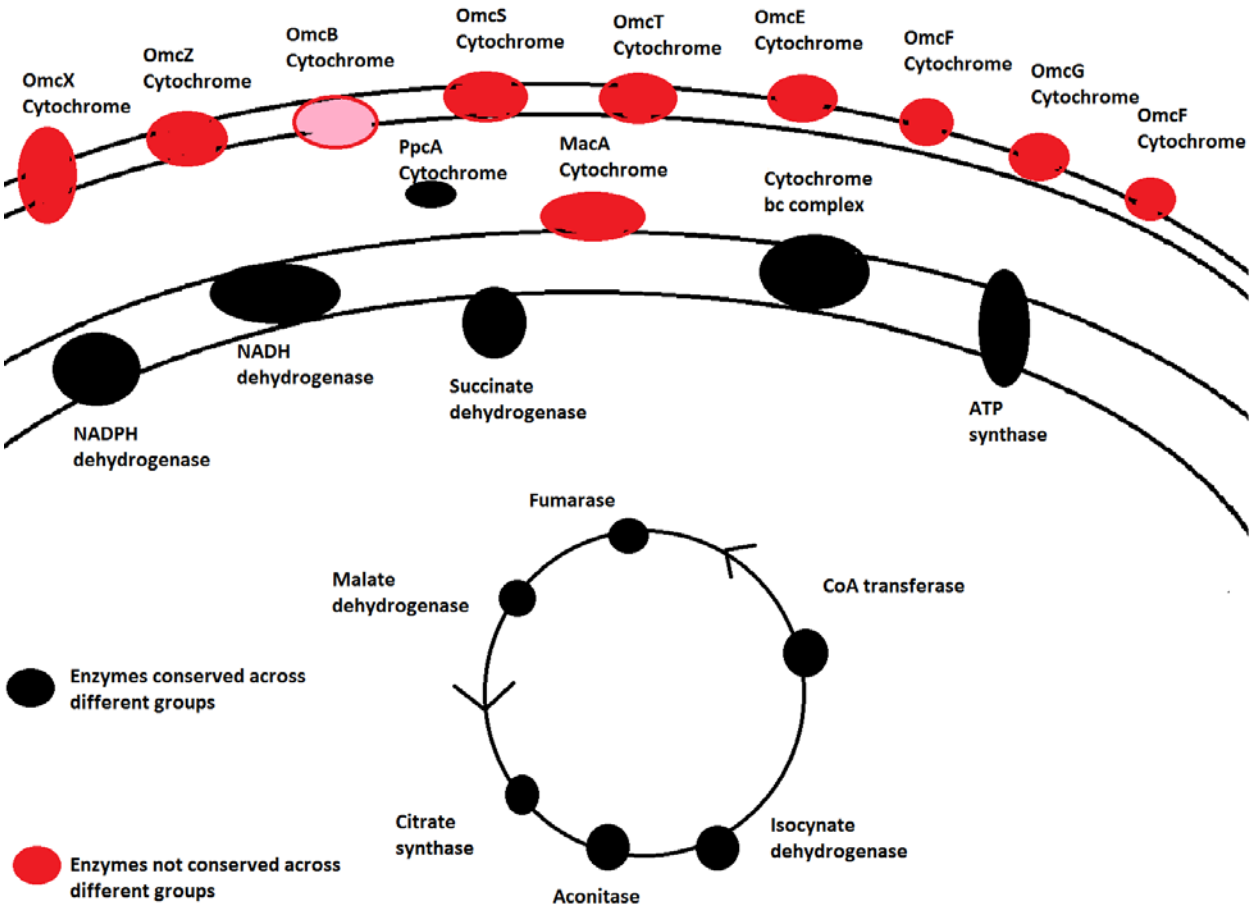

Figure 1.1: The pathways of energy metabolism conserved across different species of *Geobacter*.

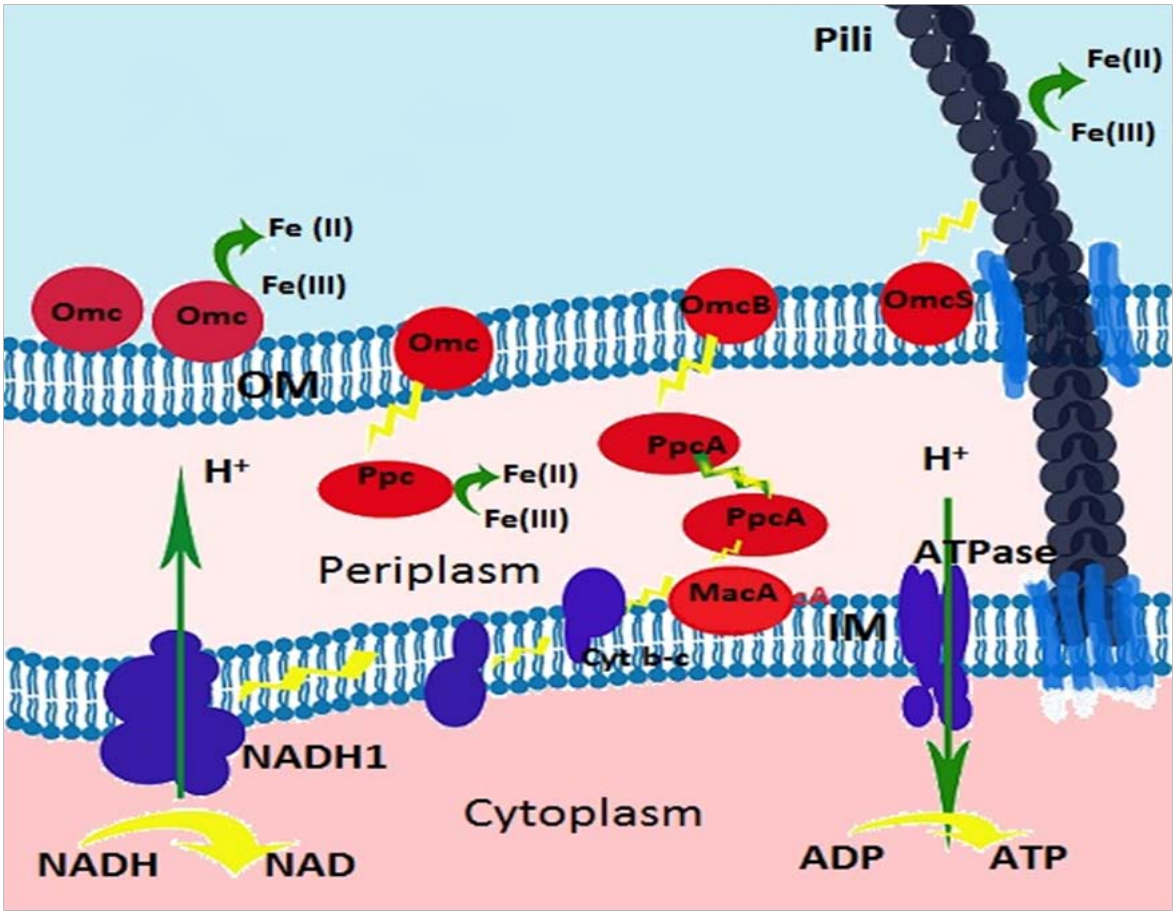

Figure 1.2: The model for dissimilatory metal reduction by *Geobacter*. Energy is conserved by proton pumping across inner membrane. Electron transfer across the cell membrane takes place.

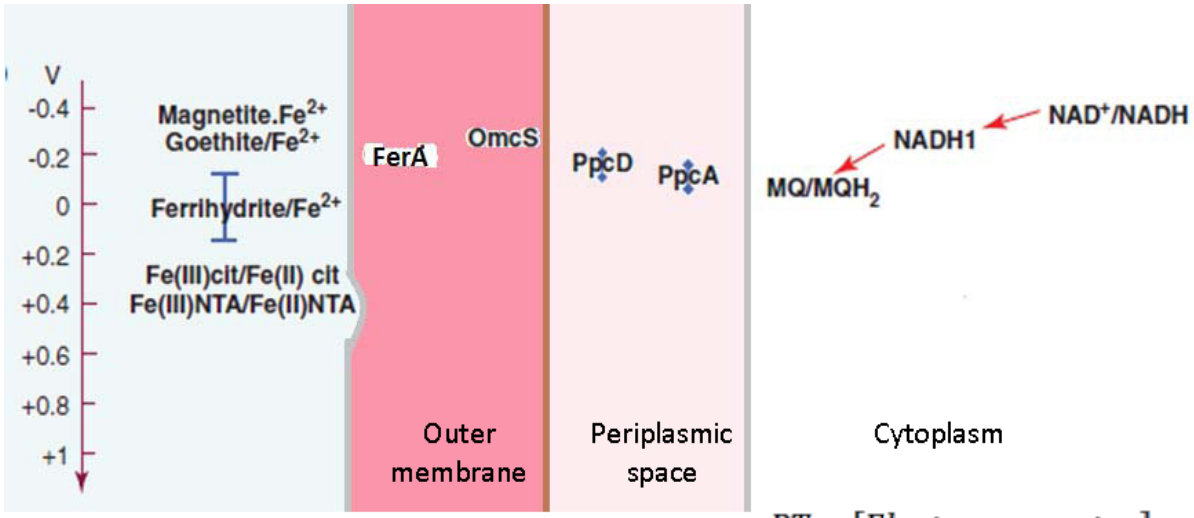

$$\Delta G = -nF\,\Delta E \qquad E = E^{o} + \frac{RT}{nF}\ln\frac{[Electron\ acceptor]}{[Electron\ donor]}$$

Figure 1.3: Transfer of electron across bacteria along the potential gradient. Redox potential of many outer membrane protein is yet unknown.

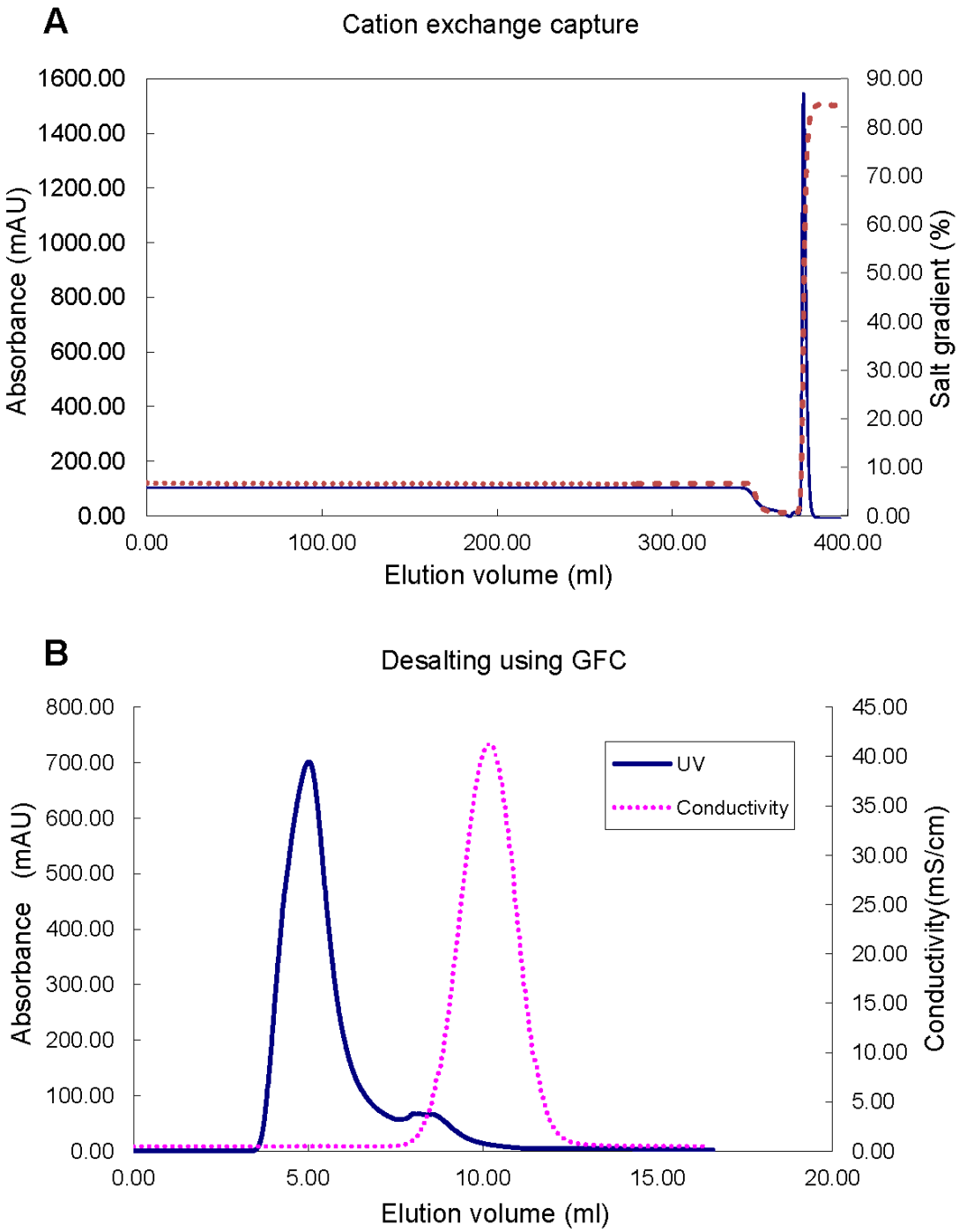

Figure 2.1: A. Chromatogram of PpcA capture step from the periplasmic fraction using cation exchange resin. Protein is eluted with a step gradient in salt concentration.

B. Chromatogram of PpcA desalting by buffer exchange using gel filtration column. Protein is elutes first (monitored by UV signal) followed by salt (monitored by conductivity).

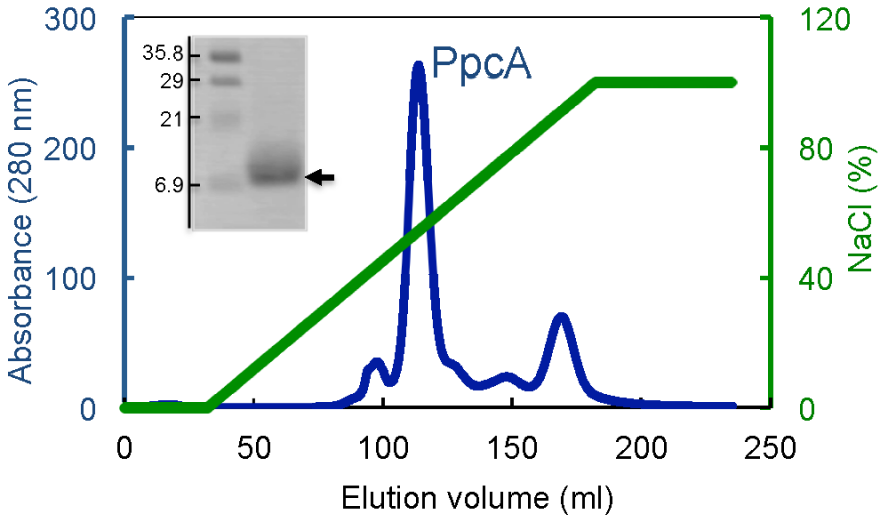

Figure 2.2: Purification of recombinant PpcA using cation exchange chromatography with a NaCl gradient. Inset, SDS-PAGE of PpcA elution peak containing the 9.6 kDa PpcA protein (arrow). Numbers at left are molecular weight markers in kDa.

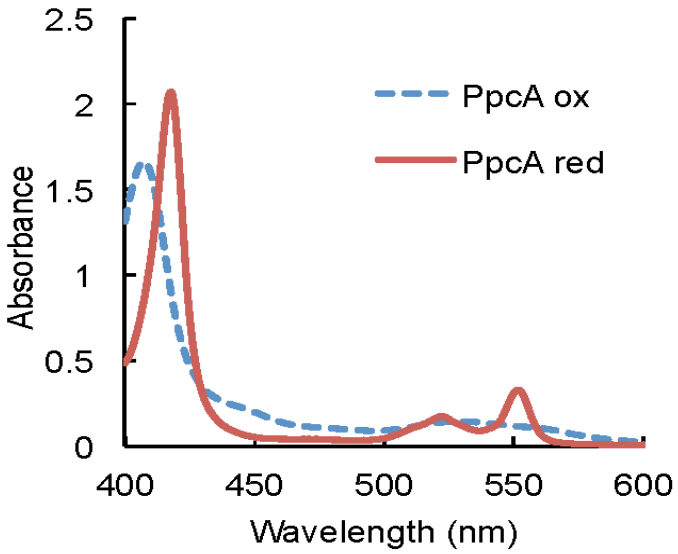

Figure 2.3: Dithionite-reduced minus oxidized spectra of recombinant PpcA protein in Tris buffer (pH 8.0) showing three absorption bands at 420, 522, and 552 nm wavelengths that are typical of *c*-type cytochromes.

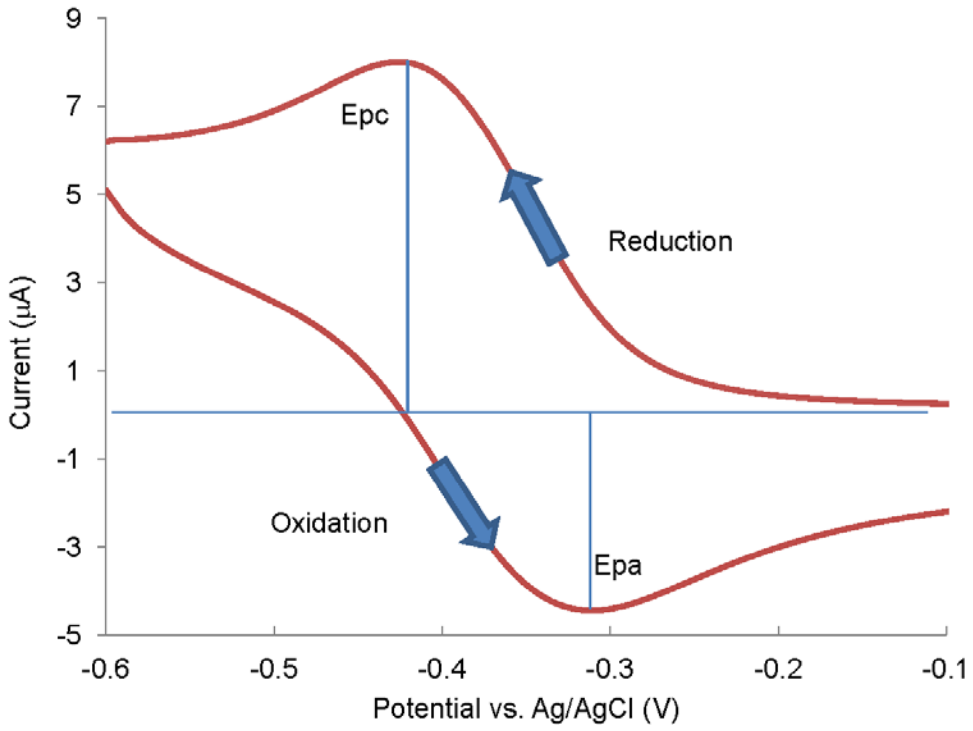

Figure 2.4: CV of PpcA in solution at SAM covered gold electrode. Cathodic current is plotted positive and anodic current is plotted negative. From the average of cathodic and anodic peak, the midpoint redox potential is calculated.

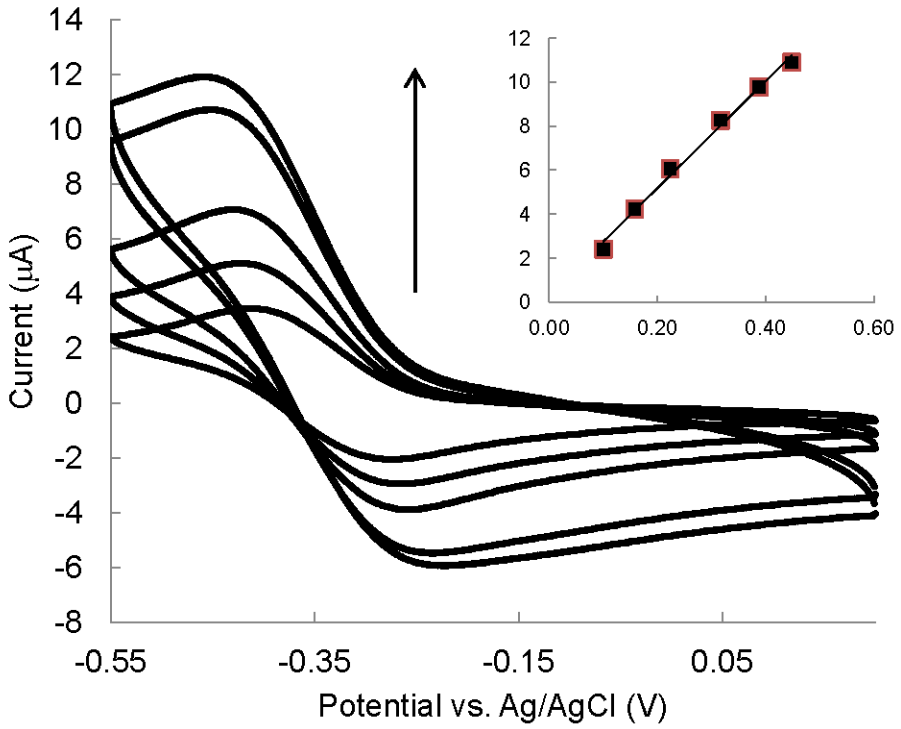

Figure 2.5: Cyclic voltammograms of PpcA in solution on a SAM coated gold electrode at increasing scan rates (arrow) of 10, 25, 50, 100, 150, and 200 mV/s (B). Inset shows the linear correlation between the cathodic peak current and the square root of scan rate for the PpcA at electrode**.**

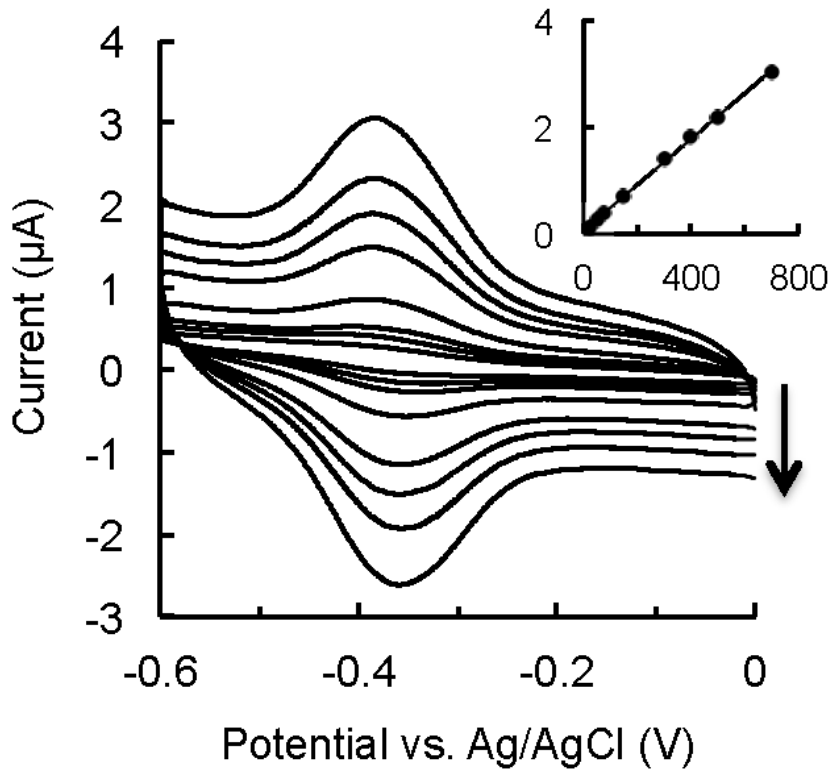

Figure 2.6: A. Cyclic voltammograms of PpcA immobilized on a SAM-functionalized gold electrode at increasing scan rates (arrow) of 25, 50, 75, 150, 300, 400, 500 and 700 mV/s **B.** Inset shows the linear correlation between the cathodic peak current and the scan rate for the PpcA biomimetic interface**.**

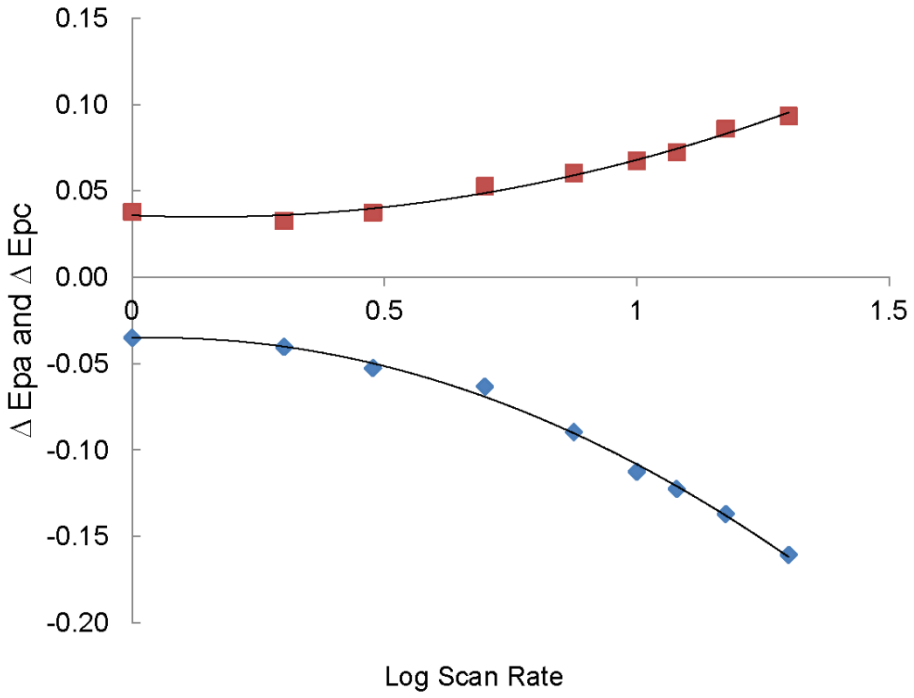

Figure 2.7: Trumpet plot obtained from the change in cathodic and anodic peak potential at various scan rates in CV experiments. The data is fitted to Laviron model to get the ET rate constants for the protein and electrode

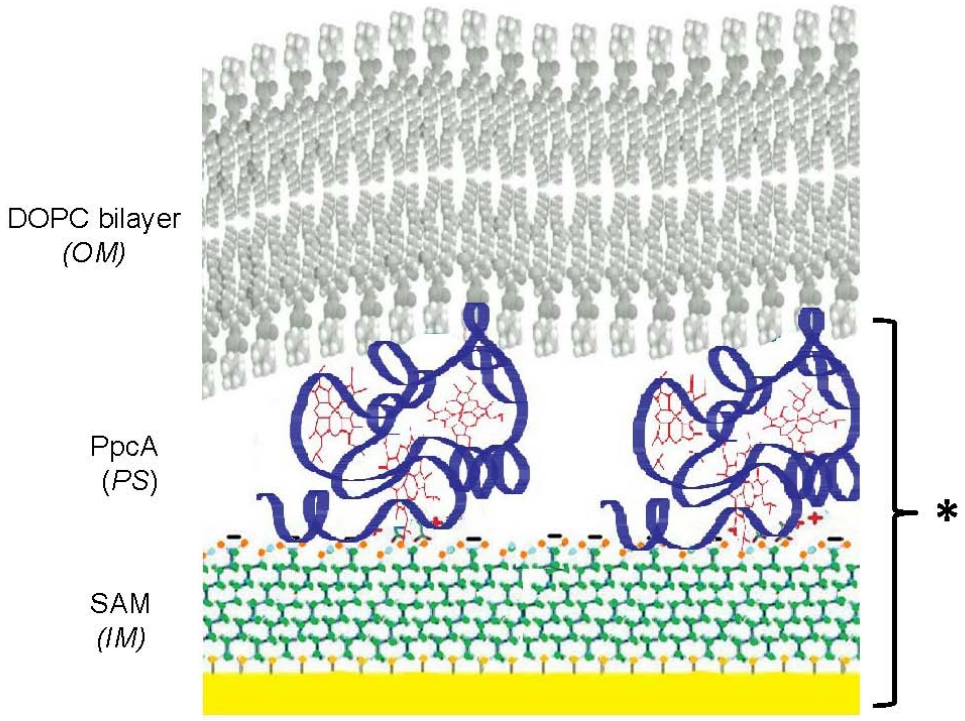

Figure 3.1: Conceptual design of the biomimetic interface. The SAM covered gold electrode serves as a mimic of an inner membrane (IM), the immobilized protein PpcA serves as a mimic of periplasmic space (PS), and the DOPC bilayer is a mimic of an outer membrane (OM).

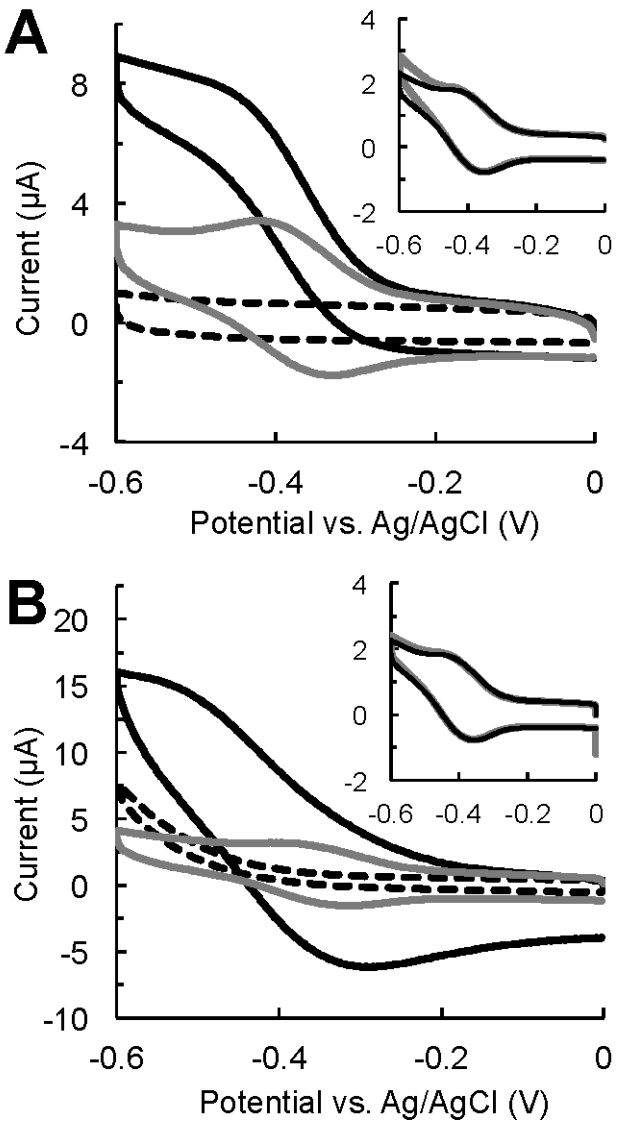

Figure 3.2: Cyclic voltammograms of PpcA interfaces in the presence (black) or absence (grey) of 200 μM Fe-NTA (A) or U acetate (B) collected at a scan rate of 500 mV/s. Insets show similar CV curves but using DOPC interfaces (PpcA interface covered with a DOPC synthetic lipid bilayer) with (black) or without (gray) 600 μM Fe-NTA (**A**) or 400 μM U acetate (**B**).

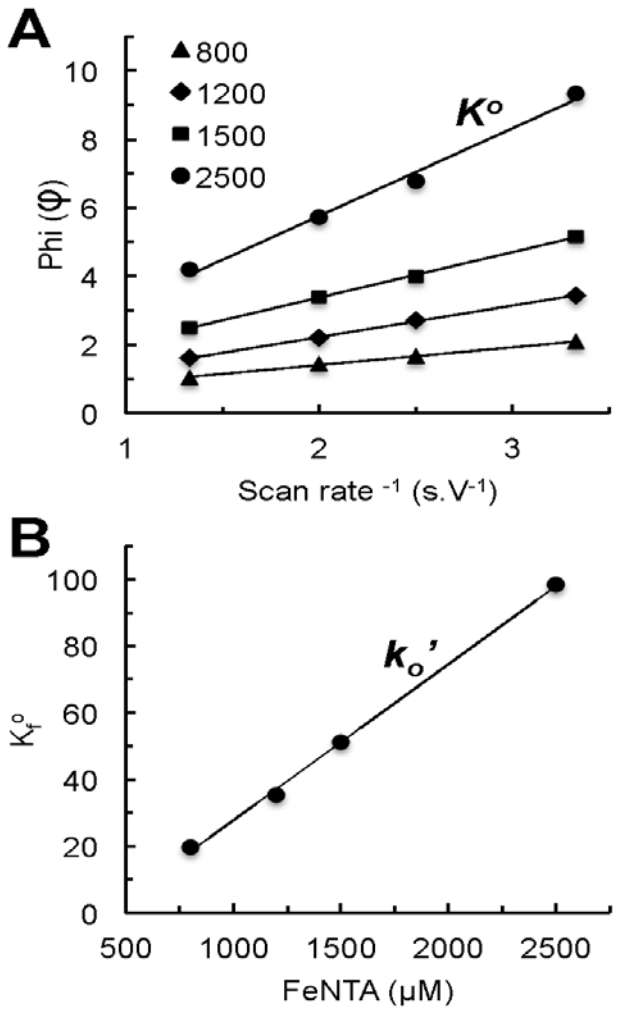

Figure 3.3: Calculation of second order rate constants k_o' for Fe-NTA reduction by cyclic voltammetry**. (A)** Linear plot between kinetic parameter (phi, φ) and the inverse of the scan rate (V/s) for Fe-NTA concentrations between 800 and 2500 μM (legend). The slope of the regression line (K^o) was used to calculate the K_f^o constant using Eq. 1, described in the Materials and Methods. (**B**) Linear correlation between the K_f^o constant and the Fe-NTA concentration, whose slope corresponds to the second order rate constant k_o'.

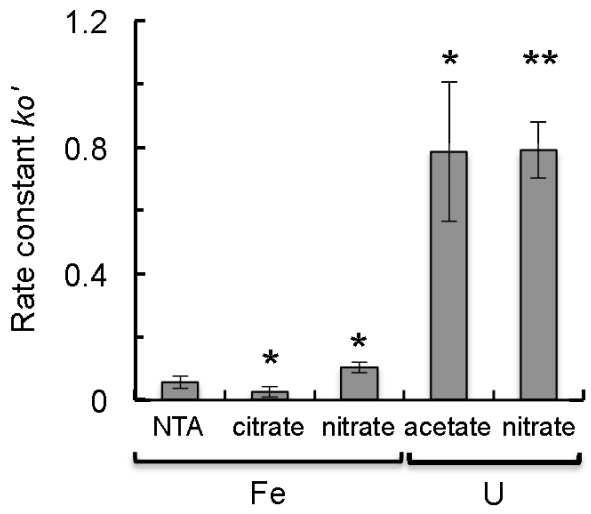

Figure 3.4: Rate constant values (k_O') of PpcA immobilized on SAM-functionalized gold electrodes for different iron and uranium electron acceptors calculated from CV curves**.** Significant differences ($p < 0.05$ or < 0.005) in *t*-test pairwise comparisons with Fe NTA are indicated with one or two stars, respectively.

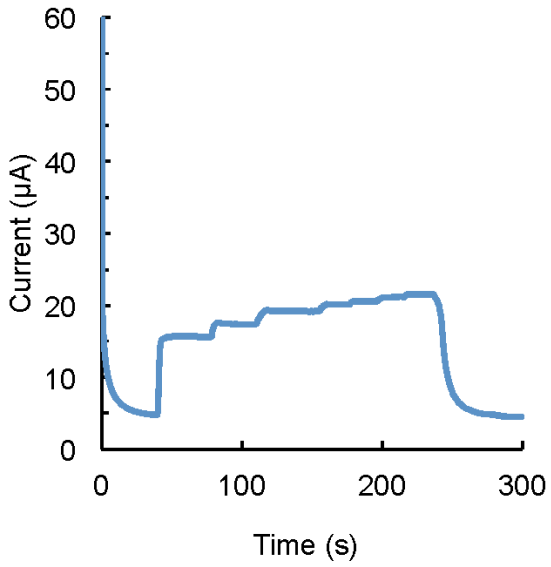

Figure 3.5: RDE voltammogram of PpcA immobilized on a SAM-functionalized gold electrode in the presence of 400 μM Fe-NTA at different rotation speeds (200, 400, 800, 1200, 1500, 1800 and 2200 rpm). The electrode potential was maintained at -500 mV against Ag/AgCl.

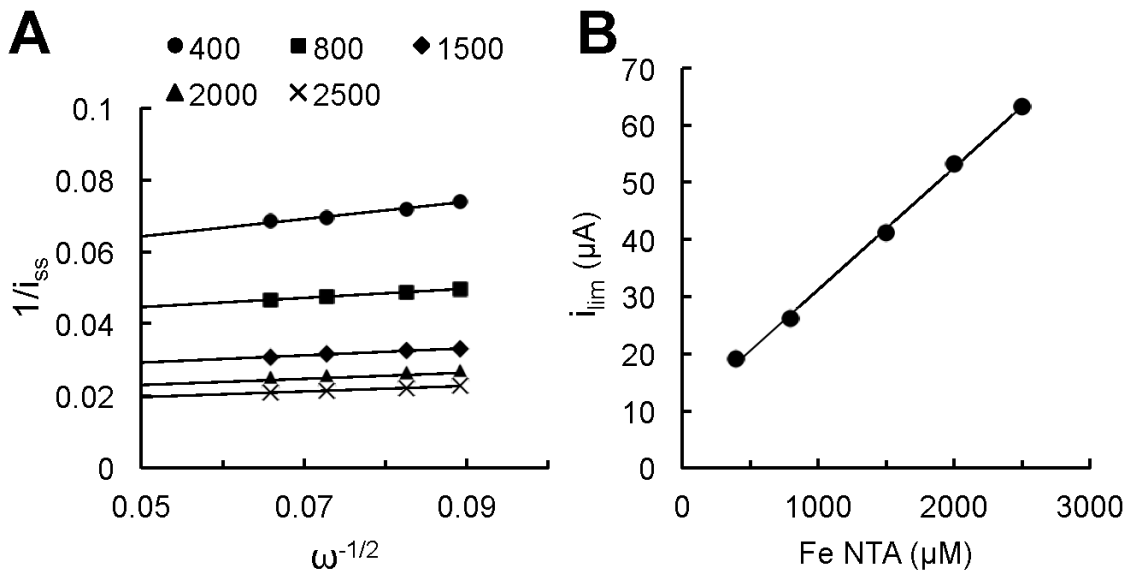

Figure 3.6: (A) Linear correspondence between cathodic currents (reverse of steady state current values or i_{ss}) of PpcA immobilized on a SAM-functionalized rotating disc gold electrode and the rotations speed ($\omega^{-1/2}$) for different concentrations of Fe-NTA (in μM). **(B)** Linear correspondence between limiting current (i_{lim}) calculated from **(A)** and Fe-NTA concentration used to calculate the second order rate constant value k_o'

Table 3.1: k_o' values for different metal acceptors obtained by cyclic voltammetry and rotating disk electrode method.

Metal species	**k_o' from CV ($x10^6$ $M^{-1}s^{-1}$)**	**k_o' from RDE ($x10^6$ $M^{-1}s^{-1}$)**
Ferric NTA	0.056 ± 0.020	0.052 ± 0.010
Ferric citrate	0.025 ± 0.010	0.012 ± 0.001
Ferric nitrate	0.103 ± 0.100	0.061 ± 0.010
Uranyl acetate	0.786 ± 0.180	ND[a]
Uranyl nitrate	0.990 ± 0.240	ND

[a] Not determined

Figure 4.1: OmpA-OmcB Amino acid sequence. Peptide sequences identified by MS are highlighted in blue. MS identified 23 unique peptides for OmcB in 151 total spectra. 380 out of 742 amino acids identified resulting in 51% coverage.

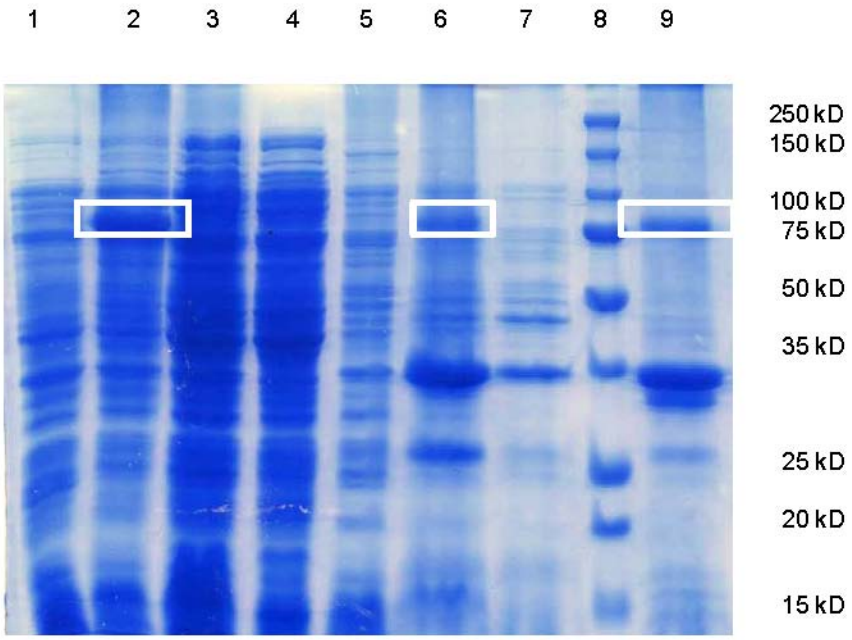

Figure 4.2: SDS PAGE profile of OmcB expression and cell fractionation. Lane 1and 2 are fermentation media samples normalized for cell density at 3 hrs and 18 hrs after inoculation. Lane 3 and 4 are crude and clarified cell lysate. Lane 5 is supernatant of ultracentrifugation step, lane 6 is membrane pellet. Lane 7 is supernatant of ultracentrifugation after sarkosyl detergent extraction and lane 9 is OM fraction lane 8 is a molecular weight marker with molecular weights shown on right in kD.

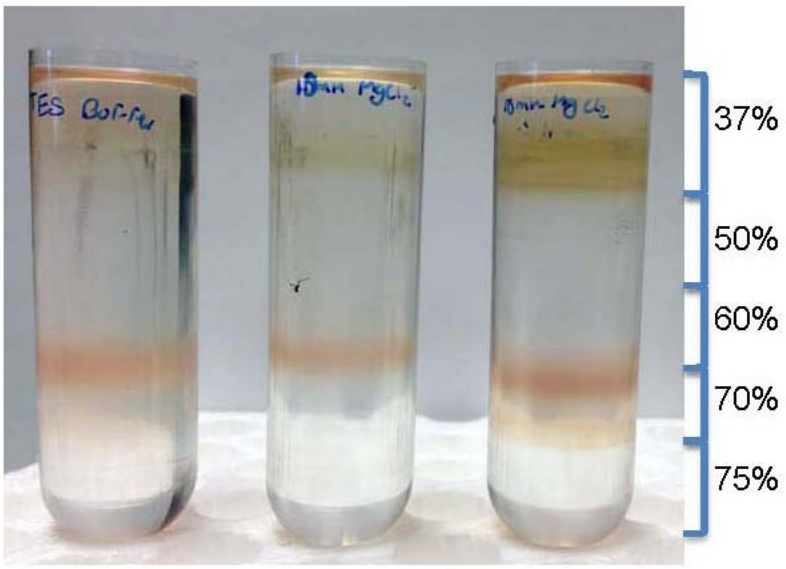

Figure 4.3: Ultracentrifugation with sucrose density gradient separates OmcB membrane fractions based on buoyant density. IM fractions are retained in 37% sucrose band, while OM fractions are located at intersection of 60 and 70% sucrose.

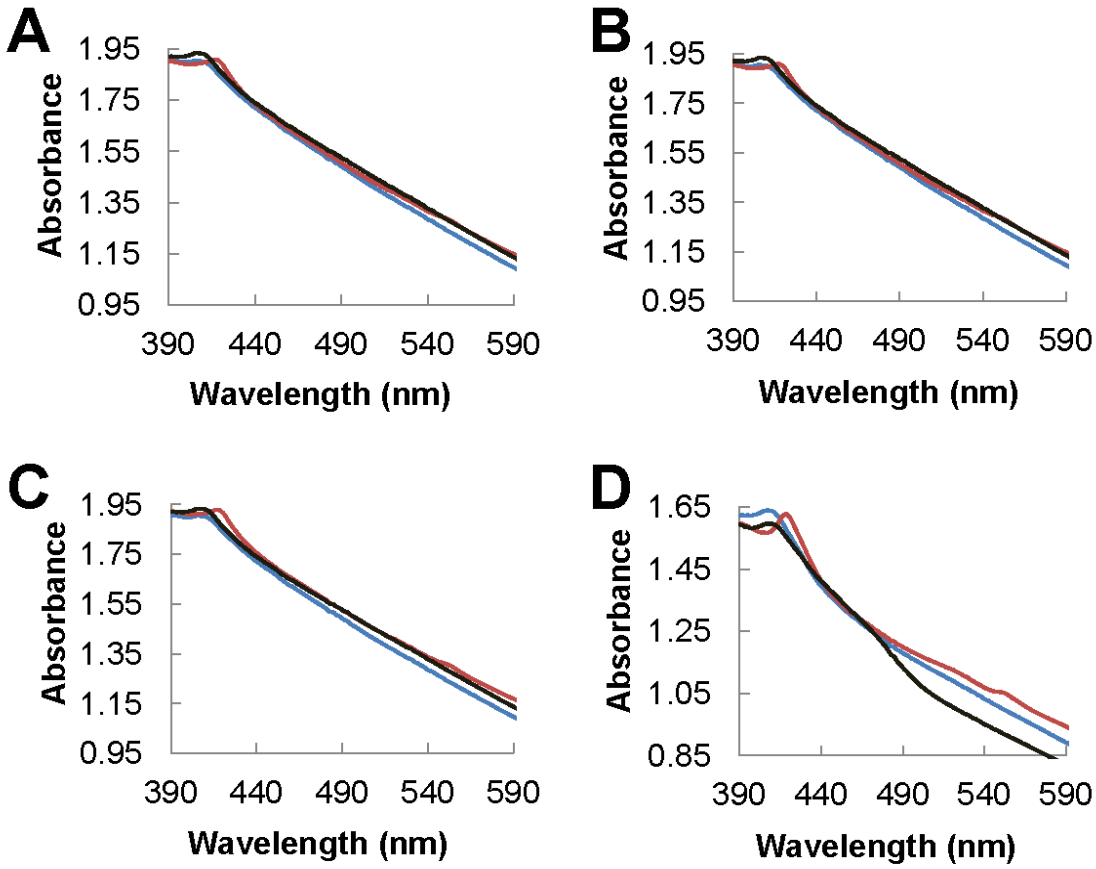

Figure 4.4: Whole cell spectroscopy of *E. coli* BL21 cells expressing OmcB. Blue line is spectra is air oxidized cells at ~ 1 mg/ml. Red Spectra showing Soret peak at 420 nm is spectra of sodium dithionite reduced cells, in some spectra the α peak at 552 nm is visible. Black spectra is spectra of reoxidized cells (observed by shift in Soret peak) with A. FeNTA, B. ferric citrate, C. riboflavin and D. ferric oxide particles.

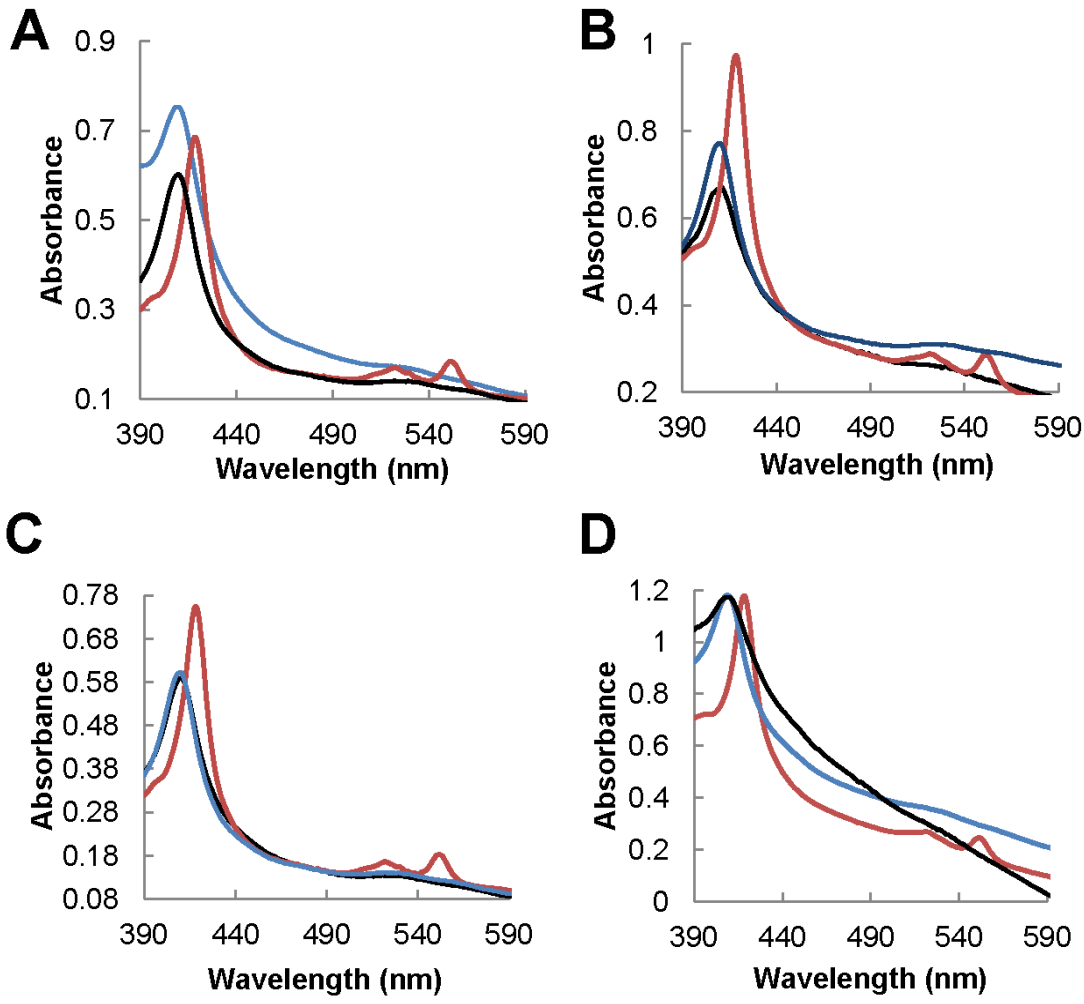

Figure 4.5: OM fragments containing OmcB reduced different metal samples. Blue spectra is air oxidized OmcB samples, red spectra is sodium dithionite reduced OmcB, and black spectra is OmcB reduced with **A.** FeNTA, **B**. Ferric citrate, **C**. UA, and **D**. Ferric oxide particles.

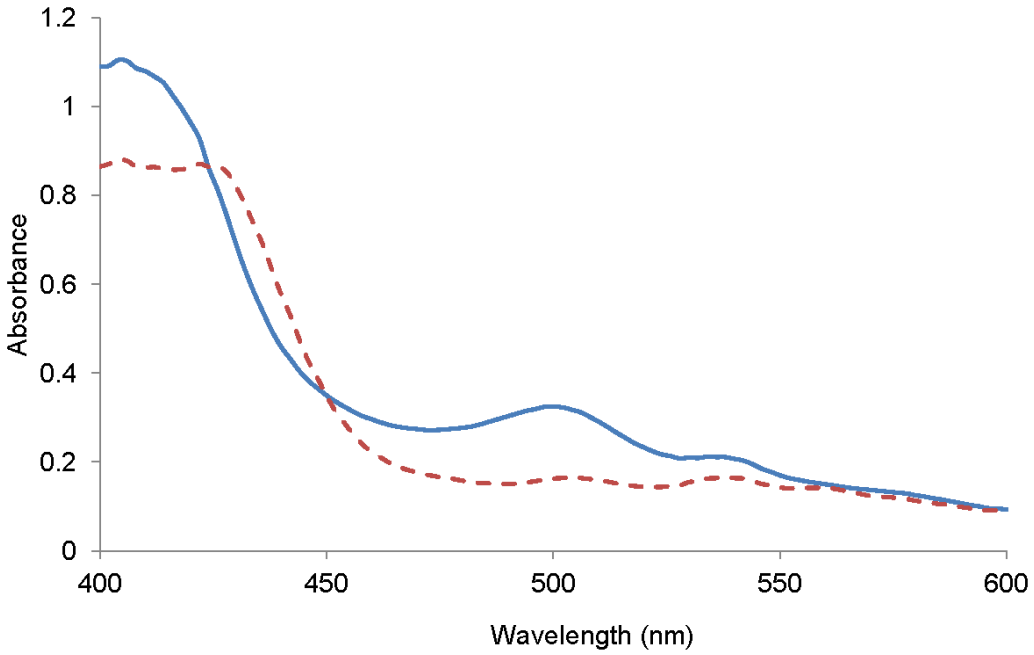

Figure 4.6: Cysteine mutation at 1 cysteine to alanine affected redox property of the OmcB. Spectra of oxidized (solid line) and sodium dithionite reduced (dashed line) OmcBc1a mutant showed peaks not related to cytochrome c protein.

Table 4.1: List of different plasmids used for OmcB expression in *E. coli.*

Primer	Sequence	Plasmid
OmpA-OmcB 5’ NdeI	5’-ACCATATGAAAAAGACAGCTATCGCGATTGCAGTGGCACTGGCTGGTTTCGCTACCGTAGCGCAGGCCTGCGGCTCCGAAAACAAGGA-3’	pET21c C-His6
OmcB XhoI 3’ His fusion	5’-GTAAGTCTCGAGCGGACGGGTCGTGCCGAGGTA-3’	
OmcB 5’ NcoI	5’-AATACCATGGGCTCCGAAAACAAGGAGGGGAC-3’	pET22b C-His6
OmcB 3’ XhoI	5’-ATATCTCGAGCGGACGGGTCGTGCCGAGGTAG-3’	
OmcB Cys mut 5’	5’-GTAGCGCAGGCCGCCGGCTCCGAAAAC-3’	pET21c C-His6 mut
OmcB Cys mut 3’	5’-GTTTTCGGAGCCGGCGGCCTGCGCTAC-3’	

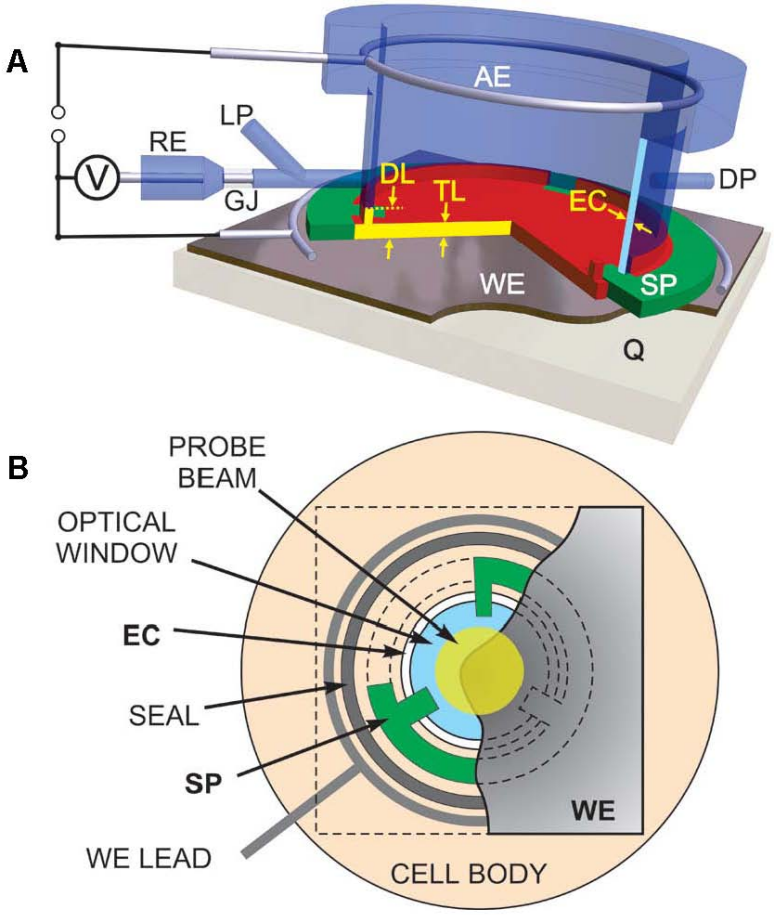

Figure 5.1: A. **Schematic diagram of an OTTLE cell.** The spacer (SP) separating the transparent window and the working electrode (WE) forms a thin layer (TE), which determines the volume of the cell. The counter or auxiliary electrode (AE) is connected to the TL via a small capillary containing supporting electrolyte (EC). Reference electrode (RE) is loaded through the loading port (LP). **B.** Schematic picture of the working electrode.

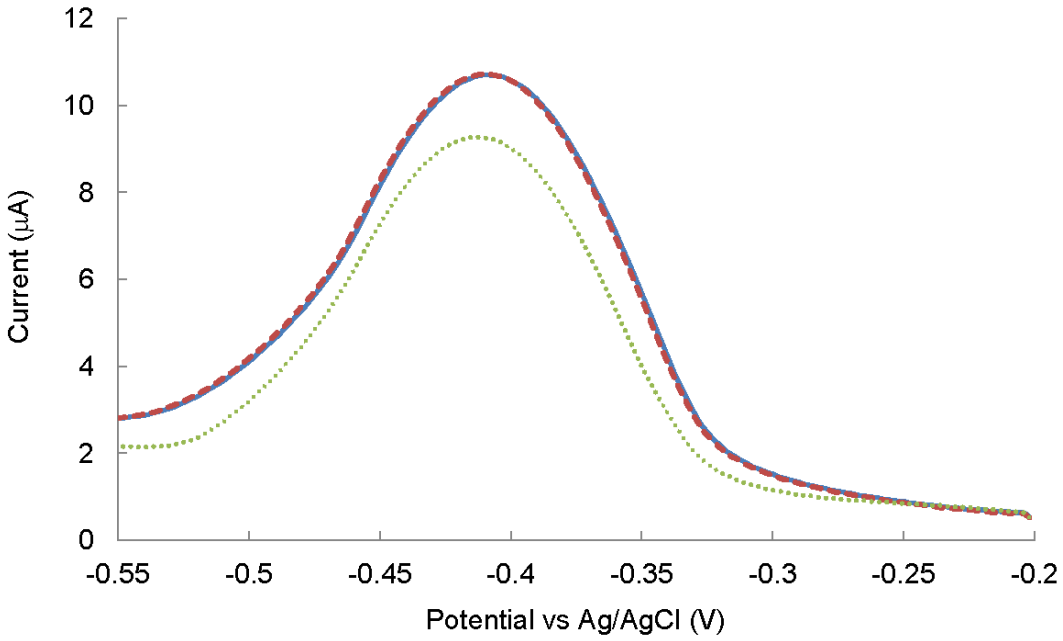

Figure 5.2: **Square wave voltammogram of PpcA adsorbed on SAM coated transparent gold electrode**. The protein response was stable for 6 hr (Solid line 1 hr and dashed line 6 hr), and the peak current decreased around 20% after 24 hr (dotted line).

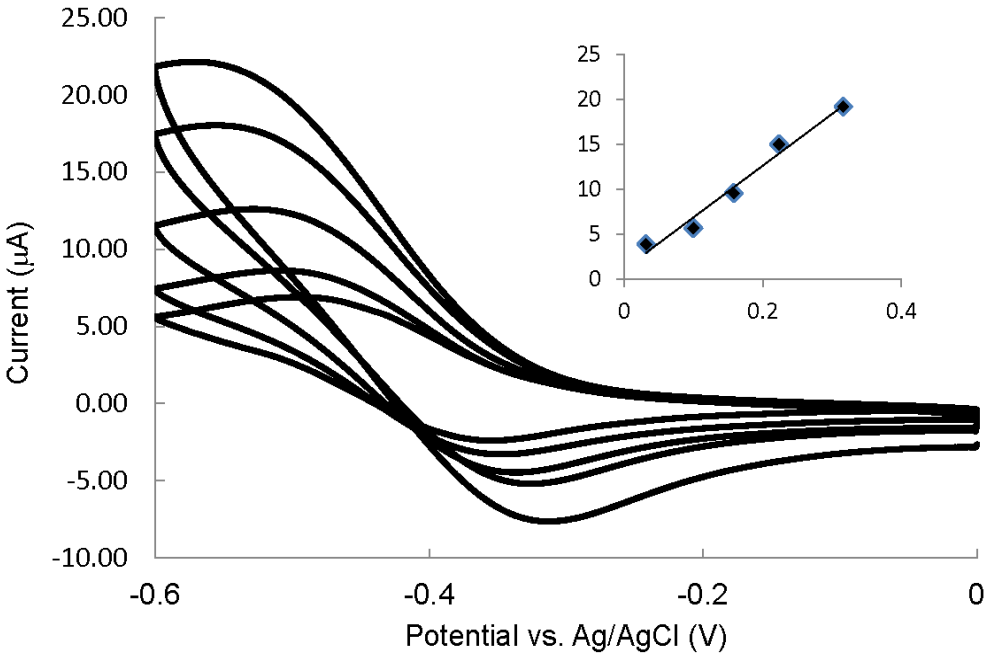

Figure 5.3: A. Cyclic voltammograms of PpcA in solution on a SAM coated gold electrode at OTTLE with increasing scan rates of 5, 10, 25, 50, and 100 mV/s **B.** Inset shows the linear correlation between the cathodic peak current and the square root of scan rate for the PpcA at the OTTLE**.**

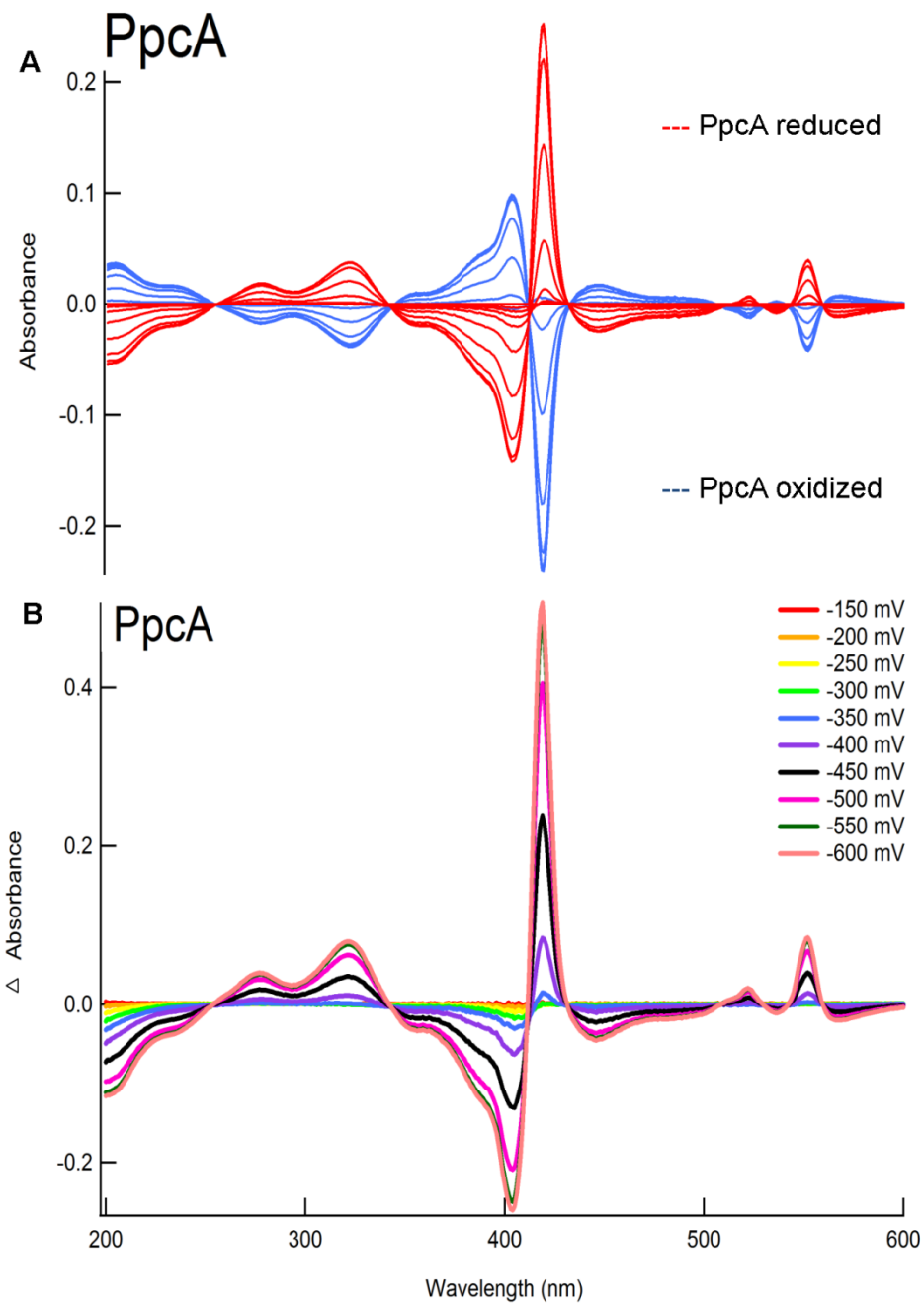

Figure 5.4: UV-vis spectroscopic response of PpcA at the OTTLE (A) Difference absorption spectra oxidized (blue) and reduced (red) PpcA **(B)** Reduced minus oxidized spectra of PpcA at different electrode potentials (vs. Ag/AgCl) showing wavelengths of interest that can be monitored as a function of redox state.

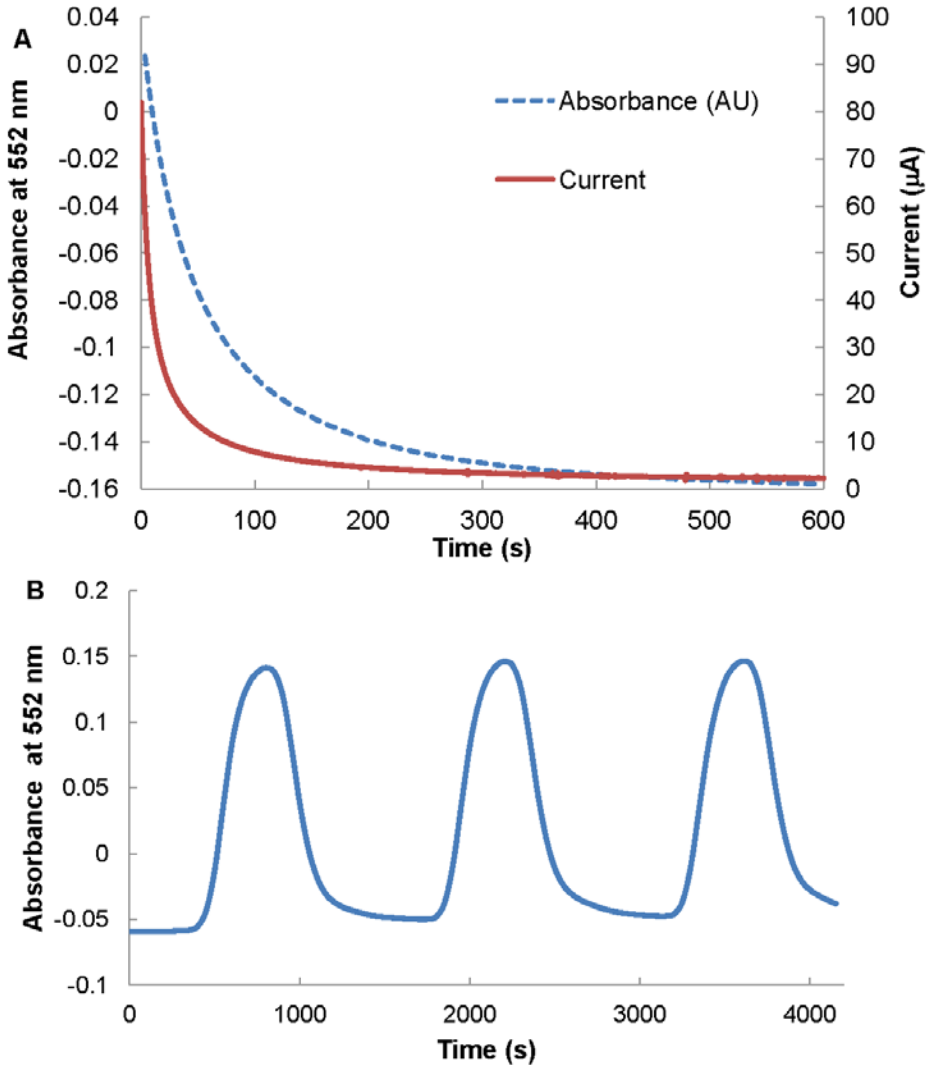

Figure 5.5: A. Chronoamperometry of PpcA at OTTLE. Kinetics of the decrease in absorbance at 552 nm follow the reduction current decay. **B.** Reproducibility of PpcA reduction at the SAM coated OTTLE show reversible and stable response of cytochrome.

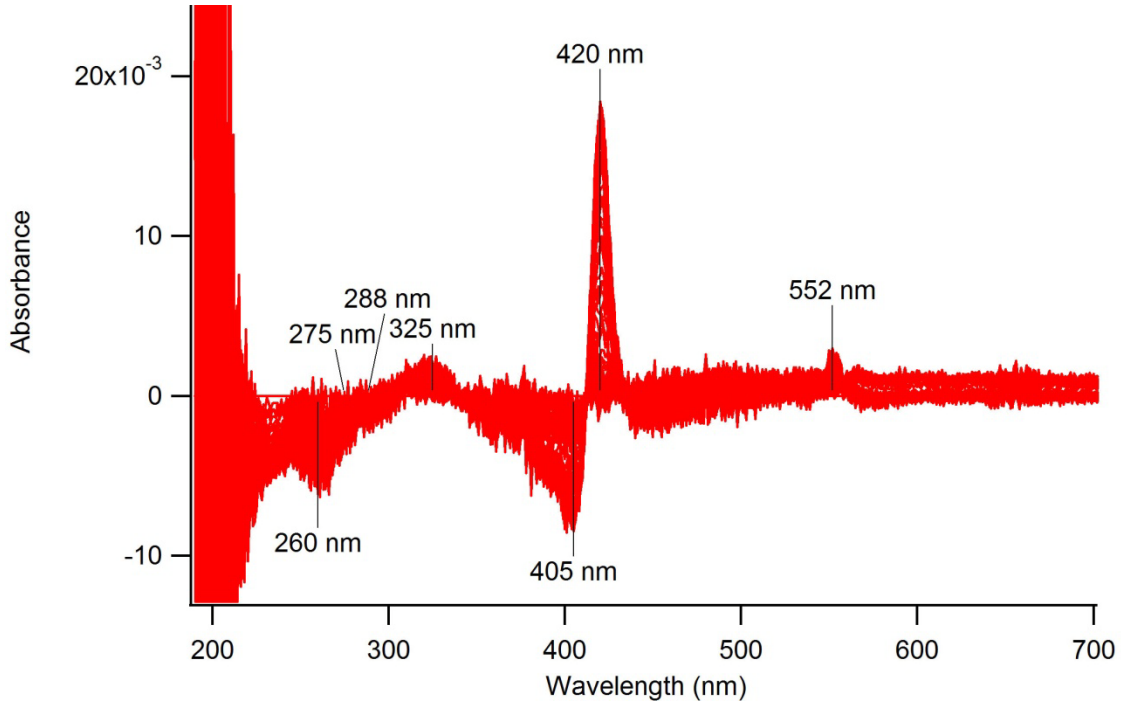

Figure 5.6: Subtraction spectra of OmcB with mediator (AQDS 50 μM) at OTTLE during the CV run at 1 mV/s. Changes in absorbance at wavelengths characteristic of cytochrome *c* proteins are observed.

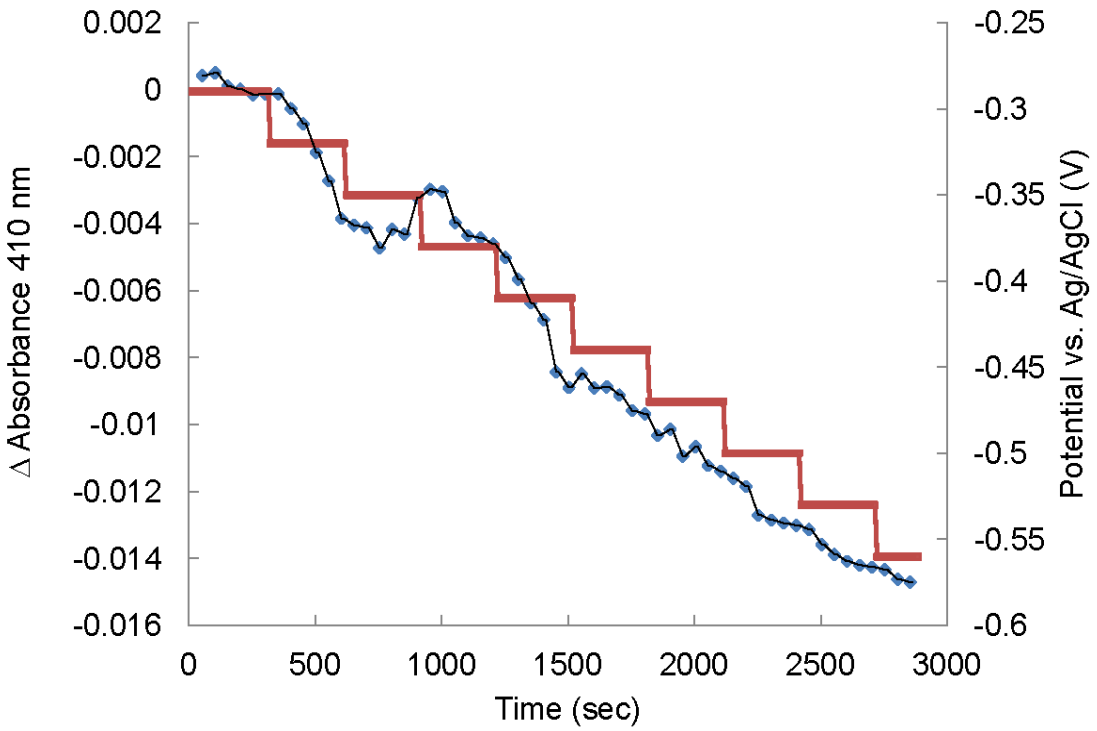

Figure 5.7: Spectroelectrochemical characterization of OmcB heme potentials using redox mediators. Change in the absorbance at 410 nm (square marker) is followed as a function of the potential (red steps). Clustering of the absorbance data at particular electrode potentials may be contributed by resolution of individual heme groups.

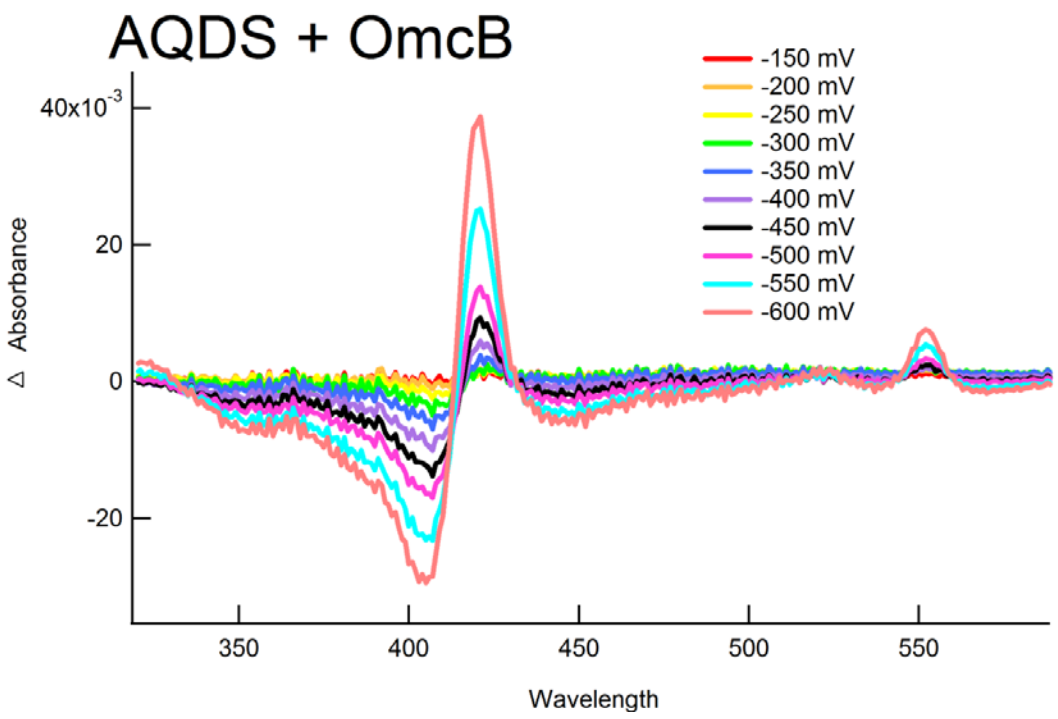

Figure 5.8: AQDS mediated reduction of OmcB membrane vesicles at OTTLE monitored by spectroscopic technique. Potential of electrode was shifted in increments of 50 mV and held at that potential for 180 sec.

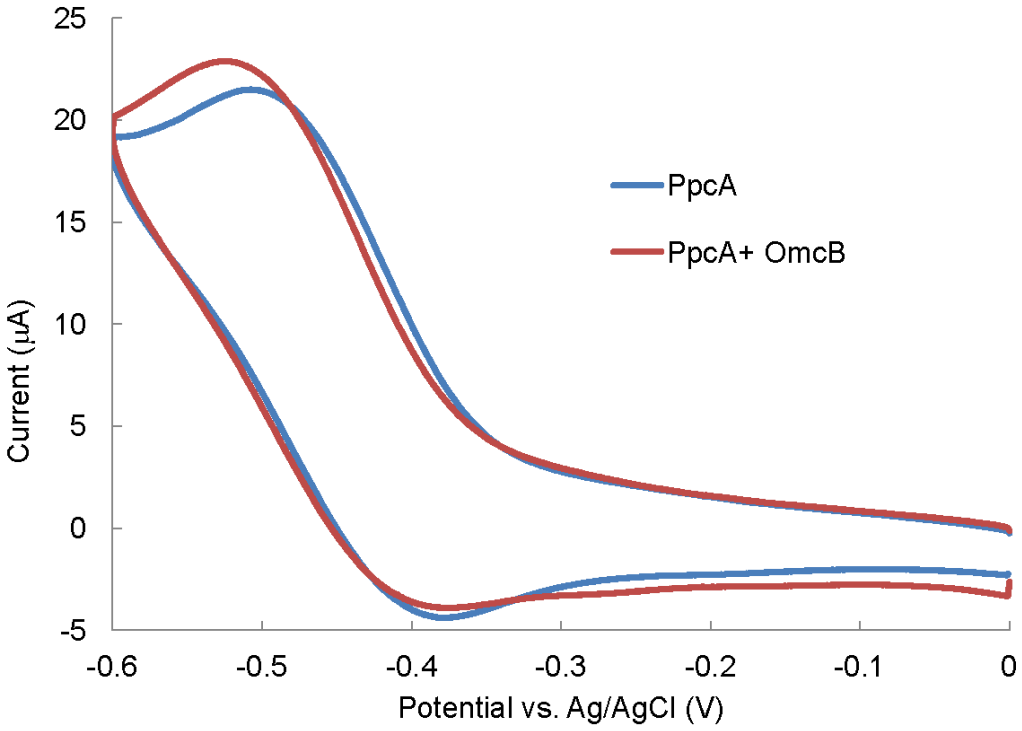

Figure 5.9: Cyclic voltammogram of PpcA with and without OmcB membrane vesicles at 50 mV/s. A small increase in the reduction current of the protein may be due to transfer of electrons from PpcA to OmcB.

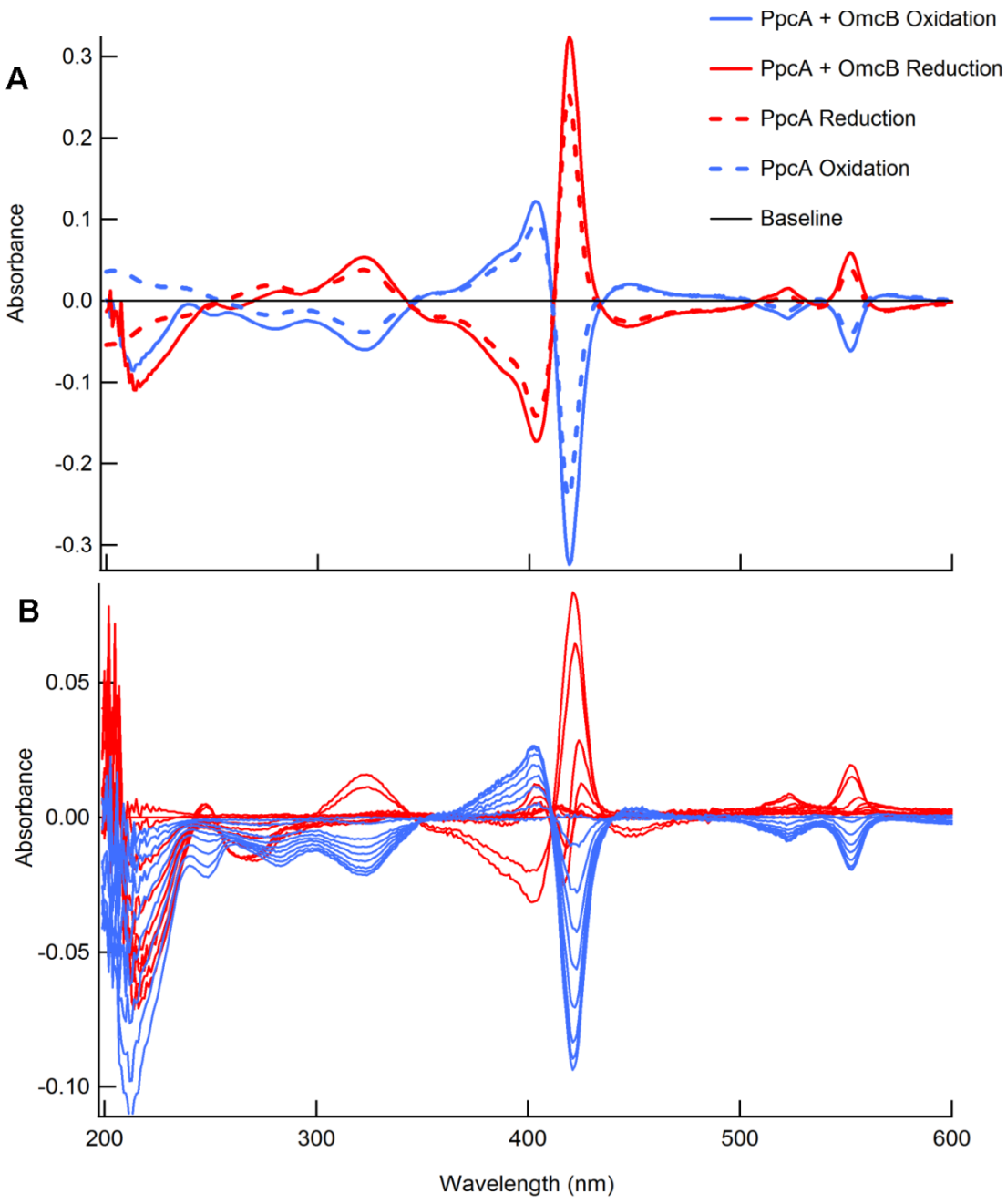

Figure 5.10: Spectroscopic response of OmcB reduction mediated by PpcA. **A**. Spectra of reduction and oxidation of PpcA with and without OmcB membrane vesicles.

B. Redox spectra of OmcB obtained from subtracting spectra of PpcA from the spectra of both proteins together in multipotential step voltammetry.

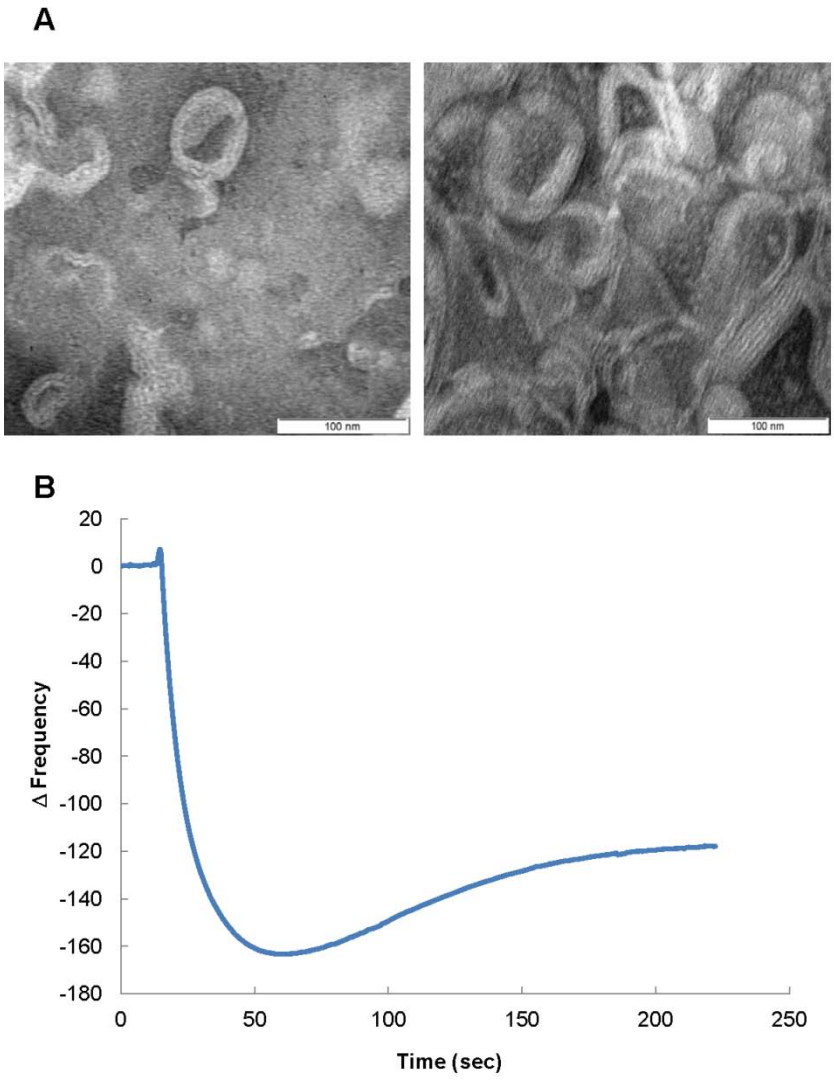

Figure 6.1: A. TEM images of DOPC liposomes prepared by sonication, taken with JEOL transmission electron microscope with accelerating voltage of 270 K.

B. QCM study showing formation of lipid bilayer on the SAM. Attachment of liposomes to the substrate, initially decreases the vibrational frequency. Rupture of liposomes to release trapped water increases the frequency.

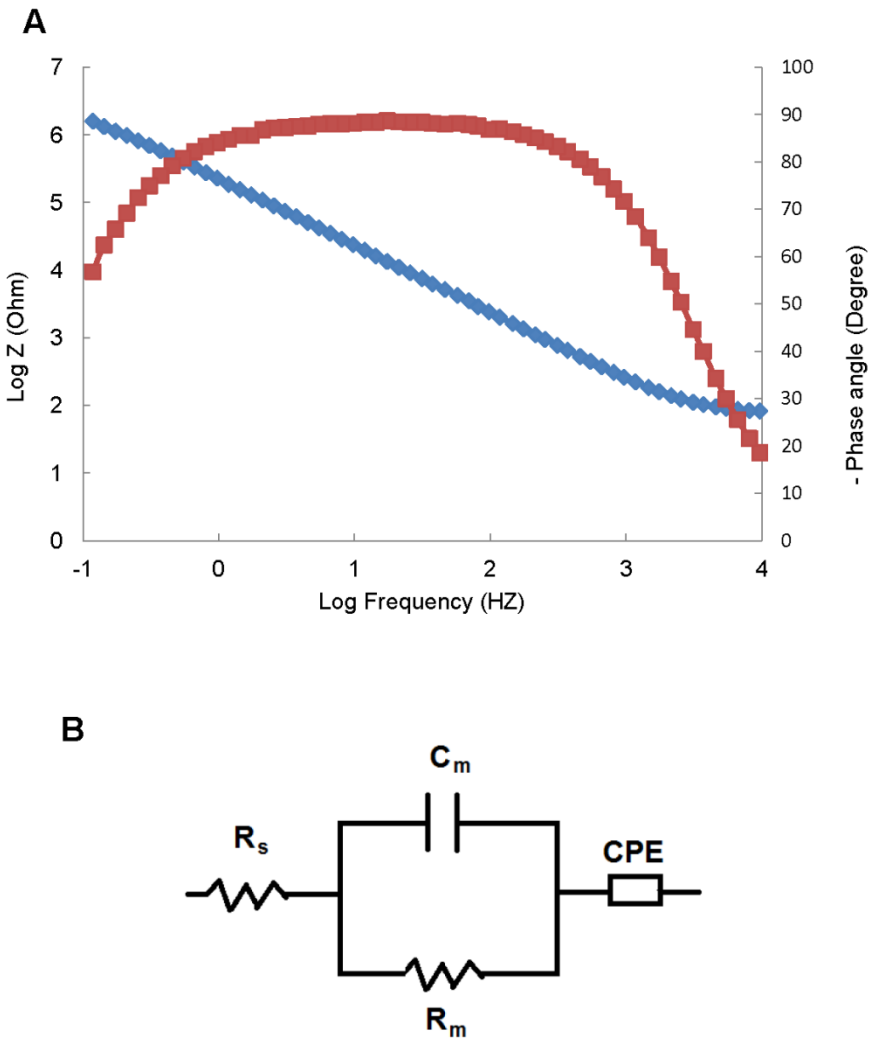

Figure 6.2: A. The phase angle and log z data plotted against log frequency for the bilayer made from proteoliposomes. The data was fitted to the equivalent circuit model shown in figure B.

B. Randles equivalent circuit model used to fit EIS data to calculate the values of electrochemical properties. R_S is the solution resistance, C_m is the capacitance of the membrane, R_m is the resistance of membrane and CPE represents the constant phase element.

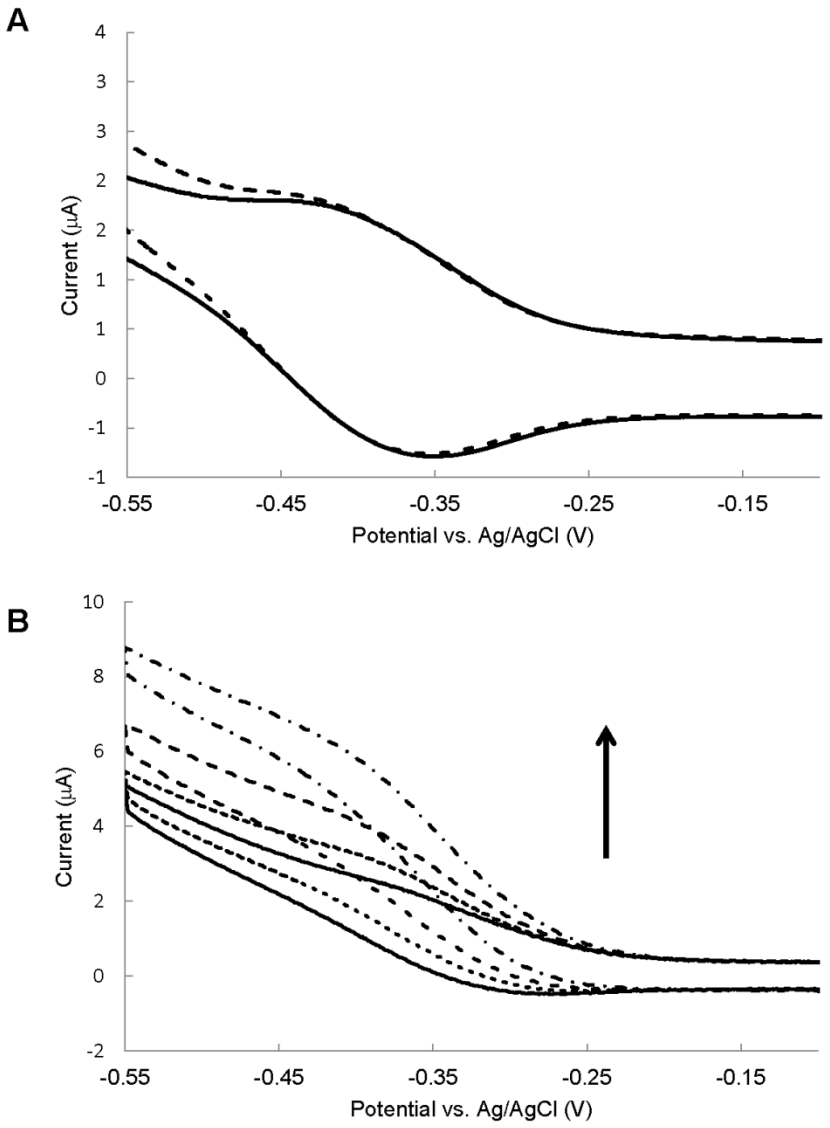

Figure 6.3 A. CV of BRACE formed with PpcA and DOPC bilayer. The redox peak of PpcA is noticed (solid line), and addition of soluble electron acceptor Fe NTA (1mM) into solution does not increase the reduction current (dashed line), indicating formation of a blocking layer. **B.** CV of BRACE formed with PpcA and OmcB proteoliposomes. The redox peak of PpcA is evident (solid line), addition of Fe NTA increased the catalytic current in a dose dependent fashion: 1 mM (dotted line), 2 mM (dashed line) and 3 mM (dashed and dotted line).

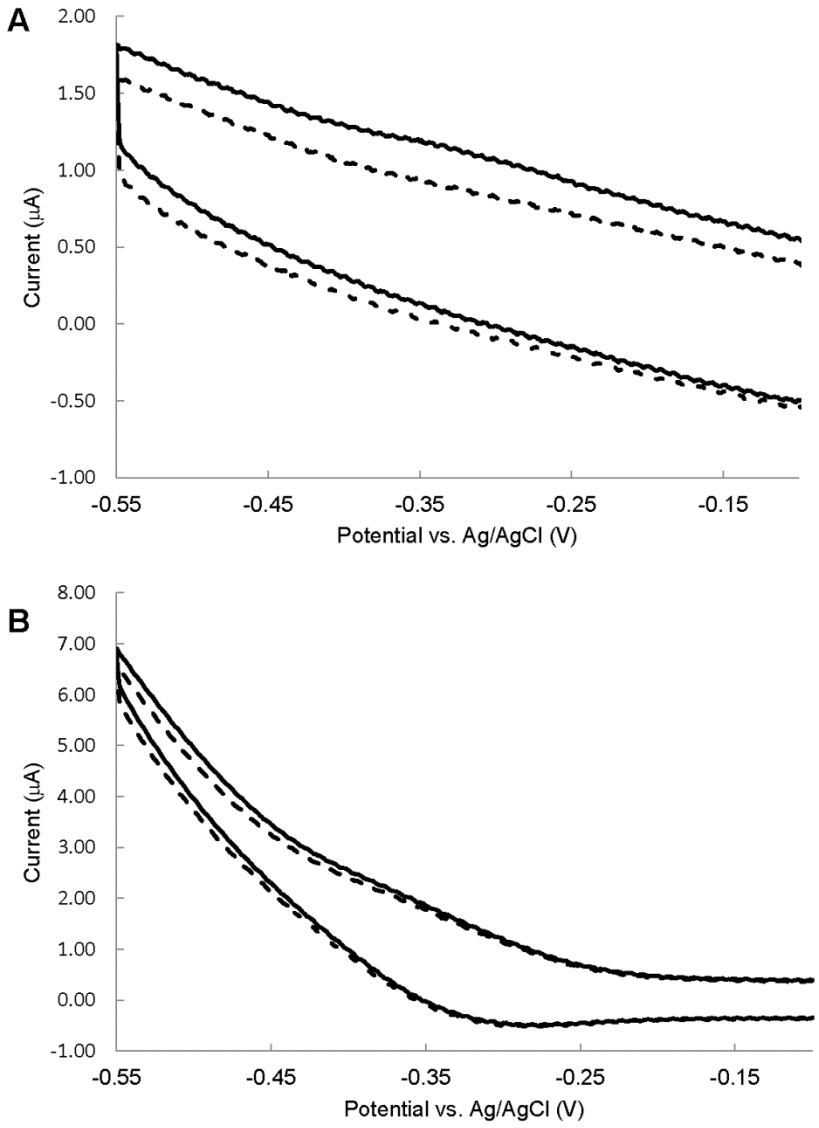

Figure 6.4 A. CV of BRACE formed with PpcA^{-heme} and OmcB proteoliposomes.

The redox peak of PpcA is absent (solid line), and addition of soluble electron acceptor Fe NTA (1mM) into solution does not increase the reduction current (dashed line). **B.** CV of BRACE formed with PpcA and OmcBc1 proteoliposomes. The redox peak of PpcA is evident (solid line), but addition of Fe NTA into solution does not increase the reduction current.

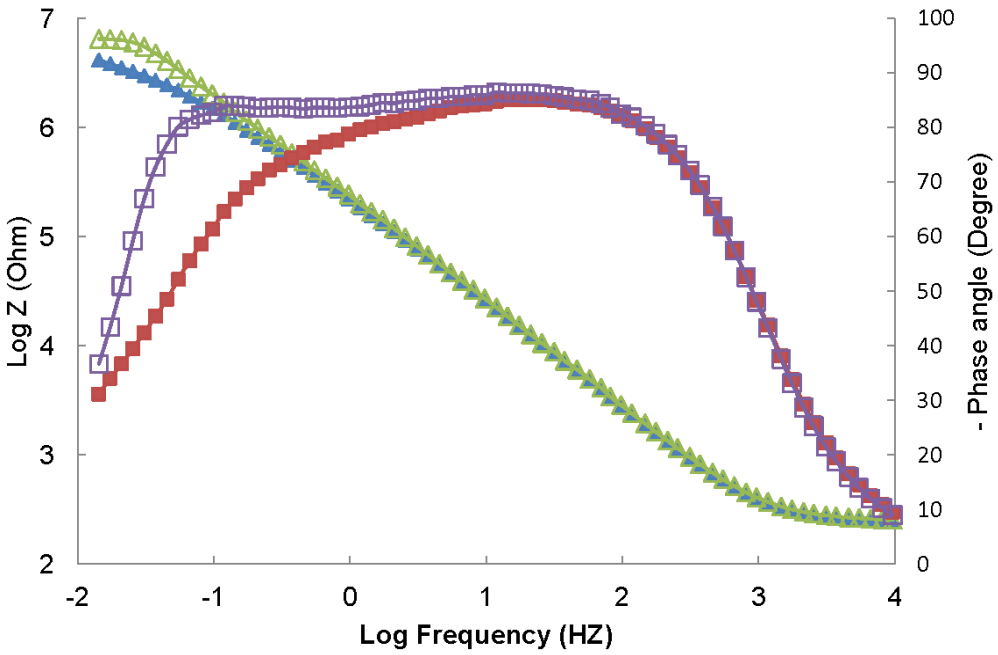

Figure 6.5: Measurement of gramicidin ion channel activity at BRACE using EIS. Impedance data for BRACE is shown before (hollow square and triangles) and 1 hr after addition 1 μM gramicidin . Drop in the resistance is evident due to the passage of sodium ions through BRACE.

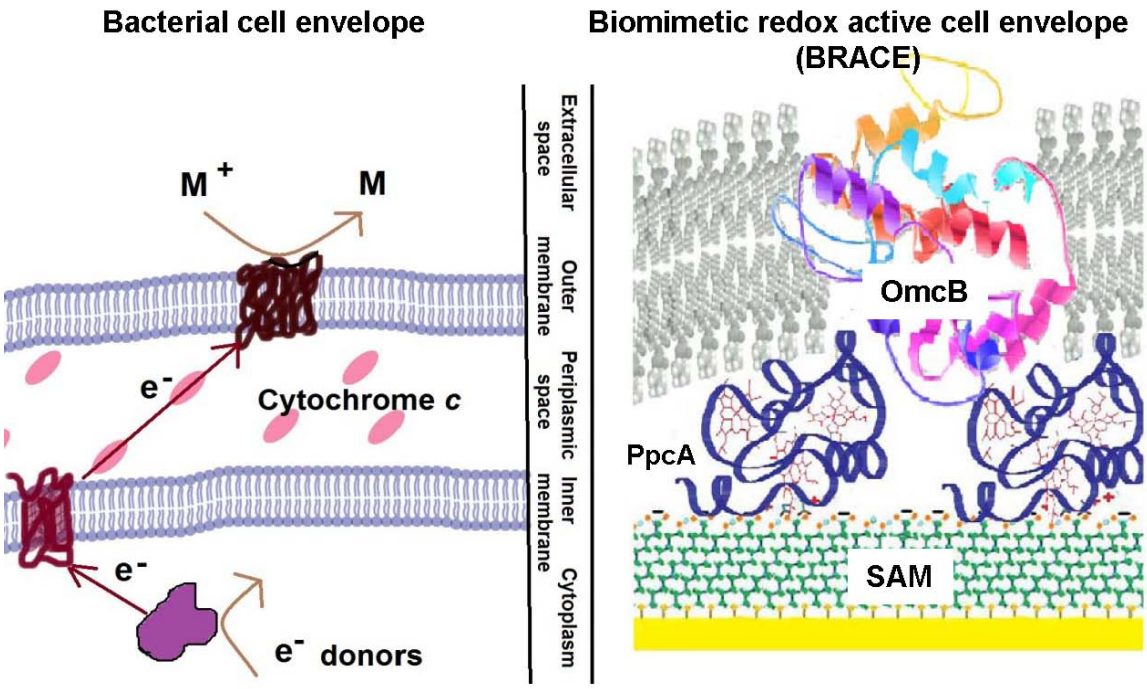

Figure 6.6: Schematic representation of *Geobacter* cell envelope (A) **and Biomimetic redox active cell envelope** (B)**.** A comparison can be made between inner membrane of the bacteria and SAM, periplasmic space cytochromes and immobilized PpcA, outer membrane and DOPC bilayer, and outer membrane cytochromes in *Geobacter* and OmcB deposited as proteoliposomes. (Figure not drawn to the scale)

Table 6.1: Reduction potentials and free energies of redox compounds

Reduction pair	**E_{env}^{*} (V)**	**ΔG (KJ/mol)**
Terminal electron acceptor		
$Fe^{3+/}Fe^{2+}$ (pH 2)	+0.77	-74.2
Fe (III)-citrate/Fe (II) citrate	+0.385	-37.1
Fe(III)-NTA/Fe(II)-NTA	+0.372	-35.9
$Ferrihydrite_{solid}/Fe^{2+}$	+0.1 to -0.1	-9.6 to 9.6
α-$FeOOH_{solid}/Fe^{2+}$	-0.274	26.4
α- Fe_2O_{3solid}/Fe^{2+}	-0.287	55.4
Fe_3O_{4solid}/Fe^{2+}	-0.314	60.6
Electron donors		
CO_2/acetate	-0.29	223.8
NAD^{+}/NADH	-0.32	61.7
Electron carriers		
Menaquinones (ox/red)	-0.067 to -0.11	12.9 to 21.2
Ubiquinone (ox/red)	+0.11	-21.2
PpcA	-0.169	16.3
OmcS	-0.212	18.3
OmcB	~ -0.18	

E_{env}^{*} : Environmentally relevant redox potentials at pH 7, except where noted

Table A .1: List of some of the detergents tried to solubilize OmcB

Detergent	Detergent class	Solubility
n-Octyl-D-glucopyranoside (OG) 0.5%, 1%, 1.5 %, 2% pH 3.5 and pH 8	Non ionic detergent	No
Dodecyl b D maltoside (DDM) 1%, 2%	Non ionic detergent	No
Polyoxyethylene 1%, 2%		No
Cell lytic™ detergent mix		No
CHAPS 1%, 2%, 4%	Zwitterionic detergent	No
Brij 35 1%	Non ionic detergent	No
MEGA-8	Non ionic detergent	No
MEGA 9 2%	Non ionic detergent	No

Table A.4.1 (cont'd)

MEGA 10 2%	**Non ionic detergent**	**No**
Sulfobetaine SB 10 2%	Zwitterionic detergent	No
Sulfobetaine SB12 2%	Zwitterionic detergent	No
Zwittergent 0.5%, 1%, 2%, 5%	Zwitterionic detergent	No
Sodium deoxycholate	Anionic detergent	No
Cetylpyridinium chloride	Cationic detergent	Slight
Cetyltrimethylammonium bromide (CTAB) 2%	Cationic detergent	Moderate
DDM2% + 6 M Urea		Moderate
OG 2% +6 M Urea		Moderate
OG 2% + 200 mM Urea		No

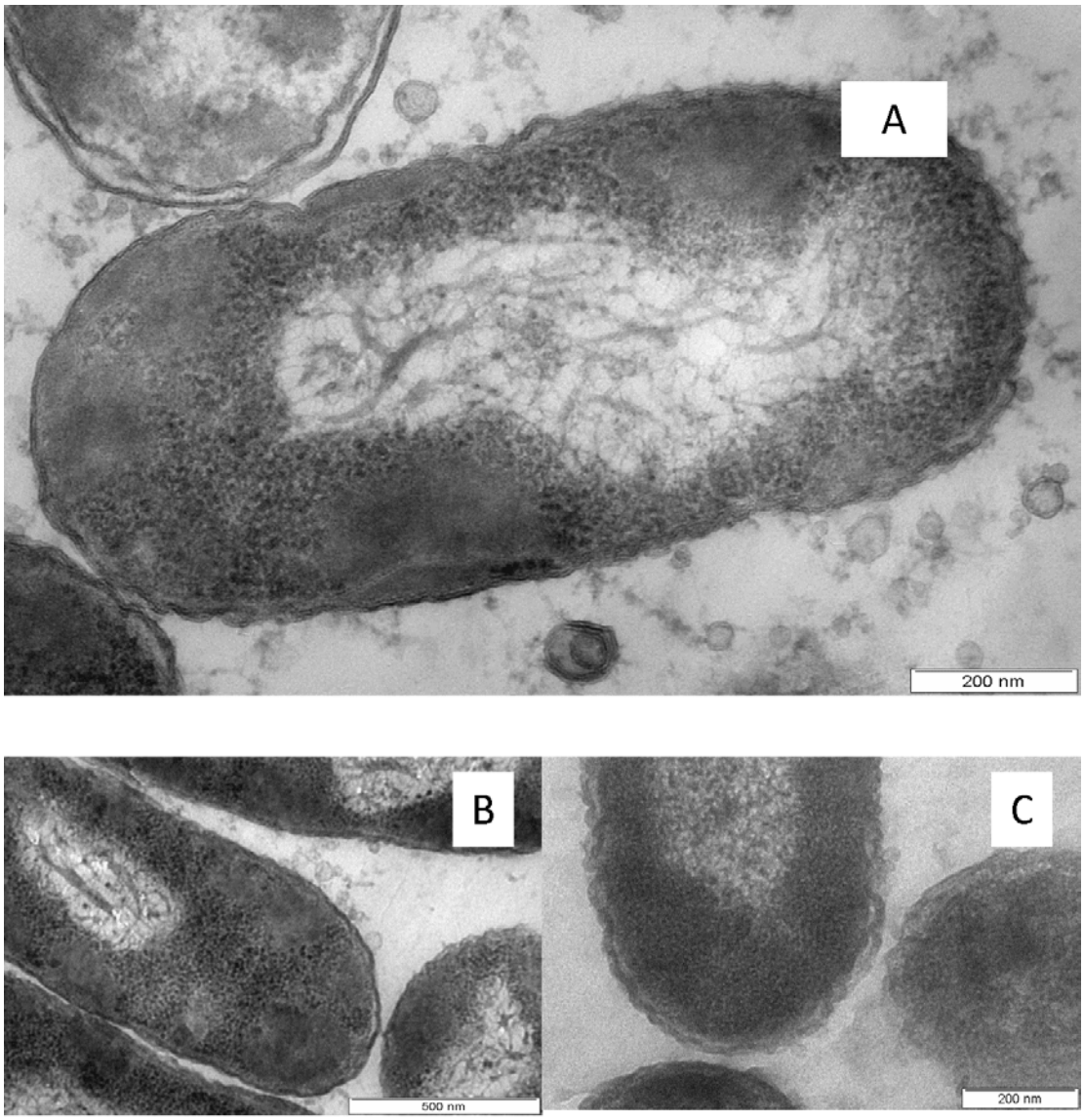

Figure A.1:A, B: TEM images of *E. coli* BL 21 cells expressing OmcB protein. The cells were harvested at the end of fermentation in the late stationary phase. **C:** TEM image of *E. coli* BL21 without the OmcB plasmid and grown under similar conditions. None of the cells displayed deposition in the periplasmic space.

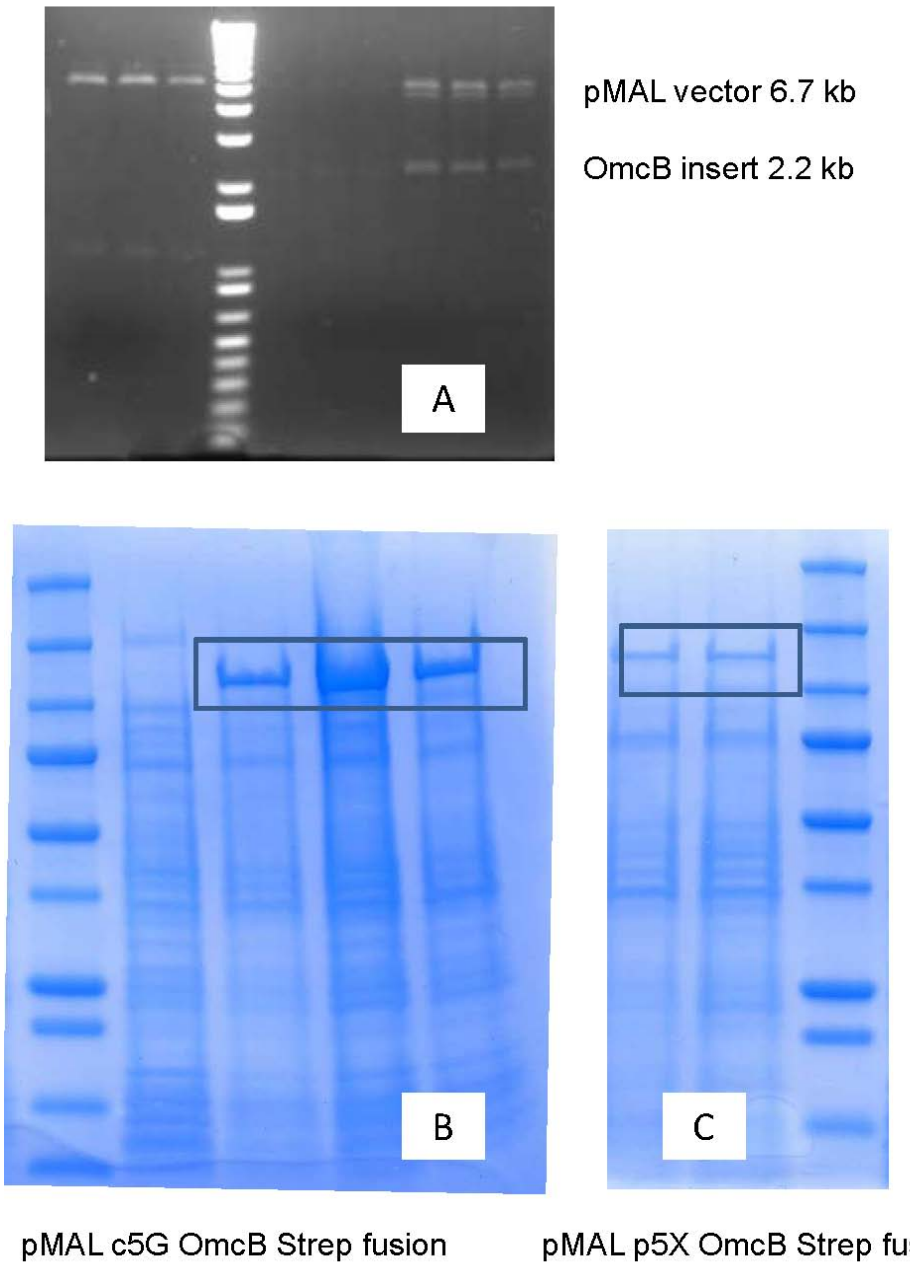

Figure A.2: A. Agarose gel electrophoresis of pMAL plasmids digested with EcoRI and NdeI restriction enzymes showed successful insertion of OmcB gene into pMAL vectors.

B. and **C.** *E. coli* cell transformed with pMAL OmcB plasmids c5G and p5X displayed a band at the expected molecular weight of the fusion protein (~125 kD).

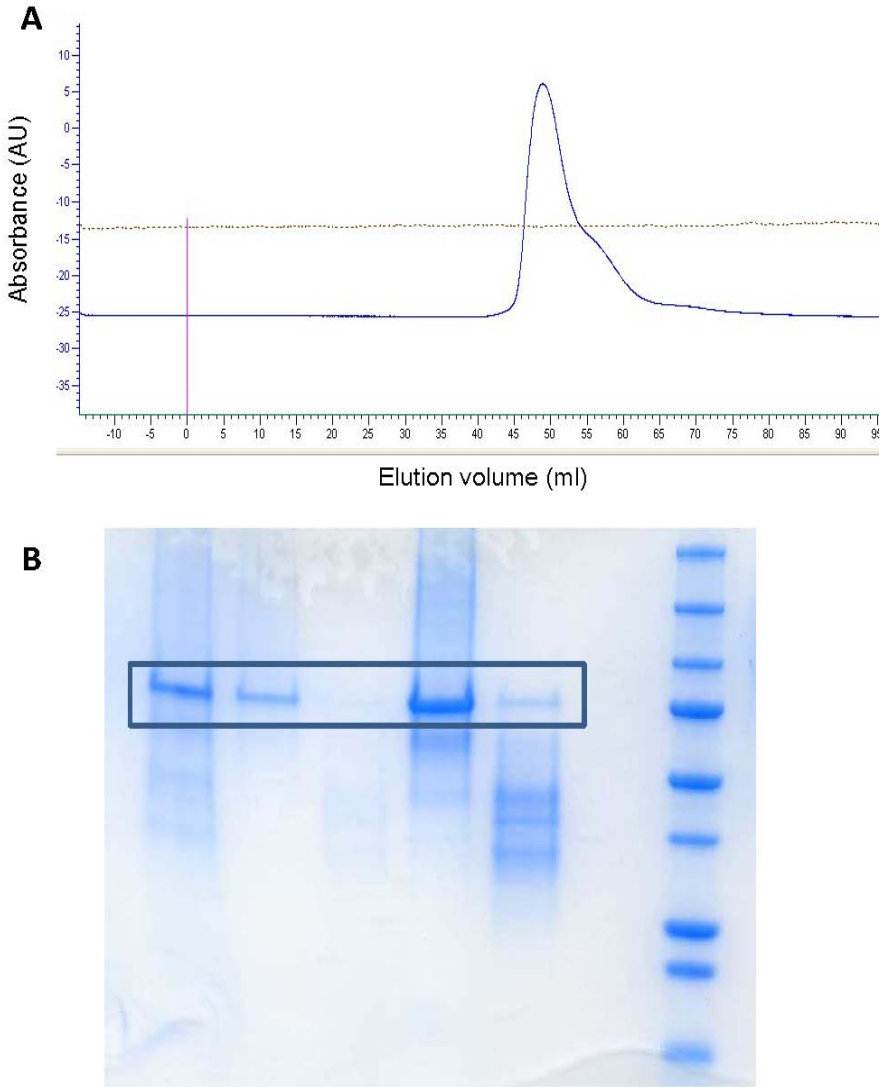

Figure A.3: A. Gel filtration chromatography of urea denatured OmcB with superdex 200^{TM} resin. **B.** Samples from the first larger peak analyzed by SDS PAGE showed presence of OmcB, while the shoulder had other membrane protein impurities.

REFERENCES

REFERENCES

1. Dullies F, Lutze W, Gong W, Nuttall HE. Biological reduction of uranium-From the laboratory to the field. Science of the Total Environment. 2010;408(24):6260-71.

2. Wall JD, Krumholz LR. Uranium reduction. Annual Review of Microbiology. Palo Alto: Annual Reviews; 2006. p. 149-66.

3. Whicker FW, Hinton TG, MacDonell MM, Pinder JE, Habegger LJ. Environment - Avoiding destructive remediation at DOE sites. Science. 2004;303(5664):1615-6.

4. Lovley DR. Bioremediation - Anaerobes to the rescue. Science. 2001;293(5534):1444-6.

5. Anderson RT, Vrionis HA, Ortiz-Bernad I, Resch CT, Long PE, Dayvault R, et al. Stimulating the in situ activity of *Geobacter* species to remove uranium from the groundwater of a uranium-contaminated aquifer. Appl Environ Microbiol. 2003;69(10):5884-91.

6. Mohapatra BR, Dinardo O, Gould WD, Koren DW. Biochemical and genomic facets on the dissimilatory reduction of radionuclides by microorganisms - A review. Miner Eng. 2010;23(8):591-9.

7. Tabak HH, Lens P, Hullebusch EDv, Dejonghe W. Developments in bioremediation of soils and sediments polluted with metals and radionuclides - 1. Microbial processes and mechanisms affecting bioremediation of metal contamination and influencing metal toxicity and transport. Reviews in Environmental Science and Bio/Technology. 2005;4(3):115-56.

8. Moon HS, McGuinness L, Kukkadapu RK, Peacock AD, Komlos J, Kerkhof LJ, et al. Microbial reduction of uranium under iron- and sulfate-reducing conditions: Effect of amended goethite on microbial community composition and dynamics. Water Research. 2010;44(14):4015-28.

9. Cardenas E, Wu WM, Leigh MB, Carley J, Carroll S, Gentry T, et al. Microbial communities in contaminated sediments, associated with bioremediation of uranium to submicromolar levels. Applied and Environmental Microbiology. 2008;74(12):3718-29.

10. Xu M, Wu W-M, Wu L, He Z, Van Nostrand JD, Deng Y, et al. Responses of microbial community functional structures to pilot-scale uranium in situ bioremediation. Isme Journal. 2010;4(8):1060-70.

11. Kotarski SF, Salyers AA. Isolation and characterization of outer membranes of Bacteroides thetaiotaomicron grown on different carbohydrates. Journal of bacteriology. 1984;158(1):102-9. Epub 1984/04/01.

12. Butler JE, Young ND, Lovley DR. Evolution of electron transfer out of the cell: comparative genomics of six *Geobacter* genomes. BMC Genomics. 2010;11.

13. Esteve-Nunez A, Sosnik J, Visconti P, Lovley DR. Fluorescent properties of c-type cytochromes reveal their potential role as an extracytoplasmic electron sink in *Geobacter sulfurreducens*. Environ Microbiol. 2008;10(2):497-505.

14. Butler JE, Young ND, Lovley DR. Evolution from a respiratory ancestor to fill syntrophic and fermentative niches: comparative genomics of six *Geobacteraceae* species. BMC Genomics. 2009;10.

15. Shelobolina ES, Coppi MV, Korenevsky AA, DiDonato LN, Sullivan SA, Konishi H, et al. Importance of c-type cytochromes for U(VI) reduction by *Geobacter sulfurreducens*. BMC Microbiol. 2007;7.

16. Taillefert M, Beckler JS, Carey E, Burns JL, Fennessey CM, DiChristina TJ. Shewanella putrefaciens produces an Fe(III)-solubilizing organic ligand during anaerobic respiration on insoluble Fe(III) oxides. J Inorg Biochem. 2007;101(11-12):1760-7.

17. Newman DK. Microbiology - How bacteria respire minerals. Science. 2001;292(5520):1312-3.

18. von Canstein H, Ogawa J, Shimizu S, Lloyd JR. Secretion of flavins by Shewanella species and their role in extracellular electron transfer. Appl Environ Microbiol. 2008;74(3):615-23.

19. Marsili E, Baron DB, Shikhare ID, Coursolle D, Gralnick JA, Bond DR. Shewanella Secretes flavins that mediate extracellular electron transfer. Proc Natl Acad Sci U S A. 2008;105(10):3968-73.

20. Qian XL, Mester T, Morgado L, Arakawa T, Sharma ML, Inoue K, et al. Biochemical characterization of purified OmcS, a c-type cytochrome required for insoluble Fe(III) reduction in *Geobacter sulfurreducens*. Biochim Biophys Acta-Bioenerg. 2011;1807(4):404-12.

21. Reardon CL, Dohnalkova AC, Nachimuthu P, Kennedy DW, Saffarini DA, Arey BW, et al. Role of outer-membrane cytochromes MtrC and OmcA in the biomineralization of ferrihydrite by Shewanella oneidensis MR-1. Geobiology. 2010;8(1):56-68.

22. Shi LA, Richardson DJ, Wang ZM, Kerisit SN, Rosso KM, Zachara JM, et al. The roles of outer membrane cytochromes of Shewanella and *Geobacter* in extracellular electron transfer. Environ Microbiol Rep. 2009;1(4):220-7.

23. Shi L, Squier TC, Zachara JM, Fredrickson JK. Respiration of metal (hydr)oxides by Shewanella and *Geobacter*: a key role for multihaem c-type cytochromes. Mol Microbiol. 2007;65(1):12-20.

24. Busalmen JP, Esteve-Nunez A, Berna A, Feliu JM. C-type cytochromes wire electricity-producing bacteria to electrodes. Angewandte Chemie-International Edition. 2008;47(26):4874-7.

25. Richter H, Nevin KP, Jia HF, Lowy DA, Lovley DR, Tender LM. Cyclic voltammetry of biofilms of wild type and mutant *Geobacter sulfurreducens* on fuel cell anodes indicates possible roles of OmcB, OmcZ, type IV pili, and protons in extracellular electron transfer. Energy & Environmental Science. 2009;2(5):506-16.

26. Nevin KP, Kim BC, Glaven RH, Johnson JP, Woodard TL, Methe BA, et al. Anode Biofilm Transcriptomics Reveals Outer Surface Components Essential for High Density Current Production in *Geobacter sulfurreducens* Fuel Cells. PLoS One. 2009;4(5).

27. Leang C, Coppi MV, Lovley DR. OmcB, a c-type polyheme cytochrome, involved in Fe(III) reduction in *Geobacter sulfurreducens*. J Bacteriol. 2003;185(7):2096-103.

28. Mehta T, Coppi MV, Childers SE, Lovley DR. Outer membrane c-type cytochromes required for Fe(III) and Mn(IV) oxide reduction in *Geobacter sulfurreducens*. Appl Environ Microbiol. 2005;71(12):8634-41.

29. Chang YJ, Long PE, Geyer R, Peacock AD, Resch CT, Sublette K, et al. Microbial incorporation of C-13-labeled acetate at the field scale: Detection of microbes responsible for reduction of U(VI). Environ Sci Technol. 2005;39(23):9039-48.

30. Reguera G, McCarthy KD, Mehta T, Nicoll JS, Tuominen MT, Lovley DR. Extracellular electron transfer via microbial nanowires. Nature. 2005;435(7045):1098-101.

31. Leang C, Qian XL, Mester T, Lovley DR. Alignment of the c-Type Cytochrome OmcS along Pili of *Geobacter sulfurreducens*. Applied and Environmental Microbiology. 2010;76(12):4080-4.

32. Cologgi DL, Lampa-Pastirk S, Speers AM, Kelly SD, Reguera G. Extracellular reduction of uranium via *Geobacter* conductive pili as a protective cellular mechanism. Proc Natl Acad Sci U S A. 2011;108(37):15248-52.

33. Malvankar NS, Vargas M, Nevin KP, Franks AE, Leang C, Kim BC, et al. Tunable metallic-like conductivity in microbial nanowire networks. Nat Nanotechnol. 2011;6(9):573-9.

34. Orellana R, Leavitt JJ, Comolli LR, Csencsits R, Janot N, Flanagan KA, et al. U(VI) Reduction by Diverse Outer Surface c-Type Cytochromes of *Geobacter sulfurreducens*. Applied and Environmental Microbiology. 2013;79(20):6369-74.

35. Bird LJ, Bonnefoy V, Newman DK. Bioenergetic challenges of microbial iron metabolisms. Trends Microbiol. 2011;19(7):330-40.

36. Grove J, Tanapongpipat S, Thomas G, Griffiths L, Crooke H, Cole J. Escherichia coli K-12 genes essential for the synthesis of c-type cytochromes and a third nitrate reductase located in the periplasm. Molecular Microbiology. 1996;19(3):467-81.

37. Kim BC, Leang C, Ding YHR, Glaven RH, Coppi MV, Lovley DR. OmcF, a putative c-type monoheme outer membrane cytochrome required for the expression of other outer membrane cytochromes in *Geobacter sulfurreducens.* Journal of Bacteriology. 2005;187(13):4505-13.

38. Kim BC, Qian XL, Ching LA, Coppi MV, Lovley DR. Two putative c-type multiheme cytochromes required for the expression of OmcB, an outer membrane protein essential for optimal Fe(III) reduction in *Geobacter sulfurreducens*. Journal of Bacteriology. 2006;188(8):3138-42.

39. Leang C, Adams LA, Chin KJ, Nevin KP, Methe BA, Webster J, et al. Adaptation to disruption of the electron transfer pathway for Fe(III) reduction in *Geobacter* sulfurreducens. J Bacteriol. 2005;187(17):5918-26.

40. Liu CX, Kota S, Zachara JM, Fredrickson JK, Brinkman CK. Kinetic analysis of the bacterial reduction of goethite. Environ Sci Technol. 2001;35(12):2482-90.

41. Liu CX, Gorby YA, Zachara JM, Fredrickson JK, Brown CF. Reduction kinetics of Fe(III), Co(III), U(VI) Cr(VI) and Tc(VII) in cultures of dissimilatory metal-reducing bacteria. Biotechnol Bioeng. 2002;80(6):637-49.

42. Marshall MJ, Plymale AE, Kennedy DW, Shi L, Wang ZM, Reed SB, et al. Hydrogenase- and outer membrane c-type cytochrome-facilitated reduction of technetium(VII) by Shewanella oneidensis MR-1. Environ Microbiol. 2008;10(1):125-36.

43. Lojou E, Bianco P, Bruschi M. Kinetic studies on the electron transfer between bacterial c-type cytochromes and metal oxides. J Electroanal Chem. 1998;452(2):167-77.

44. Shi L, Chen B, Wang Z, Elias DA, Mayer MU, Gorby YA, et al. Isolation of a high-affinity functional protein complex between OmcA and MtrC: Two outer membrane decaheme c-type cytochromes of Shewanella oneidensis MR-1. Journal of bacteriology. 2006;188(13):4705-14. Epub 2006/06/22.

45. Pitts KE, Dobbin PS, Reyes-Ramirez F, Thomson AJ, Richardson DJ, Seward HE. Characterization of the Shewanella oneidensis MR-1 decaheme cytochrome MtrA. Journal of Biological Chemistry. 2003;278(30):27758-65.

46. Gescher JS, Cordova CD, Spormann AM. Dissimilatory iron reduction in *Escherichia coli*: identification of CymA of Shewanella oneidensis and NapC of *E-coli* as ferric reductases. Molecular Microbiology. 2008;68(3):706-19.

47. Donald JW, Hicks MG, Richardson DJ, Palmer T. The c-type cytochrome OmcA localizes to the outer membrane upon heterologous expression in Escherichia coli. Journal of Bacteriology. 2008;190(14):5127-31.

48. Londer YY, Pokkuluri PR, Tiede DM, Schiffer M. Production and preliminary characterization of a recombinant triheme cytochrome c(7) from *Geobacter sulfurreducens* in *Escherichia coli*. Biochim Biophys Acta-Bioenerg. 2002;1554(3):202-11.

49. ThonyMeyer L. Biogenesis of respiratory cytochromes in bacteria. Microbiol Mol Biol Rev. 1997;61(3):337-&.

50. Bowman SEJ, Bren KL. The chemistry and biochemistry of heme c: functional bases for covalent attachment. Nat Prod Rep. 2008;25(6):1118-30.

51. Londer YY. Expression of Recombinant Cytochromes c in *E. coli*. In: Evans TC, Xu MQ, editors. Heterologous Gene Expression in *E Coli*: Methods and Protocols. Totowa: Humana Press Inc; 2011. p. 123-50.

52. Mavridou DAI, Ferguson SJ, Stevens JM. Cytochrome c assembly. IUBMB Life. 2013;65(3):209-16.

53. Sanders C, Turkarslan S, Lee DW, Daldal F. Cytochrome c biogenesis: the Ccm system. Trends Microbiol. 2010;18(6):266-74.

54. ThroneHolst M, ThonyMeyer L, Hederstedt L. *Escherichia coli* ccm in-frame deletion mutants can produce periplasmic cytochrome b but not cytochrome c. FEBS Lett. 1997;410(2-3):351-5.

55. Londer YY, Pokkuluri PR, Erickson J, Orshonsky Y, Schiffer M. Heterologous expression of hexaheme fragments of a multidomain cytochrome from *Geobacter sulfurreducens* representing a novel class of cytochromes c. Protein Expr Purif. 2005;39(2):254-60.

56. Butler JE, Young ND, Lovley DR. Evolution of electron transfer out of the cell: comparative genomics of six *Geobacter* genomes. BMC Genomics. 2010;11:40. Epub 2010/01/19.

57. Methe BA, Nelson KE, Eisen JA, Paulsen IT, Nelson W, Heidelberg JF, et al. Genome of *Geobacter sulfurreducens*: Metal reduction in subsurface environments. Science. 2003;302(5652):1967-9.

58. Pokkuluri PR, Londer YY, Duke NEC, Long WC, Schiffer M. Family of cytochrome c(7)-type proteins from *Geobacter sulfurreducens*: Structure of one cytochrome c(7) at 1.45 angstrom resolution. Biochemistry. 2004;43(4):849-59.

59. Lloyd JR, Leang C, Myerson ALH, Coppi MV, Cuifo S, Methe B, et al. Biochemical and genetic characterization of PpcA, a periplasmic c-type cytochrome in *Geobacter sulfurreducens*. Biochem J. 2003;369:153-61.

60. Lloyd JR, Chesnes J, Glasauer S, Bunker DJ, Livens FR, Lovley DR. Reduction of actinides and fission products by Fe(III)-reducing bacteria. Geomicrobiol J. 2002;19(1):103-20.

61. Morgado L, Fernandes AP, Londer YY, Bruix M, Salgueiro CA. One simple step in the identification of the cofactors signals, one giant leap for the solution structure determination of multiheme proteins. Biochem Biophys Res Commun. 2010;393(3):466-70.

62. Morgado L, Paixao VB, Salgueiro CA, Bruix M. Backbone, side chain and heme resonance assignments of the triheme cytochrome PpcA from *Geobacter sulfurreducens*. Biomol NMR Assign. 2011;5(1):113-6.

63. Morgado L, Saraiva IH, Louro RO, Salgueiro CA. Orientation of the axial ligands and magnetic properties of the hemes in the triheme ferricytochrome PpcA from *G. sulfurreducens* determined by paramagnetic NMR. FEBS Lett. 2010;584(15):3442-5.

64. Pokkuluri PR, Londer YY, Yang X, Duke NEC, Erickson J, Orshonsky V, et al. Structural characterization of a family of cytochromes c(7) involved in Fe(III) respiration by *Geobacter sulfurreducens*. Biochim Biophys Acta-Bioenerg. 2010;1797(2):222-32.

65. Morgado L, Paixao VB, Schiffer M, Pokkuluri PR, Bruix M, Salgueiro CA. Revealing the structural origin of the redox-Bohr effect: the first solution structure of a cytochrome from *Geobacter sulfurreducens*. Biochem J. 2012;441:179-87.

66. Graham LL, Beveridge TJ, Nanninga N. Periplasmic space and the concept of the periplasm. Trends in biochemical sciences. 1991;16(9):328-9. Epub 1991/09/01.

67. Graham LL, Harris R, Villiger W, Beveridge TJ. Freeze-substitution of gram-negative eubacteria: general cell morphology and envelope profiles. Journal of bacteriology. 1991;173(5):1623-33. Epub 1991/03/01.

68. Arrio-Dupont M, Foucault G, Vacher M, Devaux PF, Cribier S. Translational diffusion of globular proteins in the cytoplasm of cultured muscle cells. Biophysical Journal. 2000;78(2):901-7.

69. Kao HP, Abney JR, Verkman AS. Determinants of the translational mobility of a small solute in cell cytoplasm. The Journal of cell biology. 1993;120(1):175-84. Epub 1993/01/01.

70. Cooper JM, Thompson G, McNeil CJ. Direct electron transfer reactions between immobilized cytochrome c and modified gold electrodes. Mol Cryst Liq Cryst Sci Technol Sect A-Mol Cryst Liq Cryst. 1993;234:409-14.

71. De Wael K, Buschop H, De Smet L, Adriaens A. Immobilization of cytochrome c on cysteamine-modified gold electrodes with EDC as coupling agent. Talanta. 2008;76(2):309-13.

72. Alonso-Lomillo MA, Gonzalo-Ruiz J, Dominguez-Renedo O, Munoz F, Arcos-Martinez MJ. CYP450 biosensors based on gold chips for antiepileptic drugs determination. Biosens Bioelectron. 2008;23(11):1733-7.

73. Baker SE, Colavita PE, Tse KY, Hamers RJ. Functionalized vertically aligned carbon nanofibers as scaffolds for immobilization and electrochemical detection of redox-active proteins. Chem Mat. 2006;18(18):4415-22.

74. Villalonga R, Tachibana S, Cao R, Ortiz PD, Gomez L, Asano Y. Supramolecular-mediated immobilisation of L-phenylalanine dehydrogenase on beta-cyclodextrin-modified gold nanospheres. J Exp Nanosci. 2006;1(2):249-60.

75. Andolfi L, Bizzarri AR, Cannistraro S. Assembling of redox proteins on Au(111) surfaces: A scanning probe microscopy investigation for application in bio-nanodevices. Thin Solid Films. 2006;515(1):212-9.

76. Ron H, Matlis S, Rubinstein I. Self-assembled monolayers on oxidized metals. 2. Gold surface oxidative pretreatment, monolayer properties, and depression formation. Langmuir. 1998;14(5):1116-21.

77. Pillai RG, Braun MD, Freund MS. Electrochemically Assisted Self-Assembly of Alkylthiosulfates and Alkanethiols on Gold: The Role of Gold Oxide Formation and Corrosion. Langmuir. 2010;26(1):269-76.

78. Chen TK, Bowden EF. Electrochemical characterization of dehaloperoxidase adsorbates on COOH/OH mixed self-assembled monolayers. J Electroanal Chem. 2013;703:23-8.

79. Jin B, Wang GX, Millo D, Hildebrandt P, Xia XH. Electric-Field Control of the pH-Dependent Redox Process of Cytochrome c Immobilized on a Gold Electrode. J Phys Chem C. 2012;116(24):13038-44.

80. Campbell-Rance DS, Doan TT, Leopold MC. Sweep, step, pulse, and frequency-based techniques applied to protein monolayer electrochemistry at nanoparticle interfaces. J Electroanal Chem. 2011;662(2):343-54.

81. Cortina-Puig M, Munoz-Berbel X, Calas-Blanchard C, Marty JL. Electrochemical characterization of a superoxide biosensor based on the co-immobilization of cytochrome c and XOD on SAM-modified gold electrodes and application to garlic samples. Talanta. 2009;79(2):289-94.

82. Chen XJJ, West AC, Cropek DM, Banta S. Detection of the Superoxide Radical Anion Using Various Alkanethiol Monolayers and Immobilized Cytochrome c. Analytical Chemistry. 2008;80(24):9622-9.

83. Monari S, Battistuzzi G, Borsari M, Millo D, Gooijer C, Van der Zwan G, et al. Thermodynamic and kinetic aspects of the electron transfer reaction of bovine cytochrome c immobilized on 4-mercaptopyridine and 11-mercapto-1-undecanoic acid films. J Appl Electrochem. 2008;38(7):885-91.

84. Bard AJ, Faulkner LR. Electrochemical methods : fundamentals and applications. 2nd ed. New York: John Wiley; 2000. xxi, 833 p. p.

85. Londer YY, Pokkuluri PR, Tiede DM, Schiffer M. Production and preliminary characterization of a recombinant triheme cytochrome c(7) from *Geobacter sulfurreducens* in *Escherichia coli*. Biochim Biophys Acta. 2002;1554(3):202-11. Epub 2002/08/06.

86. Bond AM. Chemical and Electrochemical Approaches to the Investigation of Redox Reactions of Simple Electron-Transfer Metalloproteins. Inorg Chim Acta. 1994;226(1-2):293-340.

87. Lloyd JR, Blunt-Harris EL, Lovley DR. The periplasmic 9.6-kilodalton *c*-type cytochrome of *Geobacter sulfurreducens* is not an electron shuttle to Fe(III). J Bacteriol. 1999;181(24):7647-9. Epub 1999/12/22.

88. Lloyd JR, Leang C, Hodges Myerson AL, Coppi MV, Cuifo S, Methe B, et al. Biochemical and genetic characterization of PpcA, a periplasmic c-type cytochrome in *Geobacter sulfurreducens*. Biochem J. 2003;369(Pt 1):153-61. Epub 2002/10/03.

89. Mendoza SM, Arfaoui I, Zanarini S, Paolucci F, Rudolf P. Improvements in the characterization of the crystalline structure of acid-terminated alkanethiol self-assembled monolayers on Au(111). Langmuir. 2007;23(2):582-8.

90. Nicholson RS, Shain I. Theory of Stationary Electrode Polarography. Single Scan and Cyclic Methods Applied to Reversible, Irreversible, and Kinetic Systems. Analytical Chemistry. 1964;36(4):706-23.

91. Song S, Clark RA, Bowden EF, Tarlov MJ. Characterization of cytochrome c/alkanethiolate structures prepared by self-assembly on gold. The Journal of Physical Chemistry. 1993;97(24):6564-72.

92. Bernad S, Leygue N, Korri-Youssoufi H, Lecomte S. Kinetics of the electron transfer reaction of Cytochrome c(552) adsorbed on biomimetic electrode studied by time-resolved surface-enhanced resonance Raman spectroscopy and electrochemistry. Eur Biophys J Biophys Lett. 2007;36(8):1039-48.

93. Ribera D, Labrot F, Tisnerat G, Narbonne JF. Uranium in the environment: occurrence, transfer, and biological effects. Rev Environ Contam Toxicol. 1996;146:53-89.

94. Crowley KD, Aherne JF. Managing the environmental legacy of U.S. nuclear weapons production. Amer Scientist. 2002;(Online) 90:514-26.

95. Cao B, Ahmed B, Beyenal H. Immobilization of Uranium in Groundwater Using Biofilms. In: Shah V, editor. Emerging Environmental Technologies: Springer Netherlands; 2010. p. 1-37.

96. Miller AC, McClain D. A review of depleted uranium biological effects: in vitro and in vivo studies. Rev Environ Health. 2007;22(1):75-89.

97. Mondani L, Benzerara K, Carriere M, Christen R, Mamindy-Pajany Y, Fevrier L, et al. Influence of uranium on bacterial communities: a comparison of natural uranium-rich soils with controls. PloS one. 2011;6(10):e25771. Epub 2011/10/15.

98. Lovley DR, Phillips EJP, Gorby YA, Landa ER. Microbial reduction of uranium. Nature. 1991;350:413-6.

99. Sanford RA, Wu Q, Sung Y, Thomas SH, Amos BK, Prince EK, et al. Hexavalent uranium supports growth of *Anaeromyxobacter dehalogenans* and *Geobacter* spp. with lower than predicted biomass yields. Environ Microbiol. 2007;9(11):2885-93. Epub 2007/10/10.

100. Cologgi DL, Lampa-Pastirk S, Speers AM, Kelly SD, Reguera G. Extracellular reduction of uranium via *Geobacter* conductive pili as a protective cellular mechanism. Proc Natl Acad Sci USA. 2011;108(37):15248-52. Epub 2011/09/08.

101. Gorby YA, Lovley DR. Enzymatic uranium precipitation. Environ Sci Technol. 1992;26:205-7.

102. Anderson RT, Vrionis HA, Ortiz-Bernad I, Resch CT, Long PE, Dayvault R, et al. Stimulating the *in situ* activity of *Geobacter* species to remove uranium from the groundwater of a uranium-contaminated aquifer. Appl Environ Microbiol. 2003;69(10):5884-91.

103. Chang YJ, Long PE, Geyer R, Peacock AD, Resch CT, Sublette K, et al. Microbial incorporation of 13C-labeled acetate at the field scale: detection of microbes responsible for reduction of U(VI). Environ Sci Technol. 2005;39(23):9039-48.

104. Reguera G. Electron transfer at the cell-uranium interface in *Geobacter* spp. Biochem Soc Trans. 2012;40(6):1227-32. Epub 2012/11/28.

105. Haveman SA, Holmes DE, Ding YH, Ward JE, Didonato RJ, Jr., Lovley DR. *c*-Type cytochromes in *Pelobacter carbinolicus*. Appl Environ Microbiol. 2006;72(11):6980-5. Epub 2006/08/29.

106. Morgado L, Bruix M, Pessanha M, Londer YY, Salgueiro CA. Thermodynamic characterization of a triheme cytochrome family from *Geobacter sulfurreducens* reveals mechanistic and functional diversity. Biophys J. 2010;99(1):293-301. Epub 2010/07/27.

107. Shelobolina ES, Coppi MV, Korenevsky AA, DiDonato LN, Sullivan SA, Konishi H, et al. Importance of *c*-Type cytochromes for U(VI) reduction by *Geobacter sulfurreducens*. BMC Microbiol. 2007;7:16.

108. Kim BC, Leang C, Ding YH, Glaven RH, Coppi MV, Lovley DR. OmcF, a putative *c*-Type monoheme outer membrane cytochrome required for the expression of other outer membrane cytochromes in *Geobacter sulfurreducens*. J Bacteriol. 2005;187(13):4505-13.

109. Leang C, Adams LA, Chin KJ, Nevin KP, Methe BA, Webster J, et al. Adaptation to disruption of the electron transfer pathway for Fe(III) reduction in *Geobacter sulfurreducens*. J Bacteriol. 2005;187(17):5918-26.

110. Udit AK, Hindoyan N, Hill MG, Arnold FH, Gray HB. Protein-surfactant film voltammetry of wild-type and mutant cytochrome P450BM3. Inorganic Chemistry. 2005;44(12):4109-11.

111. Parker VD, Roddick A, Seefeldt LC, Wang HJ, Zheng G. Determination of rate and equilibrium constants for the reactions between electron transfer mediators and proteins by linear sweep voltammetry. Analytical Biochemistry. 1997;249(2):212-8.

112. Jadhav SR, Zheng Y, Garavito RM, Worden RM. Functional characterization of PorB class II porin from Neisseria meningitidis using a tethered bilayer lipid membrane. Biosensors & Bioelectronics. 2008;24(4):831-5.

113. Jadhav SR, Sui DX, Garavito RM, Worden RM. Fabrication of highly insulating tethered bilayer lipid membrane using yeast cell membrane fractions for measuring ion channel activity. Journal of Colloid and Interface Science. 2008;322(2):465-72.

114. Afkar E, Reguera G, Schiffer M, Lovley DR. A novel *Geobacteraceae*-specific outer membrane protein J (OmpJ) is essential for electron transport to Fe (III) and Mn (IV) oxides in *Geobacter sulfurreducens*. BMC Microbiol. 2005;5(1):41.

115. Moreno C, Franco R, Moura I, Legall J, Moura JJG. Voltammetric Studies of the Catalytic Electron-Transfer Process between the Desulfovibrio-Gigas Hydrogenase and Small Proteins Isolated from the Same Genus. Eur J Biochem. 1993;217(3):981-9.

116. Moreno C, Costa C, Moura I, Le Gall J, Liu MY, Payne WJ, et al. Electrochemical studies of the hexaheme nitrite reductase from Desulfovibrio desulfuricans ATCC 27774. European journal of biochemistry / FEBS. 1993;212(1):79-86. Epub 1993/02/15.

117. Wang Z, Liu C, Wang X, Marshall MJ, Zachara JM, Rosso KM, et al. Kinetics of reduction of Fe(III) complexes by outer membrane cytochromes MtrC and OmcA of *Shewanella oneidensis* MR-1. Appl Environ Microbiol. 2008;74(21):6746-55. Epub 2008/09/16.

118. Gray HB, Winkler JR. Electron transfer in proteins. Annu Rev Biochem. 1996;65:537-61.

119. Winkler JR, Gray HB, Prytkova TR, Kurnikov IV, Beratan DN. Electron Transfer Through Proteins. Willner I, Katz E, editors. Oxford: Blackwell Science Publ; 2005. 15-33 p.

120. Gray HB, Winkler JR. Electron flow through metalloproteins. Biochim Biophys Acta-Bioenerg. 2010;1797(8):1563-72.

121. Brezonik PL. Principles of linear free-energy and structure-activity relationships and their applications to the fate of chemicals in aquatic systems. In: Stumm W, editor. Aquatic chemical kinetics: reaction rates of processes in natural waters. New York, NY: John Wiley and Sons, Inc.; 1990. p. 113-43.

122. Marcus RA, Sutin N. Electron transfers in chemistry and biology. Biochim Biophys Acta. 1985;811:265-322.

123. Drake PL, Hartshorn RT, Mcginnis J, Sykes AG. Ph-Dependence of Rate Constants for Reactions of Cytochrome-C with Inorganic Redox Partners and Mechanistic Implications. Inorganic Chemistry. 1989;28(7):1361-6.

124. Gray HB, Winkler JR. Electron transfer in proteins. Annu Rev Biochem. 1996;65:537-61. Epub 1996/01/01.

125. Benavides-Garcia MG, Balasubramanian K. Structural insights into the binding of uranyl with human serum protein apotransferrin. Structure and spectra of protein-uranyl interactions. Chem Res Toxicol. 2009;22(9):1613-21.

126. Vidaud C, Gourion-Arsiquaud S, Rollin-Genetet F, Torne-Celer C, Plantevin S, Pible O, et al. Structural consequences of binding of UO2(2+) to apotransferrin: can this protein account for entry of uranium into human cells? Biochemistry. 2007;46(8):2215-26. Epub 2007/02/03.

127. Liu CX, Zachara JM, Fredrickson JK, Kennedy DW, Dohnalkova A. Modeling the inhibition of the bacterial reduction of U(VI) by beta-MnO2(S)(g). Environ Sci Technol. 2002;36(7):1452-9.

128. Brookshaw DR, Pattrick RAD, Lloyd JR, Vaughan DJ. Microbial effects on mineral-radionuclide interactions and radionuclide solid-phase capture processes. Mineral Mag. 2012;76(3):777-806.

129. Lovley DR. Bioremediation of organic and metal contaminants with dissimilatory metal reduction. Journal of industrial microbiology. 1995;14(2):85-93. Epub 1995/02/01.

130. Wilkins MJ, Livens FR, Vaughan DJ, Lloyd JR. The impact of Fe(III)-reducing bacteria on uranium mobility. Biogeochemistry. 2006;78(2):125-50.

131. Speers AM, Reguera G. Electron Donors Supporting Growth and Electroactivity of *Geobacter sulfurreducens* Anode Biofilms. Appl Environ Microbiol. 2012;78(2):437-44.

132. Logan BE. Exoelectrogenic bacteria that power microbial fuel cells. Nat Rev Microbiol. 2009;7(5):375-81.

133. Franks AE, Nevin KP. Microbial Fuel Cells, A Current Review. Energies. 2010;3(5):899-919.

134. Inoue K, Qian X, Morgado L, Kim B-C, Mester T, Izallalen M, et al. Purification and Characterization of OmcZ, an Outer-Surface, Octaheme c-Type Cytochrome Essential for Optimal Current Production by *Geobacter sulfurreducens*. Applied and Environmental Microbiology. 2010;76(12):3999-4007.

135. Qian XL, Reguera G, Mester T, Lovley DR. Evidence that OmcB and OmpB of *Geobacter sulfurreducen*s are outer membrane surface proteins. FEMS Microbiol Lett. 2007;277(1):21-7.

136. Krushkal J, Leang C, Barbe J, Qu YH, Yan B, Puljic M, et al. Diversity of promoter elements in a *Geobacter sulfurreducens* mutant adapted to disruption in electron transfer. Funct Integr Genomics. 2009;9(1):15-25.

137. Holmes DE, Chaudhuri SK, Nevin KP, Mehta T, Methe BA, Liu A, et al. Microarray and genetic analysis of electron transfer to electrodes in *Geobacter sulfurreducens*. Environ Microbiol. 2006;8(10):1805-15.

138. Inoue K, Leang C, Franks AE, Woodard TL, Nevin KP, Lovley DR. Specific localization of the c-type cytochrome OmcZ at the anode surface in current-producing biofilms of *Geobacter sulfurreducens*. Environ Microbiol Rep. 2011;3(2):211-7.

139. Myers CR, Myers JM. Localization of cytochromes to the outer membrane of anaerobically grown *Shewanella putrefaciens* MR-1. Journal of bacteriology. 1992;174(11):3429-38. Epub 1992/06/01.

140. Nikaido H. Isolation of outer membranes. Methods in enzymology. 1994;235:225-34. Epub 1994/01/01.

141. Shevchenko A, Wilm M, Vorm O, Mann M. Mass spectrometric sequencing of proteins from silver stained polyacrylamide gels. Analytical Chemistry. 1996;68(5):850-8.

142. Costerto.Jw, Forsberg C, Matula TI, Buckmire FL, Macleod RA. Nutrition and metabolism of marine bacteria. XVI. Formation of protoplasts, spheroplasts, and related forms from a gram-negative marine bacterium. Journal of Bacteriology. 1967;94(5):1764-&.

143. Hobb RI, Fields JA, Burns CM, Thompson SA. Evaluation of procedures for outer membrane isolation from *Campylobacter jejun*i. Microbiology-Sgm. 2009;155:979-88.

144. Bayer ME. Areas of adhesion between wall and membrane of *Escherichia coli*. J Gen Microbiol. 1968;53:395-&.

145. Filip C, Fletcher G, Wulff JL, Earhart CF. Solubilization of the cytoplasmic membrane of *Escherichia coli* by the ionic detergent sodium-lauryl sarcosinate. Journal of bacteriology. 1973;115(3):717-22. Epub 1973/09/01.

146. Nekrasova O, Tagway A, Ignatova A, Feofanov A, Kirpichnikov M. Studying of Membrane Localization of Recombinant Potassium Channels in *E.coli*. Acta Naturae. 2009;1(1):91-5.

147. Gauthier A, Puente JL, Finlay BB. Secretin of the enteropathogenic *Escherichia coli* type III secretion system requires components of the type III apparatus for assembly and localization. Infect Immun. 2003;71(6):3310-9.

148. Richter K, Buecking C, Schicklberger M, Gescher J. A simple and fast method to analyze the orientation of c-type cytochromes in the outer membrane of Gram-negative bacteria. Journal of Microbiological Methods. 2010;82(2):184-6.

149. Tommassen J. Fallacies of *E. coli* cell fractionations and consequences thereof for protein export models. Microbial Pathogenesis. 1986;1(3):225-8.

150. Jensen HM, Albers AE, Malley KR, Londer YY, Cohen BE, Helms BA, et al. Engineering of a synthetic electron conduit in living cells. Proc Natl Acad Sci U S A. 2010;107(45):19213-8.

151. Fernandes AP, Couto I, Morgado L, Londer YY, Salgueiro CA. Isotopic labeling of c-type multiheme cytochromes overexpressed in *E-coli*. Protein Expr Purif. 2008;59(1):182-8.

152. Kaderbhai MA, Ugochukwu CC, Lamb DC, Kelly SL. Targeting of active human cytochrome P4501A1 (CYP1A1) to the periplasmic space of *Escherichia coli*. Biochem Biophys Res Commun. 2000;279(3):803-7.

153. Londer YY, Pokkuluri PR, Orshonsky V, Orshonsky L, Schiffer M. Heterologous expression of dodecaheme "nanowire" cytochromes *c* from *Geobacter sulfurreducens*. Protein Expr Purif. 2006;47(1):241-8.

154. Londer YY, Giuliani SE, Peppler T, Collart FR. Addressing Shewanella oneidensis "cytochromome": The first step towards high-throughput expression of cytochromes c. Protein Expr Purif. 2008;62(1):128-37.

155. Leang C, Coppi MV, Lovley DR. OmcB, a *c*-type polyheme cytochrome, involved in Fe(III) reduction in *Geobacter sulfurreducens*. J Bacteriol. 2003;185(7):2096-103.

156. Qian X, Reguera G, Mester T, Lovley DR. Evidence that OmcB and OmpB of *Geobacter sulfurreducens* are outer membrane surface proteins. FEMS Microbiol Lett. 2007;277(1):21-7. Epub 2007/11/08.

157. Seddon AM, Curnow P, Booth PJ. Membrane proteins, lipids and detergents: not just a soap opera. Biochim Biophys Acta-Biomembr. 2004;1666(1-2):105-17.

158. Garavito RM, Ferguson-Miller S. Detergents as tools in membrane biochemistry. Journal of Biological Chemistry. 2001;276(35):32403-6.

159. Prive GG. Detergents for the stabilization and crystallization of membrane proteins. Methods. 2007;41(4):388-97.

160. Bessette PH, Aslund F, Beckwith J, Georgiou G. Efficient folding of proteins with multiple disulfide bonds in the *Escherichia coli* cytoplasm. Proc Natl Acad Sci U S A. 1999;96(24):13703-8.

161. Biolabs NE. Available from: https://www.neb.com/protocols/1/01/01/electroporation-protocol-c2986.

162. Lebendiker M, Danieli T. Purification of Proteins Fused to Maltose-Binding Protein. In: Walls D, Loughran ST, editors. Protein Chromatography: Methods and Protocols. Totowa: Humana Press Inc; 2011. p. 281-93.

163. Mollan TL, Jia Y, Banerjee S, Wu G, Timothy Kreulen R, Tsai A-L, et al. Redox properties of human hemoglobin in complex with fractionated dimeric and polymeric human haptoglobin. Free radical biology & medicine. 2014;69:265-77.

164. Knipp M, Yang F, Berry RE, Zhang H, Shokhirev MN, Walker FA. Spectroscopic and functional characterization of nitrophorin 7 from the blood-feeding insect Rhodnius prolixus reveals an important role of its isoform-specific n-terminus for proper protein function. Biochemistry. 2007;46(46):13254-68.

165. Kumbhakar D, Sarkar B, Das A, Das AK, Mobin SM, Fiedler J, et al. Valence structures of the diastereomeric complexes meso- and rac- Ru-2(acac)(4)(mu-Q) (n) (n=2-, 1-, 0, 1+, 2+) with the multiple quinonoid bridging ligand Q=1,2,4,5-tetraimino-3,6-diketocyclohexane. Dalton Trans. 2009(43):9645-52.

166. Ivashenko O, van Herpt JT, Feringa BL, Rudolf P, Browne WR. Electrochemical Write and Read Functionality through Oxidative Dimerization of Spiropyran Self-Assembled Mono layers on Gold. J Phys Chem C. 2013;117(36):18567-77.

167. Millo D. Spectroelectrochemical analyses of electroactive microbial biofilms. Biochem Soc Trans. 2012;40:1284-90.

168. Paxton WF, Kleinman SL, Basuray AN, Stoddart JF, Van Duyne RP. Surface-Enhanced Raman Spectroelectrochemistry of TTF-Modified Self-Assembled Monolayers. J Phys Chem Lett. 2011;2(10):1145-9.

169. Schwaighofer A, Steininger C, Hildenbrandt DM, Srajer J, Nowak C, Knoll W, et al. Time-Resolved Surface-Enhanced IR-Absorption Spectroscopy of Direct Electron Transfer to Cytochrome c Oxidase from R. sphaeroides. Biophysical Journal. 2013;105(12):2706-13.

170. Wang TT, Bai J, Jiang X, Nienhaus GU. Cellular Uptake of Nanoparticles by Membrane Penetration: A Study Combining Confocal Microscopy with FTIR Spectroelectrochemistry. ACS Nano. 2012;6(2):1251-9.

171. Zedler L, Kupfer S, de Moraes IR, Wachtler M, Beckert R, Schmitt M, et al. Trapped in imidazole: how to accumulate multiple photoelectrons on a black-absorbing ruthenium complex. Chemistry (Weinheim an der Bergstrasse, Germany). 2014;20(13):3793-9.

172. Dunsch L. Recent Advances in in situ multi-spectroelectrochemistry. J Solid State Electrochem. 2011;15(7-8):1631-46.

173. Hofbauer S, Gysel K, Bellei M, Hagmuller A, Schaffner I, Mlynek G, et al. Manipulating Conserved Heme Cavity Residues of Chlorite Dismutase: Effect on Structure, Redox Chemistry, and Reactivity. Biochemistry. 2014;53(1):77-89.

174. Kaim W, Fiedler J. Spectroelectrochemistry: the best of two worlds. Chem Soc Rev. 2009;38(12):3373-82.

175. Bernad S, Mantele W. An innovative spectroelectrochemical reflection cell for rapid protein electrochemistry and ultraviolet/visible/infrared spectroscopy. Analytical Biochemistry. 2006;351(2):214-8.

176. Anderson JL, Kuwana T, Hartzell CR. Spectroelectrochemical investigations of stoichiometry and oxidation-reduction potentials of cytochrome c oxidase components in the presence of carbon monoxide: the "invisible" copper. Biochemistry. 1976;15(17):3847-55. Epub 1976/08/24.

177. Benken WV, Kuwana T. Preparation and properties of thin gold and platinum films on glass or quartz for transparent electrodes. Analytical Chemistry. 1970;42(9):1114-&.

178. Cerda JF, Guzman CX, Zhang H, Amendola EJ, Castorino JD, Millet N, et al. Spectroelectrochemical measurements of redox proteins by using a simple UV/visible cell. Electrochemistry Communications. 2013;33:76-9.

179. Keesey RL, Ryan MD. Spectroelectrochemical elucidation of the kinetics of two closely spaced electron transfers. J Electroanal Chem. 2012;677:56-62.

180. Iwaki M, Giotta L, Akinsiku AO, Schagger H, Fisher N, Breton J, et al. Redox-induced transitions in bovine cytochrome bc(1) complex studied by perfusion-induced ATR-FTIR spectroscopy. Biochemistry. 2003;42(38):11109-19.

181. Rusling JF, Nassar AEF. Enhanced electron transfer for myoglobin in surfactant films on electrodes. J Am Chem Soc. 1993;115(25):11891-7.

182. Brzozowska M, Oberts BP, Blanchard GJ, Majewski J, Krysinski P. Design and Characterization of Novel Tether Layer for Coupling of a Bilayer Lipid Membrane to the Surface of Gold. Langmuir. 2009;25(16):9337-45.

183. Rich PR, Breton J. Attenuated total reflection Fourier transform infrared studies of redox changes in bovine cytochrome c oxidase: Resolution of the redox Fourier transform infrared difference spectrum of heme a(3). Biochemistry. 2002;41(3):967-73.

184. Ashur I, Schulz O, McIntosh CL, Pinkas I, Ros R, Jones AK. Transparent Gold as a Platform for Adsorbed Protein Spectroelectrochemistry: Investigation of Cytochrome c and Azurin. Langmuir. 2012;28(13):5861-71.

185. Wu YH, Hu SS. Voltammetric investigation of cytochrome c on gold coated with a self-assembled glutathione monolayer. Bioelectrochemistry. 2006;68(1):105-12.

186. Bloch DA, Borisov VB, Mogi T, Verkhovsky MI. Heme/heme redox interaction and resolution of individual optical absorption spectra of the hemes in cytochrome bd from *Escherichia coli*. Biochim Biophys Acta-Bioenerg. 2009;1787(10):1246-53.

187. Dai Y, Zheng Y, Swain GM, Proshlyakov DA. Equilibrium and Kinetic Behavior of Fe(CN)(6)(3-/4-) and Cytochrome c in Direct Electrochemistry Using a Film Electrode Thin-Layer Transmission Cell. Analytical Chemistry. 2011;83(2):542-8.

188. Yildiz A, Kissinger PT, Reilley CN. Evaluation of an improved thin-layer electrode. Analytical Chemistry. 1968;40(7):1018-24.

189. Donley C, Dunphy D, Paine D, Carter C, Nebesny K, Lee P, et al. Characterization of indium-tin oxide interfaces using X-ray photoelectron spectroscopy and redox processes of a chemisorbed probe molecule: Effect of surface pretreatment conditions. Langmuir. 2002;18(2):450-7.

190. Donner S, Li HW, Yeung ES, Porter MD. Fabrication of optically transparent carbon electrodes by the pyrolysis of photoresist films: Approach to single-molecule spectroelectrochemistry. Analytical Chemistry. 2006;78(8):2816-22.

191. Dai Y, Proshlyakov DA, Zak JK, Swain GM. Optically transparent diamond electrode for use in IR transmission spectroelectrochemical measurements. Analytical Chemistry. 2007;79(19):7526-33.

192. Richardson JN, Osisek AJ, Dyer AL. Spectroelectrochemical measurements at colloidal an multilayer optically transparent electrodes. Electroanalysis. 2003;15(19):1567-70.

193. Castner JF, Hawkridge FM. Heterogeneous electron-transfer kinetic parameters of metalloproteins as studied by channel-flow hydrodynamic voltammetry. Journal of Electroanalytical Chemistry and Interfacial Electrochemistry. 1983;143(1-2):217-32.

194. Lin SR, Jiang XE, Wang LX, Li GH, Guo LP. Adsorption Orientation of Horse Heart Cytochrome c on a Bare Gold Electrode Hampers Its Electron Transfer. J Phys Chem C. 2012;116(1):637-42.

195. Dong S, Niu J, Cotton TM. Ultraviolet/visible spectroelectrochemistry of redox proteins. Methods in enzymology. 1995;246:701-32. Epub 1995/01/01.

196. Dutton PL. Redox potentiometry: determination of midpoint potentials of oxidation-reduction components of biological electron-transfer systems. Methods in enzymology. 1978;54:411-35.

197. Arciero DM, Collins MJ, Haladjian J, Bianco P, Hooper AB. Resolution of the four hemes of cytochrome c554 from Nitrosomonas europaea by redox potentiometry and optical spectroscopy. Biochemistry. 1991;30(48):11459-65. Epub 1991/12/03.

198. Aulenta F, Di Maio V, Ferri T, Majone M. The humic acid analogue antraquinone-2,6-disulfonate (AQDS) serves as an electron shuttle in the electricity-driven microbial dechlorination of trichloroethene to cis-dichloroethene. Bioresource Technology. 2010;101(24):9728-33.

199. Doong RA, Lee CC, Lien CM. Enhanced dechlorination of carbon tetrachloride by *Geobacter sulfurreducens* in the presence of naturally occurring quinones and ferrihydrite. Chemosphere. 2014;97:54-63.

200. Hurtley S. Location, Location, Location INTRODUCTION. Science. 2009;326(5957):1205-.

201. Polka JK, Silver PA. Building synthetic cellular organization. Mol Biol Cell. 2013;24(23):3585-7.

202. Agapakis CM, Boyle PM, Silver PA. Natural strategies for the spatial optimization of metabolism in synthetic biology. Nat Chem Biol. 2012;8(6):527-35.

203. Arends JBA, Verstraete W. 100 years of microbial electricity production: three concepts for the future. Microb Biotechnol. 2012;5(3):333-46.

204. Prakash D, Gabani P, Chandel AK, Ronen Z, Singh OV. Bioremediation: a genuine technology to remediate radionuclides from the environment. Microb Biotechnol. 2013;6(4):349-60.

205. Han XJ, Qi GD, Xu XT, Wang L. Lipid Bilayer Membrane Arrays: Fabrication and Applications. Adv Biochem Eng Biotechnol. 2013;131:121-52.

206. Jadhav SR, Rao KS, Zheng Y, Garavito RM, Worden RM. Voltage dependent closure of PorB class II porin from Neisseria meningitidis investigated using impedance spectroscopy in a tethered bilayer lipid membrane interface. J Colloid Interface Sci. 2013;390:211-6.

207. Gruber B, Konig B. Self-Assembled Vesicles with Functionalized Membranes. Chem-Eur J. 2013;19(2):438-48.

208. Shen YX, Saboe PO, Sines IT, Erbakan M, Kumar M. Biomimetic membranes: A review. J Membr Sci. 2014;454:359-81.

209. Fragneto G, Charitat T, Daillant J. Floating lipid bilayers: models for physics and biology. Eur Biophys J Biophys Lett. 2012;41(10):863-74.

210. Pavlik LL, Grigoriev PA, Shubina VS, Blejyants DA, Moshkov DA. Interaction of dopamine with artificial phospholipid membranes. Biofizika. 2008;53(1):66-72.

211. Marchioretto M, Podobnik M, Dalla Serra M, Anderluh G. What planar lipid membranes tell us about the pore-forming activity of cholesterol-dependent cytolysins. Biophys Chem. 2013;182:64-70.

212. Tien HT, Ottova-Leitmannova A. Planar lipid bilayers (BLMs) and their applications. 1st ed. Boston: Elsevier; 2003. x, 1034 p. p.

213. Bally M, Bailey K, Sugihara K, Grieshaber D, Voros J, Stadler B. Liposome and Lipid Bilayer Arrays Towards Biosensing Applications. Small. 2010;6(22):2481-97.

214. Janshoff A, Steinem C. Transport across artificial membranes - an analytical perspective. Anal Bioanal Chem. 2006;385(3):433-51.

215. Peng ZQ, Tang JL, Han XJ, Wang EK, Dong SJ. Formation of a supported hybrid bilayer membrane on gold: A sterically enhanced hydrophobic effect. Langmuir. 2002;18(12):4834-9.

216. Messersmith RE, Nusz GJ, Reed SM. Using the Localized Surface Plasmon Resonance of Gold Nanoparticles To Monitor Lipid Membrane Assembly and Protein Binding. J Phys Chem C. 2013;117(50):26725-33.

217. Black JC, Cheney PP, Campbell T, Knowles MK. Membrane curvature based lipid sorting using a nanoparticle patterned substrate. Soft Matter. 2014;10(12):2016-23.

218. Jing YJ, Trefna H, Persson M, Kasemo B, Svedhem S. Formation of supported lipid bilayers on silica: relation to lipid phase transition temperature and liposome size. Soft Matter. 2014;10(1):187-95.

219. Attwood SJ, Choi Y, Leonenko Z. Preparation of DOPC and DPPC Supported Planar Lipid Bilayers for Atomic Force Microscopy and Atomic Force Spectroscopy. Int J Mol Sci. 2013;14(2):3514-39.

220. Kung LA, Kam L, Hovis JS, Boxer SG. Patterning hybrid surfaces of proteins and supported lipid bilayers. Langmuir. 2000;16(17):6773-6.

221. Kongsuphol P, Fang KB, Ding Z. Lipid bilayer technologies in ion channel recordings and their potential in drug screening assay. Sensors and Actuators B-Chemical. 2013;185:530-42.

222. Dodd CE, Johnson BRG, Jeuken LJC, Bugg TDH, Bushby RJ, Evans SD. Native *E. coli* inner membrane incorporation in solid-supported lipid bilayer membranes. Biointerphases. 2008;3(2):FA59-FA67.

223. Marx KA. Quartz crystal microbalance: A useful tool for studying thin polymer films and complex biomolecular systems at the solution-surface interface. Biomacromolecules. 2003;4(5):1099-120.

224. Arugula MA, Zhang YY, Simonian AL. Biosensors as 21st Century Technology for Detecting Genetically Modified Organisms in Food and Feed. Analytical Chemistry. 2014;86(1):119-29.

225. Marx KA, Zhou T, Sarma R. Quartz crystal microbalance measurement of self-assembled micellar tubules of the amphiphilic decyl ester of D-tyrosine and their enzymatic polymerization. Biotechnol Prog. 1999;15(3):522-8.

226. Cho N-J, Kanazawa KK, Glenn JS, Frank CW. Employing two different quartz crystal microbalance models to study changes in viscoelastic behavior upon transformation of lipid vesicles to a bilayer on a gold surface. Analytical Chemistry. 2007;79(18):7027-35.

227. Keller CA, Kasemo B. Surface specific kinetics of lipid vesicle adsorption measured with a quartz crystal microbalance. Biophysical Journal. 1998;75(3):1397-402.

228. Valincius G, Meskauskas T, Ivanauskas F. Electrochemical Impedance Spectroscopy of Tethered Bilayer Membranes. Langmuir. 2012;28(1):977-90.

229. Liu Y, Zhang Z, Zhang QX, Baker GL, Worden RM. Biomembrane disruption by silica-core nanoparticles: Effect of surface functional group measured using a tethered bilayer lipid membrane. Biochim Biophys Acta-Biomembr. 2014;1838(1):429-37.

230. Kongsuphol P, Fang KB, Ding ZP. Lipid bilayer technologies in ion channel recordings and their potential in drug screening assay. Sensors and Actuators B-Chemical. 2013;185:530-42.

231. Krishna G, Schulte J, Cornell BA, Pace RJ, Osman PD. Tethered bilayer membranes containing ionic reservoirs: Selectivity and conductance. Langmuir. 2003;19(6):2294-305.

232. Song HD, Beck TL. Temperature Dependence of Gramicidin Channel Transport and Structure. J Phys Chem C. 2013;117(8):3701-12.

233. Henning U, Rehn K, Hoehn B. Cell Envelope and Shape of *Escherichia coli* K12. Proceedings of the National Academy of Sciences. 1973;70(7):2033-6.

234. Silhavy TJ, Kahne D, Walker S. The bacterial cell envelope. Cold Spring Harb Perspect Biol. 2010;2(5):a000414. Epub 2010/05/11.

235. Torres CI, Marcus AK, Lee HS, Parameswaran P, Krajmalnik-Brown R, Rittmann BE. A kinetic perspective on extracellular electron transfer by anode-respiring bacteria. Fems Microbiol Rev. 2010;34(1):3-17.

236. DeCoursey TE. Voltage-gated proton channels: molecular biology, physiology, and pathophysiology of the H(V) family. Physiol Rev. 2013;93(2):599-652. Epub 2013/04/17.

237. Galdiero S, Galdiero M, Pedone C. beta-barrel membrane bacterial proteins: Structure, function, assembly and interaction with lipids. Curr Protein Pept Sci. 2007;8(1):63-82.

238. Khan MS, Dosoky NS, Williams JD. Engineering Lipid Bilayer Membranes for Protein Studies. Int J Mol Sci. 2013;14(11):21561-97.

239. Frasconi M, Mazzei F, Ferri T. Protein immobilization at gold-thiol surfaces and potential for biosensing. Anal Bioanal Chem. 2010;398(4):1545-64.

240. Ma W, Ying YL, Qin LX, Gu Z, Zhou H, Li DW, et al. Investigating electron-transfer processes using a biomimetic hybrid bilayer membrane system. Nat Protoc. 2013;8(3):439-50.

241. Cullison JK, Hawkridge FM, Nakashima N, Yoshikawa S. A Study of Cytochrome c Oxidase in Lipid Bilayer Membranes on Electrode Surfaces. Langmuir. 1994;10(3):877-82.

242. Knoll W, Koper I, Naumann R, Sinner EK. Tethered bimolecular lipid membranes - A novel model membrane platform. Electrochim Acta. 2008;53(23):6680-9.

243. Zlatanov I, Popova A. Penetration of Lysozyme and Cytochrome C in Lipid Bilayer: Fluorescent Study. J Membr Biol. 2011;242(2):95-103.

244. Ataka K, Giess F, Knoll W, Naumann R, Haber-Pohlmeier S, Richter B, et al. Oriented attachment and membrane reconstitution of his-tagged cytochrome c oxidase to a gold electrode: In situ monitoring by surface-enhanced infrared absorption spectroscopy. J Am Chem Soc. 2004;126(49):16199-206.

245. Brooks SC, Fredrickson JK, Carroll SL, Kennedy DW, Zachara JM, Plymale AE, et al. Inhihition of bacterial U(VI) reduction by calcium. Environ Sci Technol. 2003;37(9):1850-8.